UILU-ENG-73-2009

CIVIL ENGINEERING STUDIES
STRUCTURAL RESEARCH SERIES NO. 399

EFFECTS OF TWO-DIMENSIONAL EARTHQUAKE MOTION ON A REINFORCED CONCRETE COLUMN

By
A. E. AKTAN
D. A. W. PECKNOLD
M. A. SOZEN

A Report on a Research
Project Sponsored by
THE NATIONAL SCIENCE FOUNDATION
Research Grant GI 29934

UNIVERSITY OF ILLINOIS
at URBANA-CHAMPAIGN
URBANA, ILLINOIS
MAY 1973

EFFECTS OF TWO-DIMENSIONAL EARTHQUAKE MOTION ON A REINFORCED CONCRETE COLUMN

by

A. E. Aktan
D.A.W. Pecknold
M. A. Sozen

A Report on a Research Project Sponsored by
THE NATIONAL SCIENCE FOUNDATION
Research Grant GI 29934

UNIVERSITY OF ILLINOIS
URBANA, ILLINOIS
May, 1973

ACKNOWLEDGEMENT

This report is based on a thesis written by A. E. Aktan.

The IBM 360/75 computer system of the Department of Computer Science was used for the analyses.

The work was supported by National Science Foundation Grant GI 29934.

TABLE OF CONTENTS

CHAPTER		Page
1	INTRODUCTION	1
2	OUTLINE OF THE WORK	3
	2.1 The Finite-Filament Model	3
	2.2 Outline of the Moment-Curvature Response Study	4
	2.3 Outline of the Dynamic Response Study	5
3	MOMENT-CURVATURE RESPONSE	6
	3.1 Introductory Comments	6
	3.2 Stress-Strain Characteristics for Steel, Confined and Unconfined Concrete	7
	3.3 Comparison of the Analytical Model with Test.	9
	3.4 Column Section for 2D Moment-Curvature Study.	10
	3.5 2D Moment-Curvature Response	10
	3.6 Index for 2D Response	12
	3.7 Concluding Comments	14
4	DYNAMIC RESPONSE	16
	4.1 Introductory Comments	16
	4.2 Test Column	17
	4.3 Variables in the Dynamic Response Study	18
	4.4 2D Dynamic Response	20
	4.5 Static Reconstruction of Dynamic 2D Displacement Patterns	25
	4.6 Concluding Comments	26
5	SUMMARY AND CONCLUSIONS	29
	5.1 Object and Scope	29
	5.2 Moment-Curvature Response	29
	5.3 Dynamic Response	30
	5.4 Conclusions	31
LIST OF REFERENCES		33
TABLES		36
FIGURES		39

Page

APPENDIX

A	THE PROPERTIES OF A REINFORCED CONCRETE SECTION...	103
B	THE PROPERTIES OF A REINFORCED CONCRETE ELEMENT...	111
C	PROCEDURE FOR DYNAMIC ANALYSIS.....	120
D	NOTATION.....	129

LIST OF TABLES

Table		Page
4.1	Ground Acceleration Records (Fig. 4.1 - 4.4).....	36
4.2	Relative Intensity and Scaling Factors of Ground Acceleration Records.....	37
4.3	Maximum Column Top Drifts, Shears and System Energy (Fig. 4.14 - 4.43).....	38

LIST OF FIGURES

Figure		Page
2.1	Column, Segment, Checkpoint and Filaments.....	39
2.2	Column Model and Filament Configuration (Units Inches).....	40
3.1	Stress-Strain Characteristics of Reinforcing Steel.....	41
3.2	Stress-Strain Characteristics of Confined and Unconfined Concrete.....	42
3.3	Test Column (BK5) Section and Filament Representation (Units Inches).....	43
3.4	Comparison of Analytical and Test Responses.....	44
3.5	1D Moment-Curvature Response of the Column Section.....	45
3.6	Axial Load-Bending Moment-Yield Curvature Interaction Diagram of the Column Section.....	46
3.7	Curvature Histories for 2D Response Study.....	47
3.8	1D and 2D Moment-Curvature Responses.....	48
3.9	1D and 2D Moment-Curvature Responses.....	49
3.10	1D and 2D Moment-Curvature Responses.....	50
3.11	Primary Curves for First Direction.....	51
3.12	Second Direction Transition from 45^{o} Primary Curve to 0^{o} Primary Curve.....	52
3.13	Second Direction Transition from 45^{o} Primary Curve to 60^{o} Primary Curve.....	53
3.14	First Direction Transition from 45^{o} Primary Curve to 30^{o} Primary Curve.....	54
3.15	Transition to 0^{o} Primary Curve.....	55
4.1	Ground Acceleration-Time Histories, 1971 Pacoima, 1940 El Centro, and 1952 Taft Records (First ten sec.).	56
4.2	10 Second Elastic Response Spectra, 1971 Pacoima Record, 0%, 5%, and 20% Damping.....	57

Figure		Page
4.3	10 Second Elastic Response Spectra, 1940 El Centro Record, 0%, 5%, and 20% Damping.....	58
4.4	10 Second Elastic Response Spectra, 1952 Taft Record, 0%, 5%, and 20% Damping.....	59
4.5	Relative Displacement-Time Histories, Pacoima Record, Initial Period 0.7 Seconds.....	60
4.6	Relative Displacement-Time Histories, Pacoima Record, Initial Period 1.5 Seconds.....	61
4.7	Relative Displacement-Time Histories, El Centro Record, Initial Period 0.7 Seconds.....	62
4.8	Relative Displacement-Time Histories, El Centro Record, Initial Period 1.5 Seconds.....	63
4.9	Relative Displacement-Time Histories, Pacoima Record, Relative Intensity 4, Initial Period 0.7 Seconds.....	64
4.10	2D Column Top Displacements, Pacoima Record, Relative Intensity 4, Initial Period 0.7 Seconds.....	65
4.11	Mass Acceleration-Time Histories, Pacoima Record, Relative Intensity 4, Initial Period 0.7 Seconds.....	66
4.12	Force-Displacement Responses, Pacoima Record, Relative Intensity 4, Initial Period 0.7 Seconds.....	67
4.13	Force-Displacement Responses, Pacoima Record, Relative Intensity 4, Initial Period 0.7 Seconds.....	68
4.14	Relative Displacement-Time Histories, Pacoima Record, Relative Intensity 6, Initial Period 0.7 Seconds.....	69
4.15	2D Column Top Displacements, Pacoima Record, Relative Intensity 6, Initial Period 0.7 Seconds.....	70
4.16	Mass Acceleration-Time Histories, Pacoima Record, Relative Intensity 6, Initial Period 0.7 Seconds.....	71
4.17	Force-Displacement Responses, Pacoima Record, Relative Intensity 6, Initial Period 0.7 Seconds.....	72

Figure		Page
4.18	Force-Displacement Responses, Pacoima Record, Relative Intensity 6, Initial Period 0.7 Seconds.....	73
4.19	Relative Displacement-Time Histories, El Centro Record, Relative Intensity 6, Initial Period 0.7 Seconds.....	74
4.20	2D Column Top Displacements, El Centro Record, Relative Intensity 6, Initial Period 0.7 Seconds.....	75
4.21	Mass Acceleration-Time Histories, El Centro Record, Relative Intensity 6, Initial Period 0.7 Seconds.....	76
4.22	Force-Displacement Responses, El Centro Record, Relative Intensity 6, Initial Period 0.7 Seconds.....	77
4.23	Force-Displacement Responses, El Centro Record, Relative Intensity 6, Initial Period 0.7 Seconds.....	78
4.24	Relative Displacement-Time Histories, Taft Record, Relative Intensity 6, Initial Period 0.7 Seconds.....	79
4.25	2D Column Top Displacements, Taft Record, Relative Intensity 6, Initial Period 0.7 Seconds.....	80
4.26	Mass Acceleration-Time Histories, Taft Record, Relative Intensity 6, Initial Period 0.7 Seconds.....	81
4.27	Force-Displacement Responses, Taft Record, Relative Intensity 6, Initial Period 0.7 Seconds.....	82
4.28	Force-Displacement Responses, Taft Record, Relative Intensity 6, Initial Period 0.7 Seconds.....	83
4.29	Relative Displacement-Time Histories, Pacoima Record, Relative Intensity 6, Initial Period 1.5 Seconds.....	84
4.30	2D Column Top Displacements, Pacoima Record, Relative Intensity 6, Initial Period 1.5 Seconds.....	85
4.31	Mass Acceleration-Time Histories, Pacoima Record, Relative Intensity 6, Initial Period 1.5 Seconds.....	86
4.32	Force-Displacement Responses, Pacoima Record, Relative Intensity 6, Initial Period 1.5 Seconds.....	87
4.33	Force-Displacement Responses, Pacoima Record, Relative Intensity 6, Initial Period 1.5 Seconds.....	88
4.34	Relative Displacement-Time Histories, El Centro Record, Relative Intensity 6, Initial Period 1.5 Seconds.....	89

Figure		Page
4.35	2D Column Top Displacements, El Centro Record, Relative Intensity 6, Initial Period 1.5 Seconds.....	90
4.36	Mass Acceleration-Time Histories, El Centro Record, Relative Intensity 6, Initial Period 1.5 Seconds.....	91
4.37	Force-Displacement Responses, El Centro Record, Relative Intensity 6, Initial Period 1.5 Seconds.....	92
4.38	Force-Displacement Responses, El Centro Record, Relative Intensity 6, Initial Period 1.5 Seconds.....	93
4.39	Relative Displacement-Time Histories, Taft Record, Relative Intensity 6, Initial Period 1.5 Seconds.....	94
4.40	2D Column Top Displacements, Taft Record, Relative Intensity 6, Initial Period 1.5 Seconds.....	95
4.41	Mass Acceleration-Time Histories, Taft Record, Relative Intensity 6, Initial Period 1.5 Seconds.....	96
4.42	Force-Displacement Responses, Taft Record, Relative Intensity 6, Initial Period 1.5 Seconds.....	97
4.43	Force-Displacement Responses, Taft Record, Relative Intensity 6, Initial Period 1.5 Seconds.....	98
4.44	Curvature History Representations of 2D Column Top Displacements.....	99
4.45	1D and 2D Moment-Curvature Responses.....	100
4.46	1D and 2D Moment-Curvature Responses.....	101
4.47	1D and 2D Moment-Curvature Responses.....	102
A.1	Section and Filament Displacements, Section Stress Resultants.....	109
A.2	Stress-Strain Relation of a Filament.....	110
B.1	Finite Element, End Forces and Displacements.....	119
C.1	Single Mass System.....	127
C.2	Schematic Representation of the Iteration Procedure....	128

Chapter 1

INTRODUCTION

The 1971 San Fernando earthquake provided a large field laboratory where existing earthquake resistant design concepts were tested. An important conclusion reached after the investigations on the effects of this earthquake was that strong ground shaking estimated to be in the 30% to 50%G range resulted in extreme damage to many modern structures, designed and built according to the seismic code (22) provisions. Although the immediate reaction to this phenomenon was that the minimum code provisions were insufficient in the case of such ground acceleration intensities, other implications also need consideration. Analyses, carried out with the existing procedures, on models of the Olive View Medical Center, one of the modern structures that had extensive damage by the earthquake (8), were not successful in explaining the extent of damage even considering the highest estimates of the ground shaking intensity in the location of this structure (2,11). This points out a deficiency in the existing laboratory and analytical representation procedures of the actual structures and conditions that occur during earthquakes.

An unrealistic assumption in the analytical or laboratory modeling of space frame systems under earthquake excitation is representing the actual multi-dimensional system by a planar model and subjecting this model to only one component of the base excitation. There is no field or laboratory investigation which supports the usual procedure of neglecting the multi-dimensional interaction that occurs during an earthquake if the

structure is strained well into the inelastic range. On the contrary, existing studies on elasto-plastic models indicate that interactions can have significant effects on the response of such systems (17,19).

Although there has been a considerable number of studies on the dynamic response of reinforced concrete in recent years (7, 18, 25), effects of multi-dimensional interaction on the dynamic response of reinforced concrete have received virtually no attention. This study was carried out to obtain information on the static and dynamic multi-dimensional response of reinforced concrete. A finite-filament model, outlined in section 2.1 and described in detail in Appendices A, B and C, was developed for this purpose. This model assumes a column segment to consist of filaments along its long axis (Fig. 2.1) and develops the system properties through the stress-strain hysteresis characteristics and history of these filaments during analysis.

The report is divided into five chapters. The second chapter outlines the finite-filament model and the following two chapters. A study of the effects of two-dimensional interaction on the static moment-curvature response of a reinforced concrete section under load reversals is presented in chapter three. Chapter four gives the results of multi-dimensional dynamic response analyses of a single mass system. A summary and the general conclusions of the complete study are presented in chapter five. In all the static and dynamic analyses one-dimensional responses of the system are also provided for the purposes of comparison and correlating two-dimensional response to one-dimensional responses.

Chapter 2

OUTLINE OF THE WORK

2.1 The Finite-Filament Model

The finite-filament model assumes a column segment consists of uniaxially stressed filaments along its long axis (Fig. 2.1). The cross sectional geometry and stress-strain properties of these filaments can be varied. A number of sections along the column segment are prescribed as checkpoints to follow stress-strain histories of the filaments.

The properties of a column section are expressed in terms of its moment-curvature relation. Assuming that plane sections remain plane after deformation and the stress for a filament can be obtained from the strain history at its centroid, the axial force and two orthogonal moments on the section are related to the centroidal strain and two orthogonal curvatures.

The load-displacement relation for the column segment is obtained by assuming the displaced shape of its long axis can be expressed as a third degree polynomial. The geometry described by this assumption is used to relate internal displacements at the checkpoints to the end displacements. The section properties at each checkpoint are weighed and incorporated into the formulation of the stiffness of the column segment by the virtual work principle as described in detail in Appendix B.

The use of this model in the dynamic analysis of a system is as follows:

(a) The columns are divided into segments (Fig. 2.1b). Segments are broken into filaments. The stress-strain characteristics of different groups of filaments are prescribed. Checkpoints are assigned along the segment to follow the stress-strain histories of the filaments.

(b) At the beginning of each time step the stiffness of the system is specified and the displacement configuration of each column segment is obtained. At the checkpoints the stress-strain state of the filaments corresponding to this displacement configuration and their strain histories are evaluated.

(c) If the updated filament properties indicate a different system stiffness than the predicted, a new stiffness is developed and the displacement configuration is corrected. When the displacement configuration and the resulting filament stress-strain states do not contradict the predicted stiffness, the dynamic equilibrium is satisfied at the time step.

2.2 Outline of the Moment-Curvature Response Study

The multi-dimensional moment-curvature response of a spiral column section was investigated. The confined concrete inside the spiral and the unconfined concrete of the shell was simulated by a network of polar filaments (Fig. 2.2). Steel bars were represented by circular filaments.

The developed relation for the section properties, giving the axial load and the bending moments in terms of the centroidal strain and curvatures was used. Defining the axial load and a curvature history for the section, the centroidal strain was first obtained by iterative procedures and the two orthogonal moments were computed. To observe the effects of the interaction of both moment responses, the one-dimensional responses of the section to

the projections of the curvature history on two orthogonal axes were also obtained. Investigation of two orthogonal moments and curvatures instead of the resultant moment and curvature was useful in correlating multi-dimensional response to one-dimensional responses.

2.3 Outline of the Dynamic Response Study

A typical interior column of the Olive View Medical Center which was damaged by the 1971 San Fernando earthquake was selected as the model for the study. Half scale models of this column were tested at the University of Illinois, Structural Research Laboratory (11). The section of the column was the subject of the moment-curvature study (Fig. 2.2).

Two horizontal components of the 1971 Pacoima Dam, 1940 El Centro and 1952 Taft records were scaled and used as ground acceleration data for a study of the single and multi-dimensional acceleration, displacement and shear-displacement hysteresis responses of the column. Analyses were carried out for two different elastic uncracked periods, 0.7 seconds and 1.5 seconds. The first period corresponded to the fundamental period of the Olive View Medical Center. Energy input and dissipation characteristics were also studied.

Chapter 3

MOMENT-CURVATURE RESPONSE

3.1 Introductory Comments

Moment-curvature response provides information on the stiffness, moment capacity and energy dissipation characteristics of a reinforced concrete section. It is possible to extrapolate this information in the construction of a hypothetical load-displacement model for dynamic analysis purposes. Studies on one-dimensional moment-curvature (1, 12, 14) and load-displacement (5, 6, 25) responses proposing hypothetical models have provided valuable tools for inelastic dynamic response analysis of reinforced concrete by other researchers (7, 18).

The moment-curvature study presented in this chapter was carried out to investigate the effects of multi-dimensional interaction on the inelastic response and the possibility of constructing a multi-dimensional moment-curvature model.

The relation between moments and curvatures derived by the finite-filament concept was used. A fixed axial load was assumed and a curvature history prescribed. This curvature history was followed in small increments. At each increment the axial strain (corresponding to the previous history, existing axial load and curvatures at that increment) was obtained by iteration. The moments at this axial strain for the existing curvatures were then computed. Prescribing a curvature history was preferred to prescribing a moment history because of the problems posed by the latter procedure. Inversion of ill-conditioned relations between section moments and curvatures are necessitated when the moment history is prescribed, as

the section has sudden drops in stiffness under certain conditions during load reversals. On the other hand the main disadvantage of prescribing a curvature history is that the boundary conditions for member displacements are also prescribed as a byproduct of the curvature history. In actual multi-dimensional response, displacements define the curvature history.

Presentation of the multi-dimensional response posed a problem. Since the orientation of the moment and curvature resultants change with the curvature history, a plot of these quantities is not descriptive. The moment-curvature responses presented in this report show the two components of the resultant moments and curvatures in two orthogonal directions, referred to and labeled as 2D response. To provide comparisons one-dimensional responses to the projections of the curvature history on the two axes are also presented on the same figures. These are referred to and labeled as 1D response.

The detailed derivation of the moment-curvature relation is in Appendix A.

3.2 Stress-Strain Characteristics for Steel, Confined and Unconfined Concrete

A considerable number of investigations on the stress-strain characteristics of structural steel and concrete exist (9, 10, 11, 12, 23, 24). The accuracy of the postulated stress-strain relations is the major factor in a good correlation between predicted and observed responses (11). On the other hand, the virgin properties of these materials is also a very important variable in the assessment of accurate stress-strain relations (10). For the purposes of a general study, construction of very detailed and sophisticated stress-strain models is not feasible. The models used in this study reflect only the basic stress-strain characteristics of these materials.

The assumed stress-strain relation for steel is shown in Fig. 3.1. Strain reversals are assumed to have the initial slope, defined by the modulus of elasticity. After intersection with either of the two stress envelopes defined by the primary strain-hardening branches, these envelopes are followed. The modulus of elasticity, yield stress, strain hardening slope and the rupture strain define the stress-strain relation of steel.

The assumed stress-strain relations for confined and unconfined concrete are presented in Fig. 3.2. The relation for unconfined concrete is in the form of a parabola. Confined concrete is expressed by the same parabola up to the maximum stress. It is then linear with zero slope. Concrete is assumed to have no tension capacity. Unloadings for both types of concrete occur with the initial slope. If a filament has unloaded to zero stress, it cannot carry any compression until its prior strain at zero stress is exceeded. The physical interpretation is that the crack has to be closed before the cracked fibers have stress capacity upon reloading. A strong argument against this behavior if that loose concrete particles in the crack get in contact and have stress capacity before the crack is closed completely. However this phenomenon cannot be generalized for all the fibers and was not modeled. Crushing strains for confined and unconfined concretes set the failure limits for these fibers. A crushed filament cannot carry stress again and its stress is redistributed to the other filaments within the section.

The maximum stress, strain at maximum stress and the crushing strains define the behavior of confined and unconfined concrete.

3.3 Comparison of the Analytical Model with Test

Test results on 2D response of reinforced concrete under load reversals have not been reported. To compare the moment-curvature response obtained by finite-filaments with the actual response, 1D test results on half scale models of the section under study were used. These tests were conducted at the Structural Research Laboratory of the University of Illinois (11). As indicated in Fig. 3.3, certain parts of the shell concrete were neglected in the finite-filament simulation. The maximum concrete strength was assumed to be 5000 psi at a strain of 0.003. The crushing strains for shell and core concretes were assume to be 0.004 and 0.05 respectively. The yield stress and strain for steel were assumed to be 60,000 psi and 0.002, with a strain hardening slope of 1×10^6 psi. The axial load on the section was 200 kips. Stress-strain relations used for the materials were as explained in section 3.2.

During the tests, electronic differential transformers were used to measure the relative displacements on opposite faces of the column over a 13 in. reference length. These measurements were later converted into curvatures or average rotation.

Comparison of the moment-curvature response obtained during the first cycle of test BK5 and that obtained using finite-filaments is presented in Fig. 3.4. The discrepancies around the zero moment region are caused by the assumptions regarding the unloading and reloading characteristics of the materials. However the overall agreement is satisfactory for the purposes of this general study.

3.4 Column Section for 2D Moment-Curvature Study

The dimensions and filament representation of the column section are shown in Fig. 2.2. One hundred and twenty concrete and eight steel filaments were used to represent the section. The outermost layer of filaments were assumed to be unconfined concrete to represent the shell. All interior concrete filaments were prescribed as confined core concrete. The stress-strain relations for the materials described in section 3.2 were incorporated in the analysis. The limits for material stresses and strains given in section 3.3 were used. A constant axial load of 750 kips was assumed to act on the section.

The 1D moment-curvature response of the section under load reversals, demonstrating the hysteresis characteristics provided by the analytical model is presented in Fig. 3.5.

The 1D axial load-bending moment-yield curvature interaction diagram for the section is presented in Fig. 3.6. To obtain this relation, the finite-filament model was used to compute the 1D monotonic moment-curvature responses of the section under a series of axial loads. Each point of the interaction diagram was provided by one of these monotonic moment-curvature responses.

3.5 2D Moment-Curvature Response

Figure 3.7a represents the arbitrary 1D loading program for the section described in Fig. 2.2. The corresponding response is in Fig. 3.5. Any 2D curvature history is a combination of 1D curvature histories in two orthogonal directions. There is an infinite number of possible combinations.

However, to obtain information on general characteristics of 2D response, three 2D curvature histories and corresponding responses are presented in this section. The considered curvature histories are shown in Fig. 3.7. Corresponding responses are in Fig. 3.8 - 3.10.

Figure 3.7b represents a curvature history to cycling the section in the first direction and repeating cycling in the second direction. The corresponding moment-curvature responses are shown in Fig. 3.8. The first direction response coincides with the 1D response. The second direction response during the initial curvature application indicates differences from 1D response. Previous disturbance of the section in the first direction results in a loss of stiffness and moment capacity even though the curvature in that direction was erased before loadings in the second direction. The second direction response then approaches the 1D response indicating the effects of the previous disturbance become unimportant after continuing curvature application.

Figure 3.7c demonstrates only one active or acting curvature on the section during a curvature application. The previously attained curvature in the passive direction (or in the direction where curvature is held constant) is maintained while the curvature is applied in the active direction. The corresponding moment-curvature responses are presented in Fig. 3.9. The first direction response coincides with 1D response at initial curvature application. The curvature is then maintained during loading in the second direction. This results in two major differences from 1D behavior. The second direction response occurs with considerably lower stiffness, indicates lower moment capacity, while 70% of the moment reached in the first direction is lost at constant curvature. The curvature is then fixed in the second

direction and reversed in the first direction, resulting in an 80% reduction of the moment capacity of the second direction. This implies that if the curvature in the passive direction was freed, increased displacements would result due to the loss of moment capacity.

Figure 3.7d represents a continuous curvature interaction on the section after an initial loading in the first direction. The moment curvature responses in Fig. 3.10 indicate that after the initial 1D curvature, continuous 2D curvature results in a consistently lower moment capacity and energy dissipation. After the effects of the initial 1D loading is lost, the responses are almost identical in the two directions. They are also proportional to the corresponding 1D responses.

An investigation of these 2D responses indicate certain behavior patterns characteristic to 2D response. Existing or previous disturbances in one direction effect the response in the other direction. The effect of a previous disturbance tends to diminish as curvature is applied in the active direction. Continuous disturbances result in consistent reductions in stiffness, moment capacity and energy dissipation. Another important result regards the orientation of the resultant curvature on the section. When the orientation is 1D, the response approaches 1D response despite previous or existing action in the orthogonal direction. Constant orientation with respect to a direction results in responses proportional to 1D responses. These characteristics are useful in defining an index for 2D response.

3.6 Index for 2D Response

The trends in 2D response indicate the possibility of modeling by correlating to corresponding 1D responses. Possible curvature histories in

2D response result in an infinite number of orientations of the resultant curvature on the section. Construction of a hypothetical moment-curvature model for 2D response requires a certain index to indicate the behavior under various loading possibilities. This index is the interaction angle, which defines the orientation of the resultant curvature on the section in reference to one of the directions. Components of 2D moment-curvature responses of the virgin section for different interaction angles are shown in Fig. 3.11. For symmetric circular sections these 2D responses can be obtained from the 1D response corresponding to a zero interaction angle and are defined as the primary curves. The two orthogonal components of 2D response follow their corresponding primary curves during the initial curvature applications as long as the interaction angle is constant. Any change in the interaction angle during the curvature application results in the shifting of the response components to primary curves defined by the new interaction angle. This shift between the primary curves is not abrupt but is characterized by a smooth transition.

Several examples of transition between primary curves are demonstrated in Fig. 3.12 - 3.15. In Fig. 3.12, two curvature applications start with an interaction angle of 45^{o} and the angle is changed to zero. In the first case the primary curve corresponding to the 45^{o} interaction angle is followed and the response shifts to the 0^{o} primary curve when the angle changes. In the second case the angle change is delayed and the shift occurs with a different transition curve. Figure 3.13 demonstrates the shift from a 45^{o} primary curve to a 60^{o} primary curve in the second direction. Figure 3.14 represents the component of the same response in the first direction where the transition is to the 30^{o} primary curve.

When the interaction angle changes from 90^{o} to 0^{o} the transition is to the 1D response curve. Figure 3.15 demonstrates this phenomenon. The magnitude of the existing curvature in the first direction results in different transition curves. The moment-curvature responses during transition indicate a decrease in stiffness and moment capacity until the transition is completed. This decrease depends on the magnitude of the existing curvature in the passive direction.

3.7 Concluding Comments

With the concept of primary curves and transition discussed in this chapter, the main characteristics of 2D response can be summarized as follows:

(a) 1D moment response is an upper bound for the corresponding component of 2D moment response.

(b) 2D response to the initial curvature application follows the primary curves defined by the interaction angle of the applied curvature.

(c) Any changes in the interaction angle are accompanied by the transition of the response to other primary curves defined by the changed value of the interaction angle.

(d) Characteristics of this transition depend on the curvature history for a given section and axial load. The magnitude of curvature applied with the previous interaction angle and the amount of change in the interaction angle are important variables effecting transition.

(e) Construction of a hypothetical 2D moment-curvature hysteresis model requires further investigation on the transition concept. Since there are infinite possible variations of the major variables in transition, extensive study is required.

The hypothetical curvature histories used in this chapter indicate the possibility of grave reductions in stiffness, moment capacity and energy dissipation properties in 2D response compared to 1D responses. However these reductions are directly related to the curvature histories. Information on realistic curvature histories in 2D dynamic response is required to anticipate and discuss the actual effects of these characteristics.

Chapter 4

DYNAMIC RESPONSE

4.1 Introductory Comments

In spite of the rapid developments in recent years in the state of the art (3, 4, 5, 6, 7, 16, 18, 20, 25, 26), some of the major problems in inelastic response analysis of reinforced concrete remain to be investigated. Two of these problems are the following:

(a) Most analyses have been confined to 1D. The effects of multi-dimensional interaction on the dynamic response of reinforced concrete has been ignored. The 2D static moment-curvature study presented in the previous chapter indicated major differences between 2D and 1D static responses. Significant reductions in the stiffness, energy dissipation and moment resistance of a section were observed in 2D response.

(b) Previous analytical solutions have been based on primary force-displacement curves calculated for monotonic loading of the entire cross section, with hysteresis rules modifying the primary curve so determined. It is preferable to use the hysteresis rules for the response of the materials rather than for the whole section.

The object of the dynamic response study presented in this chapter is to investigate the effects of multi-dimensional interaction on the inelastic dynamic response of reinforced concrete. The finite-filament concept outlined in section 2.1 was used. The analytical method develops the system properties through the stress-strain relations of individual fibers on the sections. The continuous changes in the section properties along the members

are recognized. Any inelastic action and damage sustained by the system during dynamic excitation is a direct result of the entire previous strain histories and the specified limiting strains of the fibers. In this manner the failure of unconfined concrete fibers earlier than the confined concrete fibers, yielding of individual steel bars, strength reductions due to partial failures on different sections are all incorporated in the model.

Development of the load-displacement relation of reinforced concrete by finite-filaments is presented in Appendix B. The inelastic dynamic response analysis procedure followed in this study is given in Appendix C.

4.2 Test Column

A typical interior column of the main building of the Olive View Medical Center which was extensively damaged by the San Fernando earthquake in 1971 (8) was selected as the model for the study. The section of this column was the subject of the moment-curvature study in chapter 3. Information regarding the column section was given in section 3.4. The moment-curvature hysteresis behavior and the axial load-bending moment-yield curvature interaction diagram were given in Fig. 3.5 and 3.6.

In the dynamic analysis, the column was assumed to be a single segment fixed at both ends against rotation. Five checkpoints were used to follow the stress-strain history of the filaments. The location of these checkpoints and the finite-filament representation are shown in Fig. 2.2.

An axial load of 750 kips which reflected the average interior column load in the Olive View Medical Center was assumed. The effect of this

axial load on the lateral stiffness (P-Δ effect)of the column was incorporated in the analyses. Two different column top masses were considered in the study. These masses corresponded to uncracked elastic periods of 0.7 seconds and 1.5 seconds. The first period coincides with the fundamental natural period of the actual structure.

The first yield and crushing of the shell were computed to occur at column top displacements of 1 in. and 2 in. respectively, corresponding to base moments of 12,000 kip-in. for yield and 14,000 kip-in. for the loss of the shell. The two column top masses in conjunction with the base yield moment resulted in yield base shear coefficients of 13% and 2.5% corresponding to the initial periods of 0.7 seconds and 1.5 seconds, respectively.

In the analyses damping was provided only by the energy dissipation characteristics of the materials. Additional viscous damping was not introduced.

4.3 Variables in the Dynamic Response Study

(a) The Number of Interacting Response Dimensions

All the dynamic response analyses in this study were carried out considering response in two lateral directions. For each case studied, two 1D responses to the lateral components of the ground acceleration record were also obtained to provide comparison between 2D and 1D responses.

(b) Ground Acceleration Characteristics

The horizontal components of three ground acceleration records were used as base acceleration inputs to the system. These were the S74W and S16E components of the 1971 Pacoima Dam record, EW and NS components

of the 1940 El Centro record and the S69E and N21E components of the 1952 Taft record. The first ten seconds of these records were used in the analyses (Fig. 4.1) with scale factors as described in the next section. Elastic response spectra for the initial ten seconds of all six components are given in Fig. 4.2 - 4.4. Other pertinent data for the records are given in Table 4.1.

(c) System Characteristics

The system characteristics were varied by changing the mass on the column top. Two different masses, resulting in initial column periods of 0.7 seconds and 1.5 seconds were used. The change in the system characteristics is better characterized by the resulting yield base shear coefficients of 13% and 2.5% for the column. During the excitations the stiffness changes resulted in a wide range of periods. The initial period was useful only as a lower bound for these periods.

The varying maximum intensities of the ground acceleration records combined with the different column top masses results in a wide range of maximum displacement responses and damage sustained by the system. This was observed in a preliminary study involving five-second response analyses of the column. Displacement-time histories of the mass point for the two different column initial periods, obtained by using the unscaled Pacoima Dam and El Centro ground acceleration records as base acceleration inputs are shown in Fig. 4.5 - 4.8. These analyses indicate maximum displacement responses varying between less than one and over ten times the crushing displacement. Complete failure of the column was indicated for the Pacoima

Dam record and 1.5 seconds initial period combination. To eliminate the possibility of complete column failure and to obtain column top drifts that would be representative of the first story drifts generally expected to occur during earthquakes, in frame structures, the ground acceleration records had to be scaled. For this purpose, the relative intensity, defined as the ratio of the maximum ground acceleration in terms of acceleration due to gravity to the yield base shear coefficient, was used. After a preliminary study, scaling the ground acceleration records to obtain a relative intensity of 6 was observed to result in reasonable maximum column top drifts ranging from the crushing displacement to five times the crushing displacement in 1D analyses. The relative intensities resulting from the two different column top masses and the actual maximum intensities of the ground acceleration records are given in Table 4.2. Six case studies for the two column top masses and the three earthquake records scaled for a relative intensity of 6 are presented in the next section. One case study with the Pacoima Dam record scaled for a relative intensity of 4 and an initial period of 0.7 seconds is also given.

4.4 2D Dynamic Response

The results of seven case studies are presented in this section. In each case, the column shown in Fig. 2.2, with a fixed lumped mass at its top, was analysed three times. Two 1D responses to the first 9.6 seconds of the horizontal components of the earthquake record acting individually and a 2D response to the components acting simultaneously were obtained. Relative displacement-time history and acceleration-time histories of the mass point, force-displacement hysteresis relations and the 2D column top relative

displacements were investigated. Energy input to the system and the energy dissipated by the system were also studied. Figures 4.9 - 4.43 and Table 4.3 can be referred to for the results of the analyses.

The case studies are presented in the following.

(a) Pacoima Dam Record, Relative Intensity 4, Initial Period 0.7 Seconds

Figures 4.9 - 4.13 show the results of the analyses for this case. In Fig. 4.9, the 2D displacement response starts deviating from the 1D responses after the initial three seconds of the excitation, when the crushing displacements are exceeded and a displacement equal to twice that at crushing is obtained. After crushing occurs, the main effect of the 2D interaction is to increase the period in the S74W direction and to reverse the drift directions for both components of the response. After the initial three seconds, a permanent but stable set exceeding the crushing displacement occurs. The column top displacement curve in Fig. 4.10 indicates an initial wide loop corresponding to the maximum displacements after the first three seconds and small loops for the rest of the excitation with a shifted center at a little past the crushing displacement. A comparison of the 2D and 1D mass acceleration responses in Fig. 4.11 indicates consistently higher accelerations in 1D responses. The force displacement plots in Fig. 4.12 and 4.13 also reflect this phenomenon. The lateral load capacity in 2D response is significantly lower compared to 1D responses.

(b) Pacoima Dam Record, Relative Intensity 6, Initial Period 0.7 Seconds

In this case the ground accelerations were 50% higher than those in case (a). The responses are shown in Fig. 4.14 - 4.18. Comparison of the responses with case (a) indicates the effects of the increased ground

acceleration intensity. The displacement responses in Fig. 4.14 indicate a maximum 1D response of four times the crushing displacement in the S16E direction after which stable permanent sets at close to the crushing displacement are observed for both components. The 2D response, similar to case (a), starts deviating from 1D responses after the initial three seconds. Instead of stable oscillations at a permanent set, however, the drifts in both directions continue to increase. Each time the crushing displacement is exceeded in the corresponding 1D response, an accumulation of inelastic displacement appears to occur as a result of 2D interaction. Thus, the increase in the ground acceleration intensity results in unstable drifts of the order of eight times the crushing displacement in both directions at the end of the 9.6 seconds of excitation. It is interesting to note that the 1D drifts for this case are acceptable and are expected to occur during moderate to severe earthquakes in structures of the type represented by the model.

Another important implication of the displacement responses for this case is that the drift increase in the direction of the weaker S74W component of the ground acceleration is higher than in the more intense S16E direction. This supports one of the conclusions of the 2D moment curvature study. Damaging the section in the more active direction results in a greater decrease in moment capacity and stiffness in the other direction, leading to larger displacements. Comparison of 2D load displacement responses in Fig. 4.17 and 4.18 indicate a more significant resistance reduction in the S74W direction in 2D response. (The sudden increase in stiffness for 1D response in Fig. 4.18 is caused by the "closing of the crack" in the analysis. Under actual conditions this occurs at a slower rate than that indicated by the analysis.) Furthermore, these responses indicate a degrading of resistance

due to 2D interaction. The 1D hysteresis relations remain stable throughout the excitation. Comparison of Fig. 4.10 and 4.15 demonstrates the significant effects of the 50% increase in base acceleration intensity on the column top displacements.

(c) El Centro Record, Relative Intensity 6, Initial Period 0.7 Seconds

In this case the system characteristics and the maximum base acceleration intensity are similar to case (b). The effect of the change in the base accelerations is reflected in Fig. 4.19 - 4.23. The 2D displacements start deviating from the 1D displacements after the first second when the crushing displacement is exceeded in both directions. However, the restoring characteristic of the base acceleration restrains the inelastic displacement accumulation in 2D motion. After five seconds of excitation permanent sets in two directions take place and 2D drifts exceed the 1D drifts. The 2D, NS drift starts increasing significantly during the last second of excitation. Continuing increase of this drift would depend on whether the ground acceleration restores the drift towards the opposite direction. The column top displacements and the mass acceleration time histories are shown in Fig. 4.20 and 4.21. The hysteresis relations in Fig. 4.22 and 4.23 indicate lower resistances in 2D response. The 2D force-displacement relation for the NS direction indicates a decay in the resistance during the final stages of oscillation.

(d) Taft Record, Relative Intensity 6, Initial Period 0.7 Seconds

The results of the analyses for this case are shown in Fig. 4.24 - 4.28. The 1D displacement responses in Fig. 4.24 indicate drifts at five

times the crushing displacement of the column. The base acceleration does not display restoring characteristics, resulting in stable, permanent sets in both directions during 1D response. The results of 2D interaction for such displacement magnitudes is similar to case (b). An unstable, increasing drift in the S69E direction reaches magnitudes over twenty times the crushing displacement. The column resistance has decayed considerably by the final seconds of the excitation as demonstrated by the hysteresis relations in Fig. 4.27 and 4.28. The displacements in the N21E component are insignificant. Apparently the motion in the S69E direction governs the 2D response. The P-Δ effect plays an important role after the first six seconds of response because the base moments due to the axial load exceed the static crushing moment capacity at a drift of ten times the crushing displacement. The column top displacements and mass acceleration-time histories are presented in Fig. 4.25 and 4.26. The force-displacement relations in Fig. 4.27 and 4.28 provide a descriptive comparison between 2D and 1D responses.

The system characteristics were changed for the next three cases by increasing the column top mass. The resulting yield base shear coefficient of 2.5% characterizes systems of higher periods. Since the response characteristics are similar, these cases are presented together.

(e) Pacoima Dam, El Centro and Taft Records, Relative Intensity 6, Initial Period 1.5 Seconds

Results of the analyses for these three case studies are presented in Fig. 4.29 - 4.43. The 1D displacement responses indicate maximum displacement magnitudes changing from less than to twice crushing displacement. Permanent sets are negligible. For such response magnitudes the differences

between 1D and 2D responses were not significant. 2D interaction appears to increase the displacements slightly for one response direction while decreasing the responses and increasing the periods in the other direction. The mass acceleration-time histories and force-displacement relations display insignificant changes because of 2D interaction. The 2D resistances continue to be lower than the corresponding 1D resistances, however, no reduction in strength with load cycles was observed as in the previous cases.

(f) Energy Input

Energy input to the system and the energy dissipation of the system during excitations were also calculated. The total input and dissipated energies were computed to be equal throughout the excitations for all the analyses, providing a check of the numerical procedure. The input or absorbed energies in individual directions in 2D response were less than the energy of the corresponding direction in 1D response. Total system energies for the analyses are included in Table 4.3.

4.5 Static Reconstruction of Dynamic 2D Displacement Patterns

The dynamic response study presented in section 4.4 indicates that if relative displacements in 1D response exceed twice the crushing displacement, 2D drifts are significantly larger than 1D drifts. The 2D column top displacements in Fig. 4.15, 4.20 and 4.25 correspond to these cases. The static moment-curvature study in this section was carried out to determine whether the increasing drifts can be explained by the effects of static 2D interaction.

Assuming the displacements of the column top is caused by curvature concentrations over a length of 10 inches at both ends of the

column, representative 2D curvature histories for these displacements were obtained. These idealized curvature histories are shown in Fig. 4.44(a), (b) and (c), corresponding to the displacement patterns shown in Fig. 4.20, 4.15 and 4.25 respectively. The 2D static moment-curvature responses of the column section to these curvature histories are compared with the 1D responses to the projections of these histories in the two directions, in Fig. 4.45 - 4.47. It should be noticed that the curvature magnitudes attained in actual 1D dynamic response analyses were considerably smaller than these projections. The responses indicate significant reductions in the moment capacity and stiffness of the section due to 2D interaction. Reductions in the moment capacity of the section due to the crushing of core concrete fibers are also observed. Since curvatures resulting from eight times the crushing displacement are considered, regional crushing of confined core concrete appears possible. In these analyses the strain capacity for core concrete was prescribed as ten times the capacity of shell concrete as explained in section 3.4. Exceeding the limiting compressive strains for core concrete fibers occurs at considerably smaller curvatures in 2D response compared to 1D response. It is apparent from Fig. 4.45 - 4.47 that most of the effects of 2D interaction on the dynamic behavior are direct consequences of the observed effects of this interaction in static moment-curvature response.

4.6 Concluding Comments

The basic conclusion of the dynamic response study presented in this section is that the responses of a ductile, moment resisting, reinforced concrete space frame system under earthquake excitation can be underestimated by a 1D analysis. This does not depend on the analytical method. Even a

sophisticated analysis technique which does not consider the effects of 2D interaction can result in underestimates of displacements and system damage. This depends mainly on the magnitude of the drifts and whether the base acceleration has restoring characteristics. If a stable permanent set over twice the crushing displacement is observed as a result of 1D analysis, unstable, continuously increasing drifts and possible system failure are likely to be caused by the actual multi-dimensional excitation.

The past trend in earthquake resistant design has been towards the use of ductile, moment resisting space frames as the best defense against earthquake excitation (22). It is generally accepted that systems of this kind, analysed and designed in accordance with seismic code (22) provisions, will have inelastic displacements in the order of three to five times the yield displacement. For inelastic displacements of these magnitudes this study has shown the effects of 2D interaction to be important.

The spirally confined reinforced concrete column model displayed desirable resistance qualities in 1D response. However in 2D response a decay of lateral load capacity was observed when twice crushing displacement was exceeded. It should be noticed that the hysteresis characteristics provided by the finite-filament model do not reflect the degrading effects of shear. This is also demonstrated by the 1D moment-curvature hysteresis behavior shown in Fig. 3.5. The decay of the lateral resistance observed in 2D responses is caused by 2D flexural interaction completely. This decay should be expected to be more critical in less effectively confined systems where the effect of shear is more pronounced.

The elastic response spectra predicted the maximum 1D inelastic displacements to the NS component of the El Centro record accurately. With

this exception, the spectral displacement responses to the other five base acceleration components underestimated the actual inelastic displacements in the order of 100% as shown in Table 4.3.

The analytical model used in this study is restricted by economic considerations. Computation costs increase with the number of columns, column segments, checkpoints, filaments and the number of time increments considered in the analysis. Less expensive procedures should be developed. The 2D static moment-curvature behavior was sufficient to explain the effects of 2D interaction in dynamic response, indicating the possibility of a hypothetical 2D moment-curvature hysteresis model for less expensive dynamic analysis. The conclusions of chapter 3 should be helpful in constructing such a model.

Chapter 5

SUMMARY AND CONCLUSIONS

5.1 Object and Scope

The work described in this report was carried out to provide information on the effects of multi-dimensional interaction on the static and dynamic response of reinforced concrete. An analytical model that incorporates the stress-strain hysteresis characteristics and history of individual confined concrete, unconfined concrete and steel fibers in reinforced concrete was developed for this purpose. The specific objectives of the static and dynamic response studies were as follows:

(a) To investigate the two-dimensional moment-curvature response of a reinforced concrete section under load reversals and the possibility of constructing a static, two-dimensional moment-curvature hysteresis model in terms of one-dimensional responses.

(b) To determine the effects of two-dimensional motion on the response of single-mass systems under earthquake excitations as compared with response to one-dimensional motion.

5.2 Moment-Curvature Response

The effects of 2D interaction on the static moment-curvature response under load reversals were observed to depend on the curvature history. 2D curvature histories obtained by several combinations of 1D curvature histories indicated varying amounts of reduction in the stiffness, moment capacity and energy dissipation of the section. A curvature on the order of three times the crushing curvature of the section in one direction reduced the stiffness 50% in the other direction. Application of three times

the crushing curvature in the second direction, while maintaining the curvature constant in the first direction, resulted in an 80% reduction of the moment capacity in the first direction. Thus the interaction of the curvatures in the two directions resulted in adverse effects on the resistance of the section. 2D curvature histories obtained from 2D displacement patterns of a column under earthquake excitation indicated that with higher magnitudes of 2D curvatures on the order of ten times the crushing curvature, the reductions in the moment capacity, stiffness and energy dissipation of the section were extremely significant. Curvature magnitudes of this range could be realized only in the case of effectively confined columns. Construction of a hypothetical 2D moment-curvature model appeared possible since the static moment-curvature responses were sufficient in explaining the effects of 2D interaction on dynamic responses. An index for 2D moment-curvature response was found to be the orientation of the resultant curvature on the section and the primary curves corresponding to this orientation.

5.3 Dynamic Response

The effects of 2D interaction on the relative-displacement, mass acceleration and the force-displacement responses were observed to depend on the displacement magnitudes and base acceleration characteristics. For displacement magnitudes exceeding twice the crushing displacement, 2D interaction became critical. In the cases where less than the twice crushing displacements occurred, the 2D displacement magnitudes differed from the 1D displacement magnitudes by approximately 10%.

The magnitude of the total drift for the two-dimensional analysis depended on the characteristics of the ground motion which could be judged

by the response of the system to one-dimensional motion. If the response to 1D motion was such that the center of oscillation (current point of inelastic set) tended to remain at or be restored to a point close to its original position, effects of two-dimensional motion on drift were not critical.

The maximum mass acceleration responses and the maximum column shears were consistently higher in 1D responses. Interaction reduced the shears by decreasing the lateral resistance of the system. If twice crushing displacements were exceeded, the 2D force-displacement responses displayed decaying characteristics in the later stages of the excitation.

The total absorbed energy of the system was generally lower in 2D response. These observations on the effects of 2D interaction in dynamic response were made on base excitation durations of 9.6 seconds.

5.4 Conclusions

A reinforced concrete column with a circular symmetrically reinforced cross section carrying a single mass was subjected to the first ten seconds of the ground motion for three earthquakes (Pacoima 1971, El Centro 1940, and Taft 1952).

The analyses were made for both horizontal components of the ground motions acting individually and simultaneously. The calculated deflections for two-dimensional motion exceeded those for one-dimensional motion by 20 to 200 percent, if the calculated deflection for one-dimensional motion exceeded approximately twice the crushing deflection, which could be interpreted as the "yield" deflection for the load-displacement relationship of the column analyzed.

From the studies in this report it is concluded that if a column is to provide earthquake resistance in both horizontal directions and if planar inelastic dynamic response analysis indicates deflections on the order of twice the "yield" deflection, the actual maximum deflection of the column may exceed critically the calculated deflection.

LIST OF REFERENCES

1. Aoyama, H., "Moment-Curvature Characteristics of Reinforced Concrete Members Subjected to Axial Load and Reversal of Bending," Proc., International Symposium on Flexural Mechanics of Reinforced Concrete, Miami, Florida, November 1964.

2. Aoyama, H. and M. A. Sozen, "Dynamic Response of a Reinforced Concrete Structure with Tied and Spiral Columns," a paper submitted for presentation at the Fifth World Conference on Earthquake Engineering, Rome, Italy, 1973.

3. Blume, J. A., N. M. Newmark, and L. H. Corning, "Design of Multistory Reinforced Concrete Buildings for Earthquake Motions," Portland Cement Association, 1961.

4. Clough, R. W., "Dynamic Effects of Earthquakes," Journal of the Structural Division, ASCE, Vol. 86, No. ST4, April 1960.

5. Clough, R. W. and S. B. Johnston, "Effect of Stiffness Degradation on Earthquake Ductility Requirements, Proc., Japan Earthquake Engineering Symposium, Tokyo, 1966.

6. Giberson, M. F., "The Response of Nonlinear Multi-Story Structures Subjected to Earthquake Excitation," thesis submitted to the California Institute of Technology at Pasadena in partial fulfillment of the requirements of the degree of Doctor of Philosophy, 1967.

7. Gulkan, P. and M. A. Sozen, "Response and Energy-Dissipation of Reinforced Concrete Frames Subjected to Strong Base Motions," Civil Engineering Studies, Structural Research Series No. 377, University of Illinois, Urbana-Champaign, May 1971.

8. Jennings, P. C., ed., "Engineering Features of the San Fernando Earthquake, February 9, 1971," Earthquake Engineering Research Laboratory, EERL 71-02, California Institute of Technology, Pasadena, California, June 1971.

9. Karsan, I. D. and J. O. Jirsa, "Behavior of Concrete Under Compressive Loadings," Journal of the Structural Division, ASCE, Vol. 95, No. ST12, December 1969.

10. Karlsson, B. I., A. E. Aktan, and M. A. Sozen, "Behavior of Reinforcing Bars Subjected to Large Strain Reversals," Civil Engineering Studies, Structural Research Series No. 397, University of Illinois, Urbana-Champaign, 1973.

11. Karlsson, B. I., H. Aoyama, and M. A. Sozen, "Spirally Reinforced Concrete Columns Subjected to Loading Reversals Simulating Earthquake Effects," a paper submitted for presentation at the Fifth World Conference on Earthquake Engineering, Rome, Italy, 1973.

12. Kent, D. C., "Inelastic Behavior of Reinforced Concrete Members with Cycling Loading," thesis presented to the University of Canterbury, at Christchurch, New Zealand, in partial fulfillment of the requirements for the degree of Doctor of Philosophy, 1969.

13. Langhaar, H. L., "Energy Methods in Applied Mechanics," John Wiley and Sons, Inc., 1962.

14. Monnier, T., "The Moment-Curvature Relation of Reinforced Concrete," Institute TNO for Building Materials and Building Structures, Report No. BI-69-72, Delft, The Netherlands, September 1969.

15. Newmark, N. M., "A Method of Computation for Structural Dynamics," Journal of the Engineering Mechanics Division, ASCE, Vol. 85, No. EM3, July 1959.

16. Newmark, N. M., and E. Rosenblueth, "Fundamentals of Earthquake Engineering," Prentice Hall, 1971.

17. Nigam, N. C., "Inelastic Interactions in the Dynamic Response of Structures," thesis submitted to the California Institute of Technology at Pasadena in partial fulfillment of the requirements of the degree of Doctor of Philosophy, 1967.

18. Otani, S. and M. A. Sozen, "Behavior of Multistory Reinforced Concrete Frames During Earthquakes," Civil Engineering Studies, Structural Research Series No. 392, University of Illinois, Urbana, November 1972.

19. Pecknold, D.A.W. and M. A. Sozen, "Calculated Inelastic Structural Response to Uniaxial and Biaxial Earthquake Motions," a paper submitted for presentation at the Fifth World Conference on Earthquake Engineering Rome, Italy, 1973.

20. Penzien, J., "Elasto-plastic Response of Idealized Multi-Story Structures Subjected to a Strong Motion Earthquake," Proceedings, Second World Conference on Earthquake Engineering, Vol. II, Tokyo, 1960.

21. Przemieniecki, J. S., "Theory of Matrix Structural Analysis," McGraw-Hill, 1968.

22. "Recommended Lateral Force Requirements and Commentary," Seismology Committee, Structural Engineers Association of California, 1967.

23. Singh, A., K. H. Gerstle, and L. G. Tulin, "The Behavior of Reinforcing Steel Under Reversed Loading," Journal ASTM, Materials Research and Standards, Vol. 5, No. 1, January, 1965.

24. Sinha, B. P., K. H. Gerstle, and L. G. Tulin, "Stress-Strain Relations for Concrete Under Cyclic Loading," Proceedings ACI Journal, Vol. 61, No. 2, February 1964.

25. Takeda, T., M. A. Sozen, and N. N. Nielsen, "Reinforced Concrete Response to Simulated Earthquakes," Journal of the Structural Division, ASCE, Vol. 96, No. ST12, December 1970.

26. Veletsos, A. S. and N. M. Newmark, "Effect of Inelastic Behavior on the Response of Simple Systems to Earthquake Motions," Proceedings, Second World Conference on Earthquake Engineering, Vol. II, Tokyo, 1960.

27. Zienkiewicz, O. C., "The Finite Element Method in Engineering Science," McGraw-Hill, 1971.

Table 4.1 Ground Acceleration Records
(Fig. 4.1 - 4.4)

Ground Acceleration Record	Component	Spectrum Intensity* (in)	Maximum Acceleration* (G)
Pacoima Dam 1971	S74W	74.91	1.24(8.52 sec, S74W)
	S16E	107.47	
El Centro 1940	EW	22.93	.312(2.02 sec, NS)
	NS	35.64	
Taft 1952	S69E	18.01	.177(9.12 sec, N21E)
	N21E	17.97	

*First 10 seconds of the records were considered.

Table 4.2 Relative Intensity and Scaling Factors of Ground Acceleration Records

Ground Acceleration Record	Base Yield Shear Coefficient* (%)	Relative Intensity (G) for Full Scale Record	Acceleration Scaling factor (for relative Intensity of 6)
Pacoima Dam 1971	13	9.70	0.62
	2.5	50.80	0.12
El Centro 1940	13	2.40	2.50
	2.5	12.80	0.47
Taft 1952	13	1.36	4.40
	2.5	7.25	0.83

*Base Yield Shear Coefficients of 13% and 2.5% correspond to initial elastic periods of 0.7 seconds and 1.5 seconds respectively.

Table 4.3 Maximum Column Top Drifts, Shears and System Energy
(Fig. 4.14 - 4.43)

Ground Acceleration Record	Initial Period (sec)	Elastic Drifts (in)		Inelastic Drifts (in)				Inelastic Shears (kips)				Total Input Energy (10^7 lb-in)			
				1D		2D		1D		2D		1D		2D	
		1-1	2-2	1-1	2-2	1-1	2-2	1-1	2-2	1-1	2-2	1-1	2-2	1-1	2-2
Pacoima Dam 1971	0.7	4.40	3.70	5.37	8.08	13.48	15.16	215	240	140	190	.22	.38	.11	.30
	1.5	1.65	4.00	0.99	2.08	1.00	2.09	130	160	80	150	.004	.03	.005	.03
El Centro 1940	0.7	4.50	14.00	7.42	13.11	9.07	15.42	205	205	165	160	.35	.49	.38	.46
	1.5	1.27	3.40	4.08	3.37	4.45	2.63	160	180	160	140	.09	.12	.08	.10
Taft 1952	0.7	7.26	8.95	13.32	13.91	46.40	6.25	210	210	240	205	.53	.42	.44	.27
	1.5	4.20	2.45	2.78	1.99	3.37	1.79	180	180	140	115	.07	.05	.06	.04

Notes

(1) The crushing displacement and shear for the column were 2 inches and 155 kips respectively.
(2) Initial periods of 0.7 and 1.5 seconds corresponded to base yield shear coefficients of 13% and 2.5% respectively.
(3) First 10 seconds of the ground acceleration records were used. These were scaled to result in a relative intensity of 6 as shown in Table 4.2.
(4) Elastic displacements were obtained from 10 second elastic spectra for 0% damping and adjusted by the scaling factors in Table 4.2.
(5) The ground motion components used are as follows:

	1-1	2-2
Pacoima Dam	S74W	S16E
El Centro	EW	NS
Taft	S69E	N21E

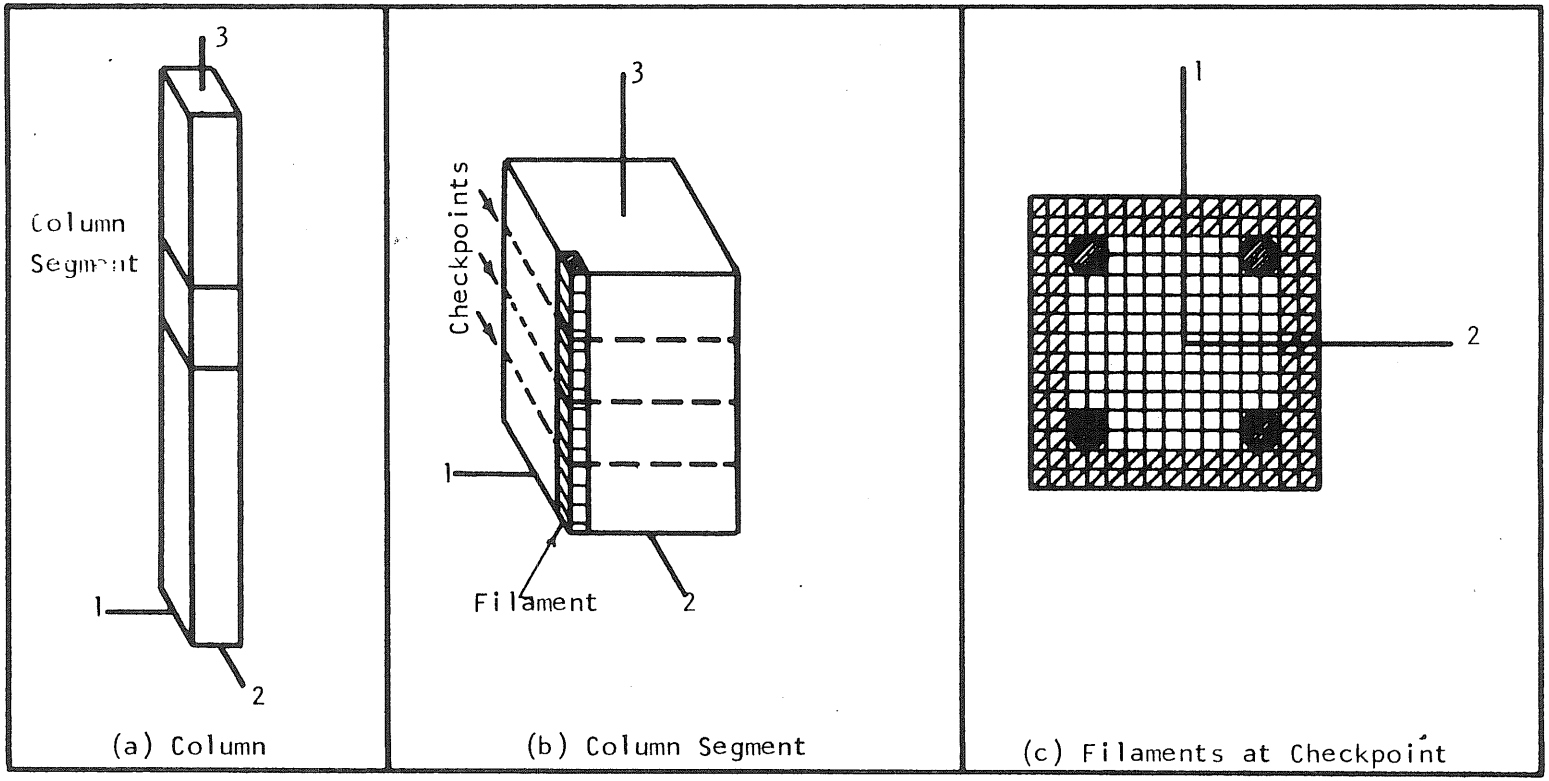

Fig. 2.1 Column, Segment, Checkpoint and Filaments

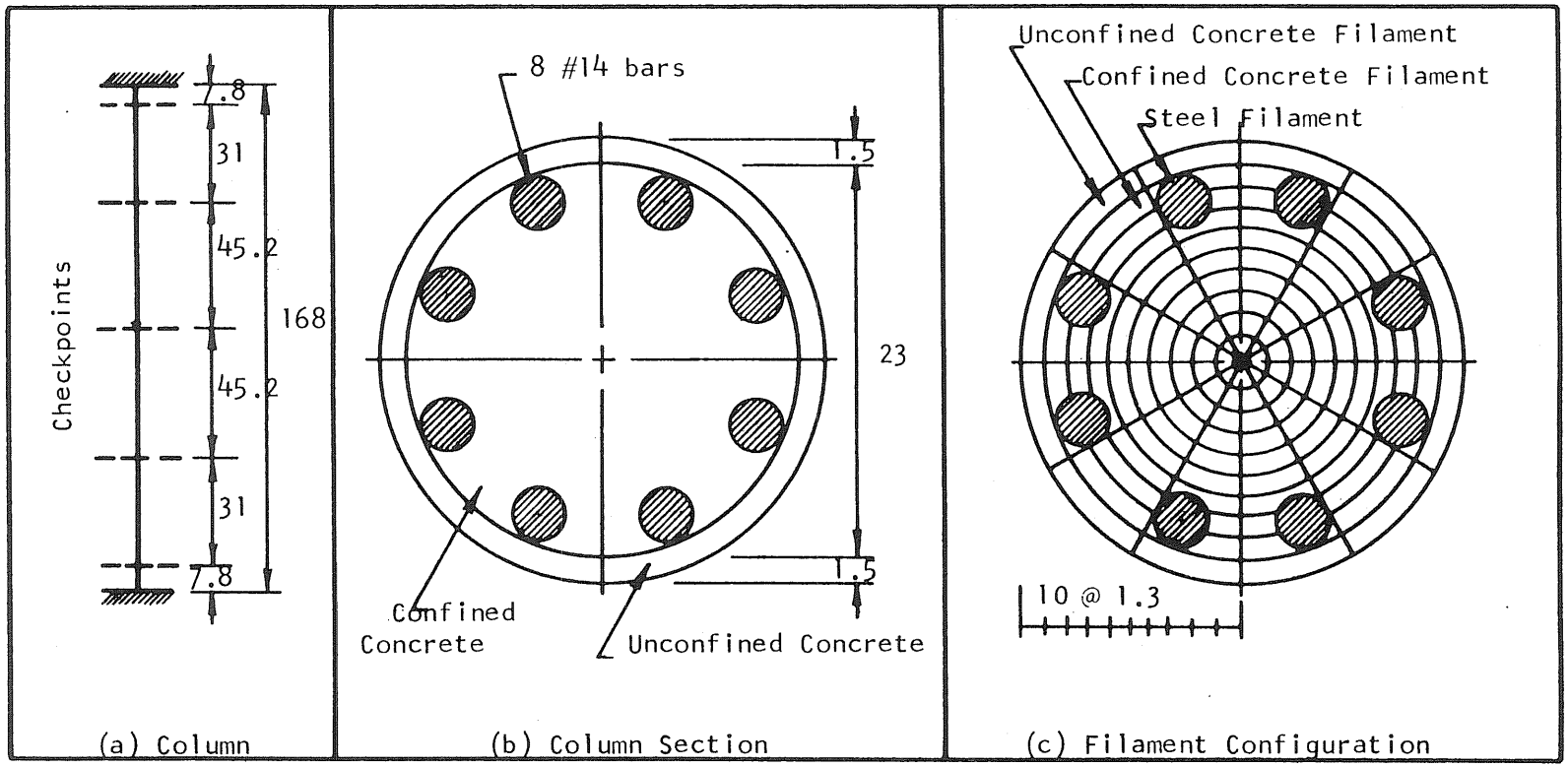

Fig. 2.2 Column Model and Filament Configuration (Units Inches)

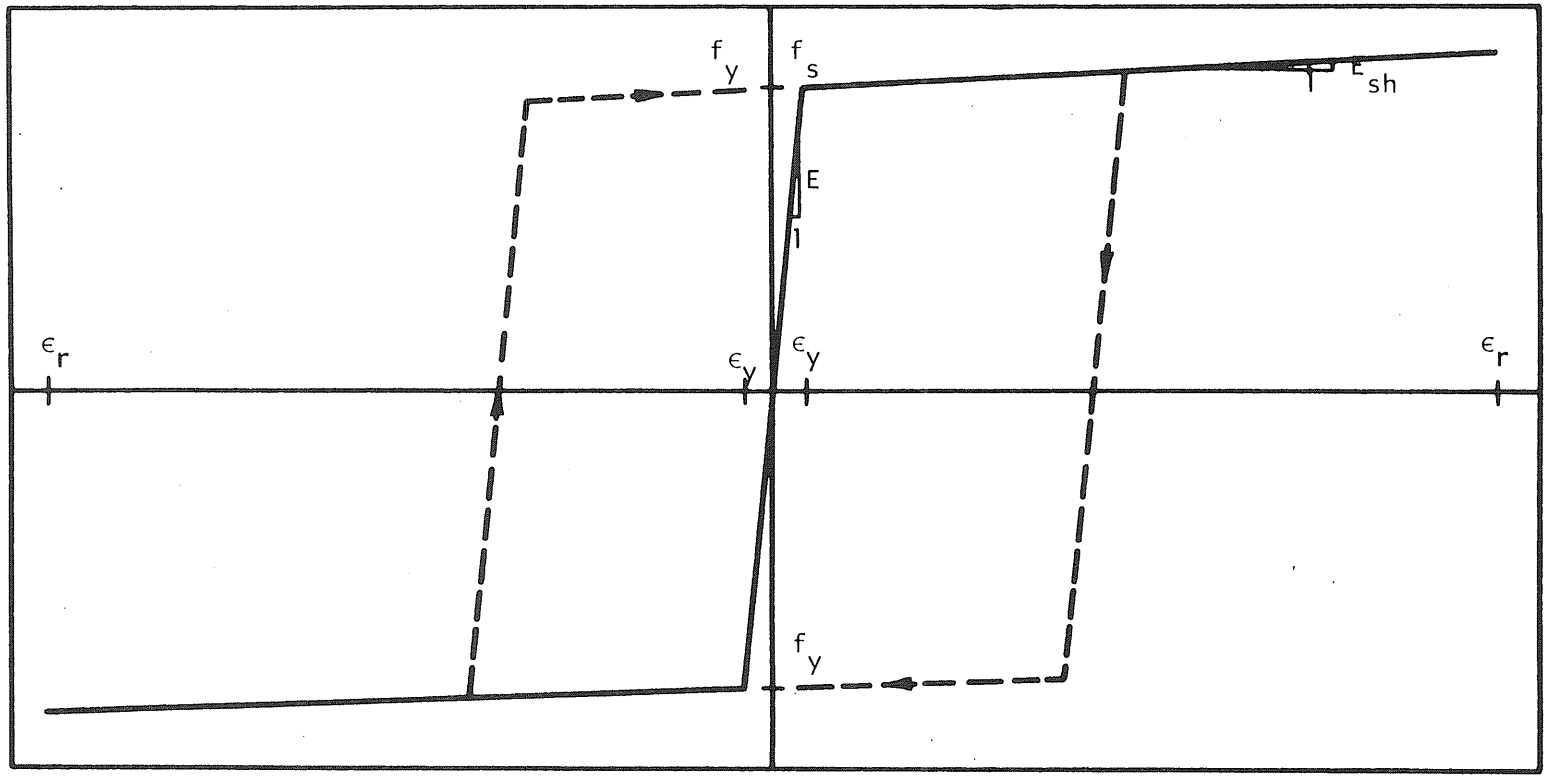

Fig. 3.1 Stress-Strain Characteristics of Reinforcing Steel

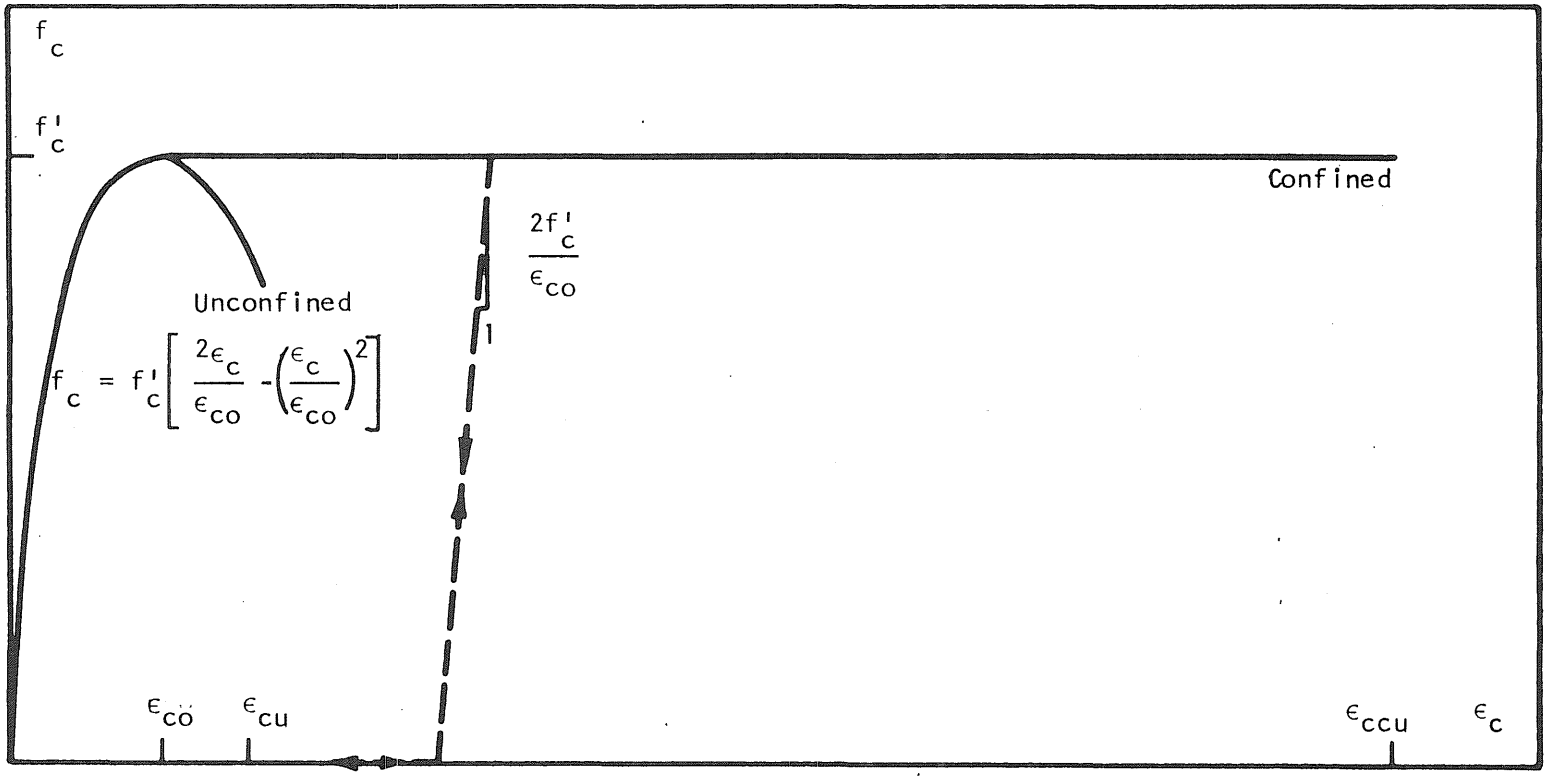

Fig. 3.2 Stress-Strain Characteristics of Confined and Unconfined Concrete

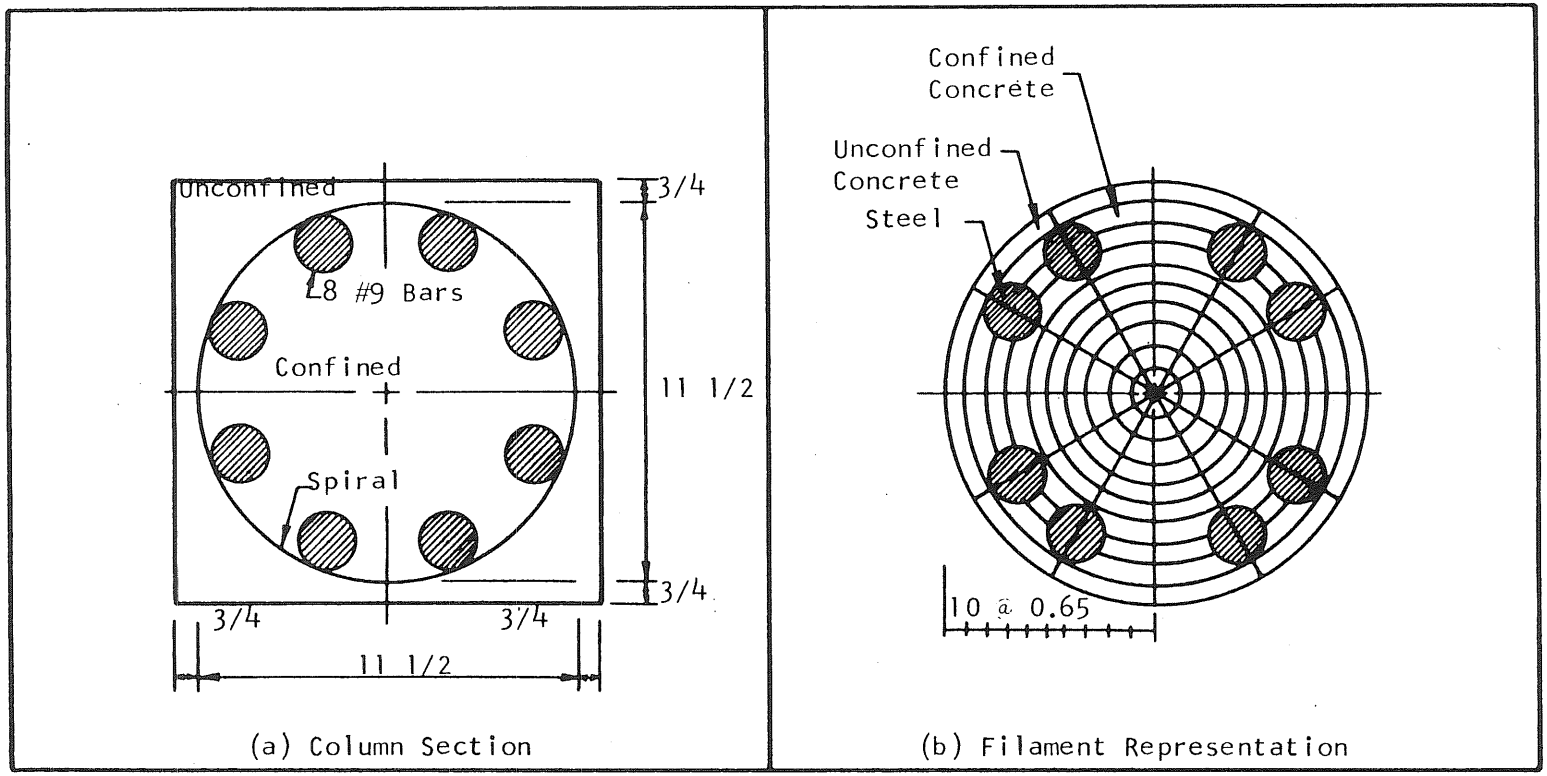

Fig. 3.3 Test Column (BK5) Section and Filament Representation (Units Inches)

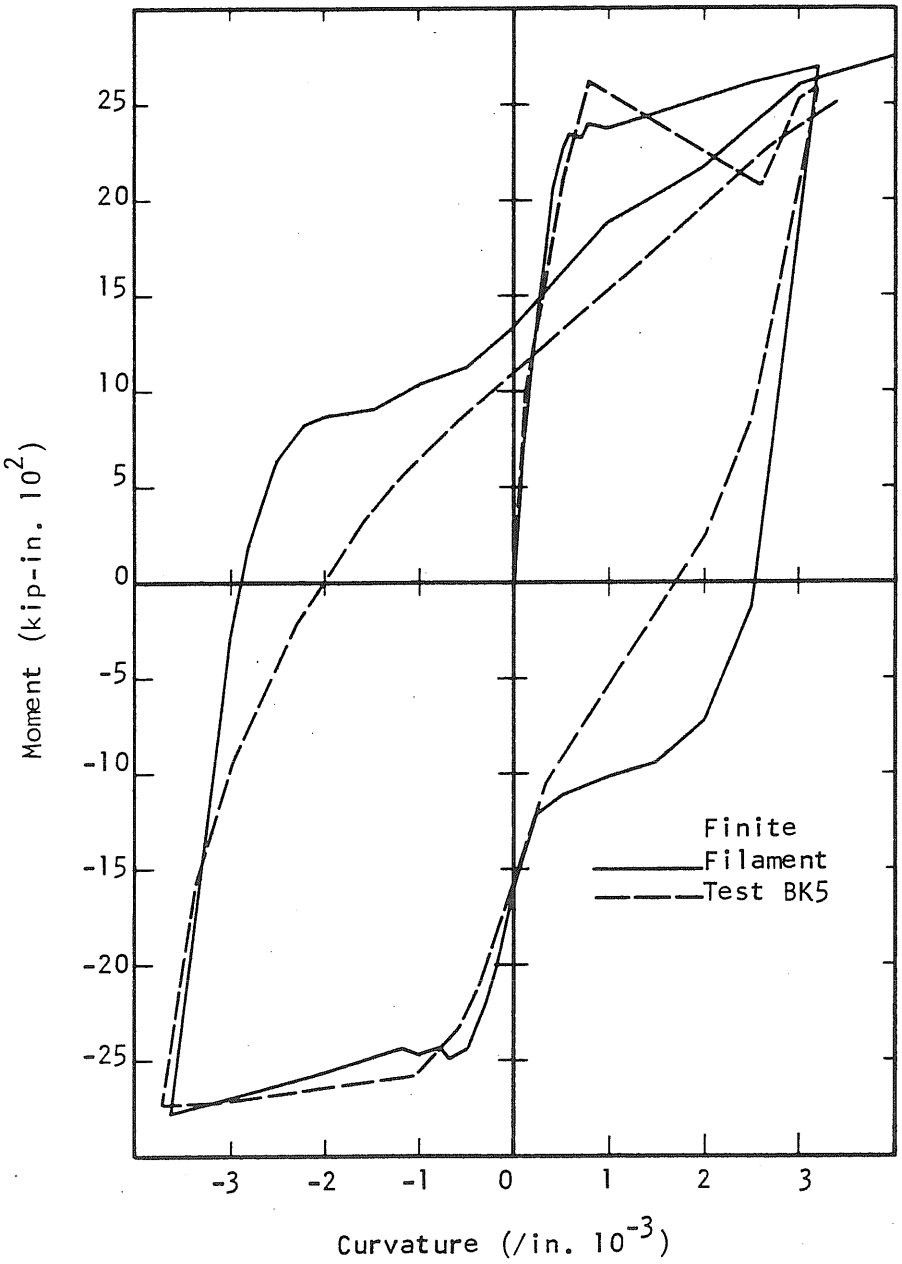

Fig. 3.4 Comparison of Analytical and Test Responses

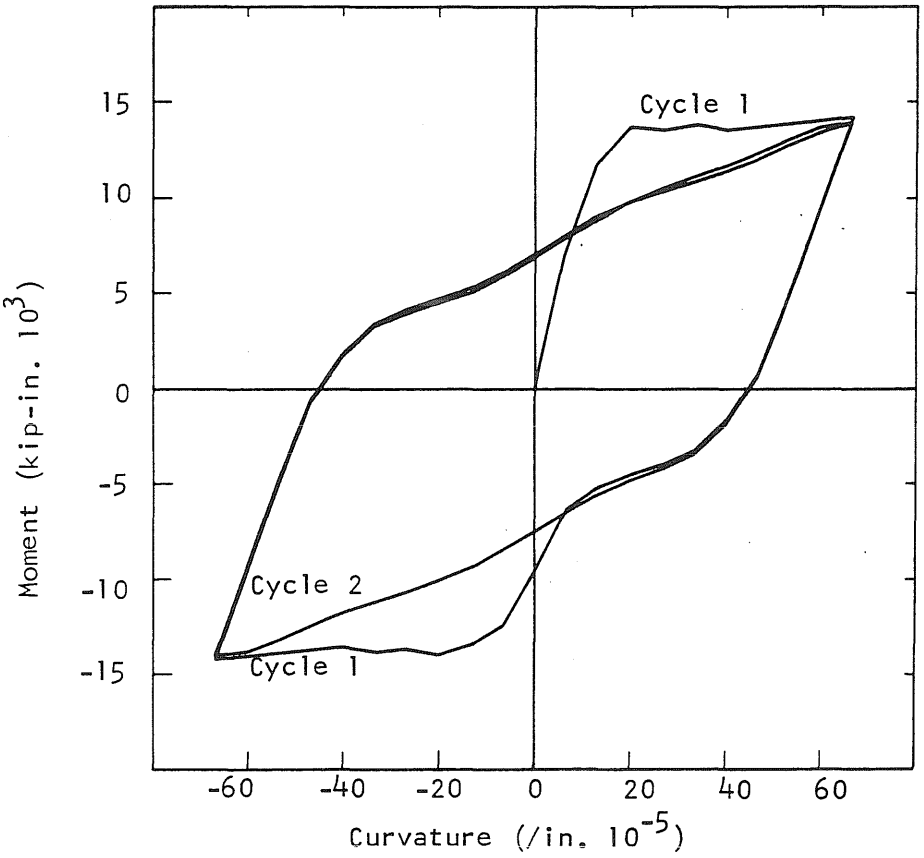

Fig. 3.5 1D Moment-Curvature Response of the Column Section

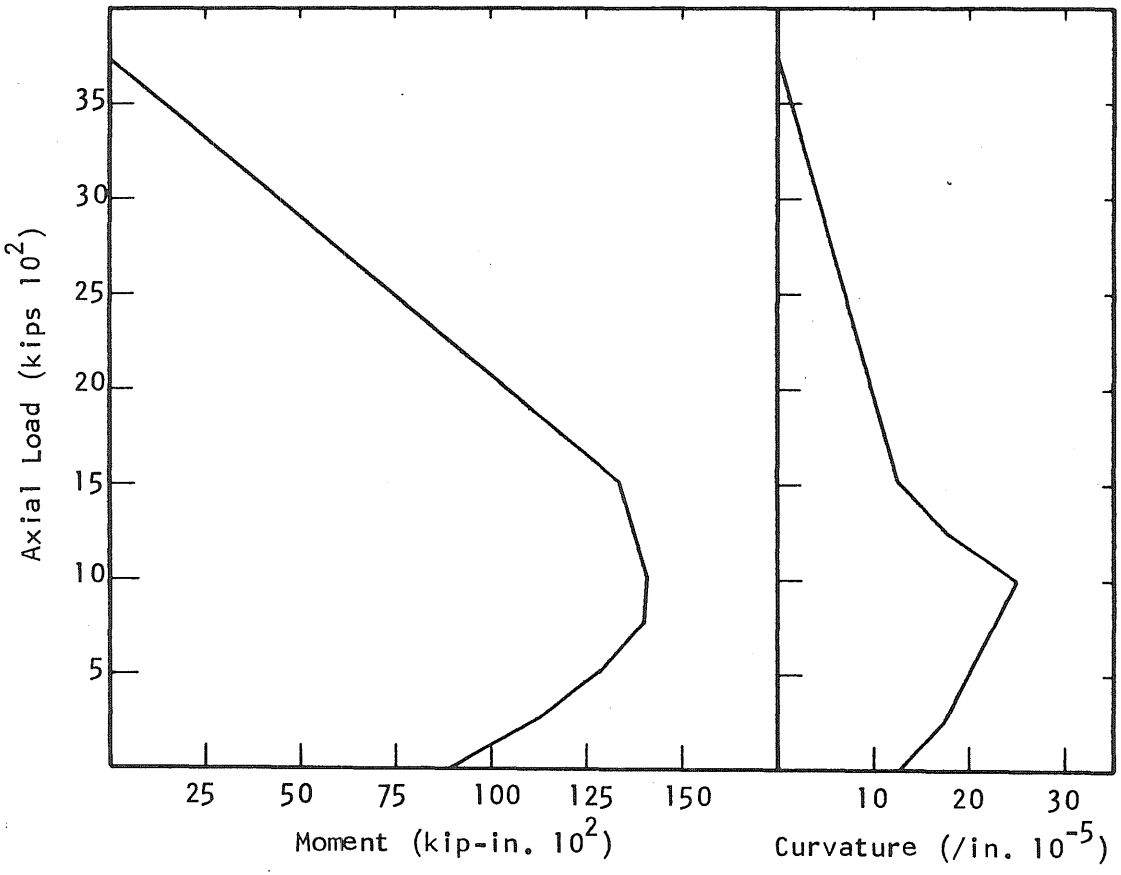

Fig. 3.6 Axial Load-Bending Moment-Yield Curvature Interaction Diagram of the Column Section

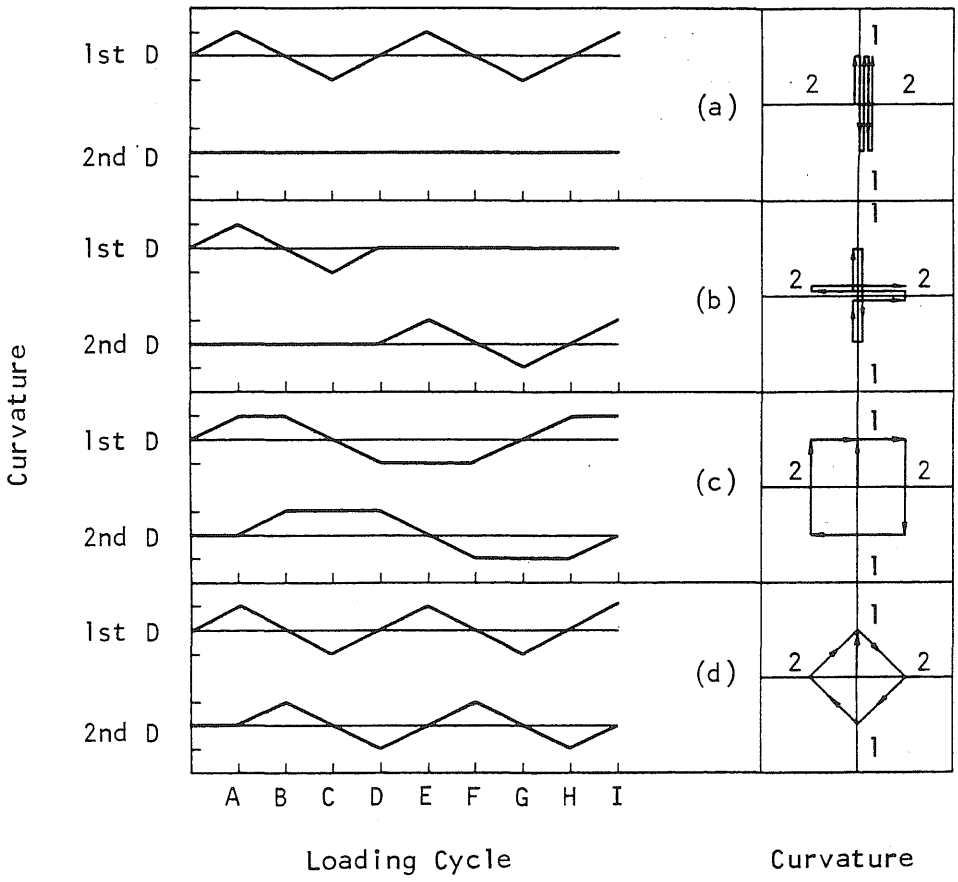

Fig. 3.7 Curvature Histories for 2D Response Study

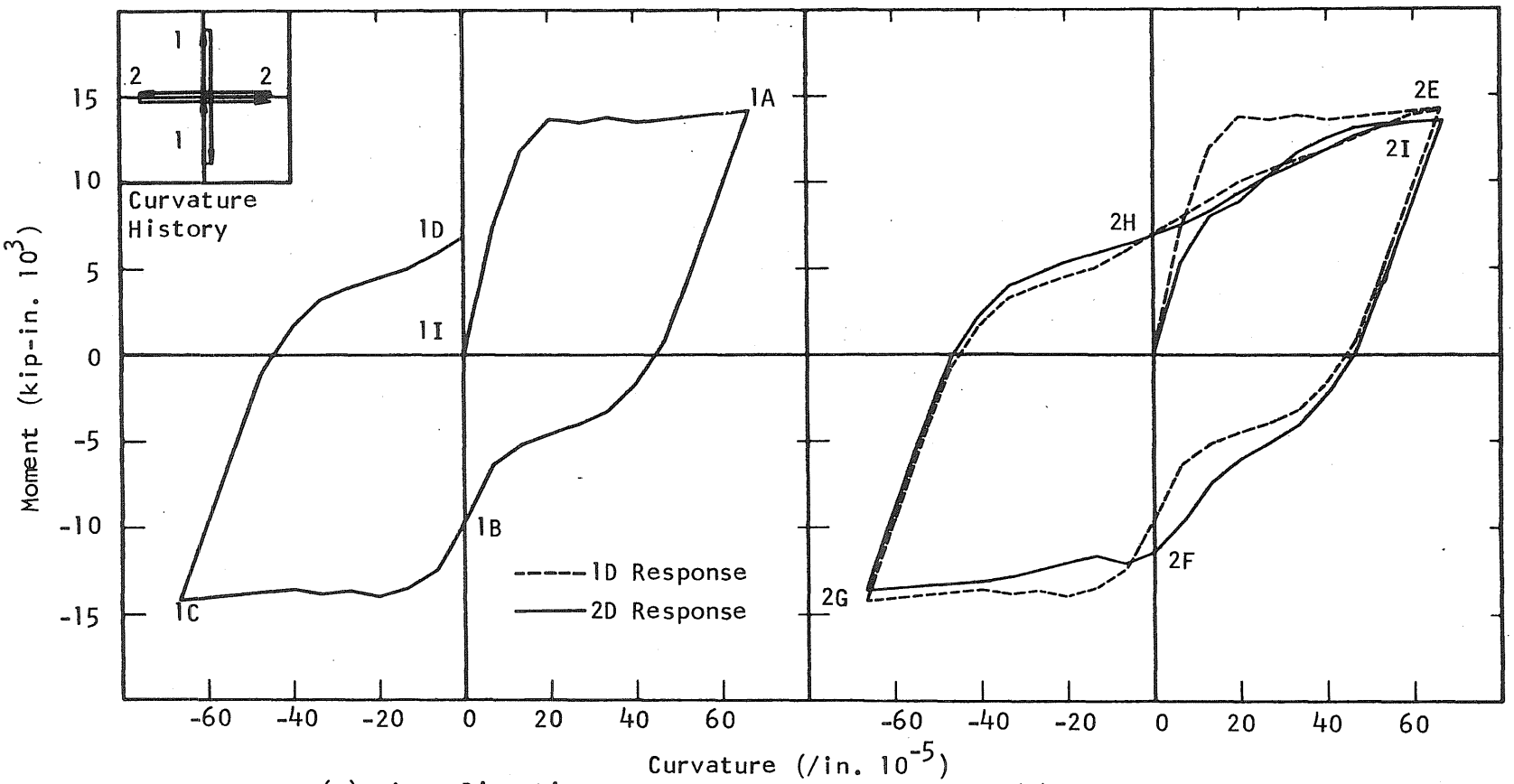

(a) First Direction (b) Second Direction

Fig. 3.8 1D and 2D Moment-Curvature Responses

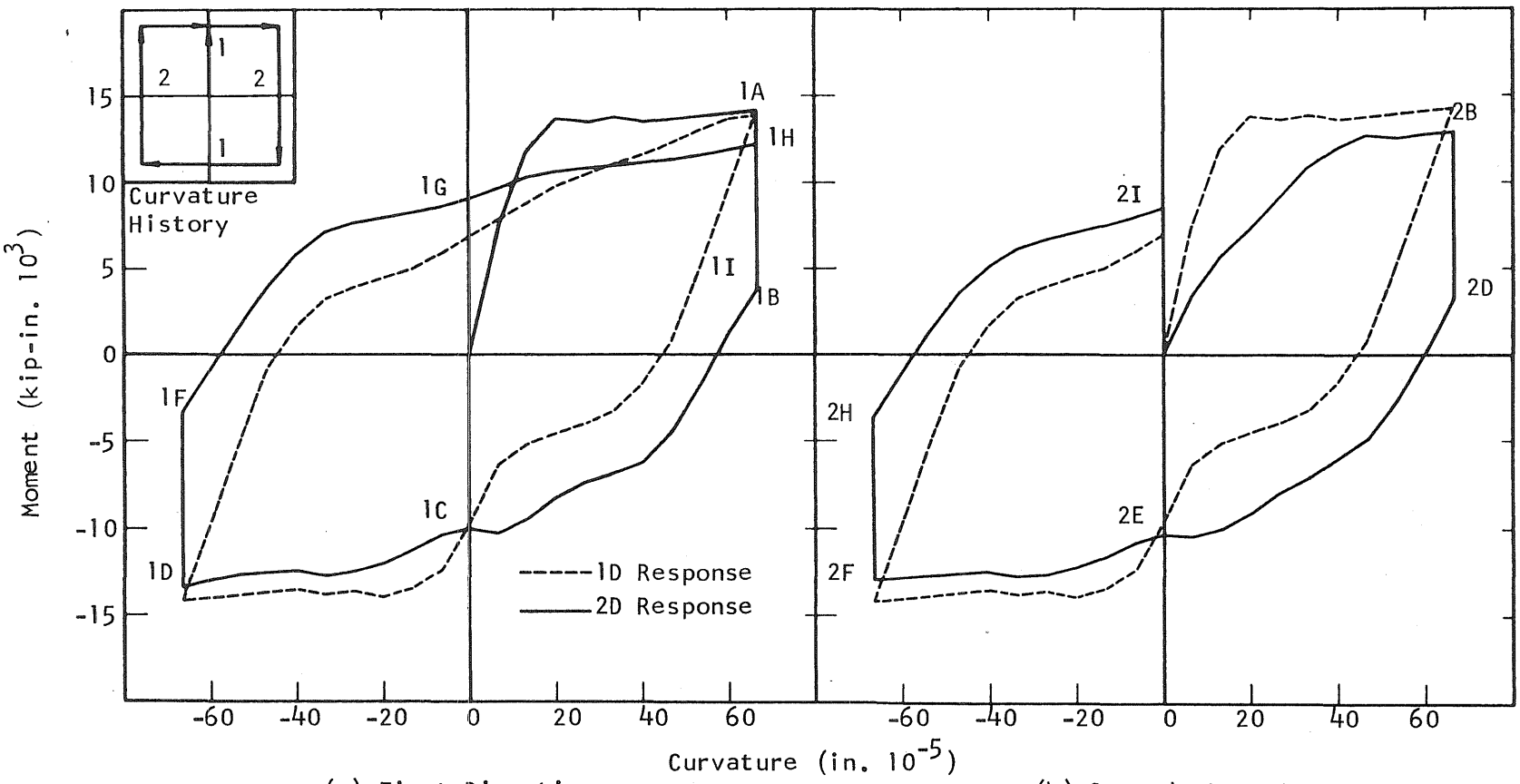

(a) First Direction (b) Second Direction

Fig. 3.9 1D and 2D Moment-Curvature Responses

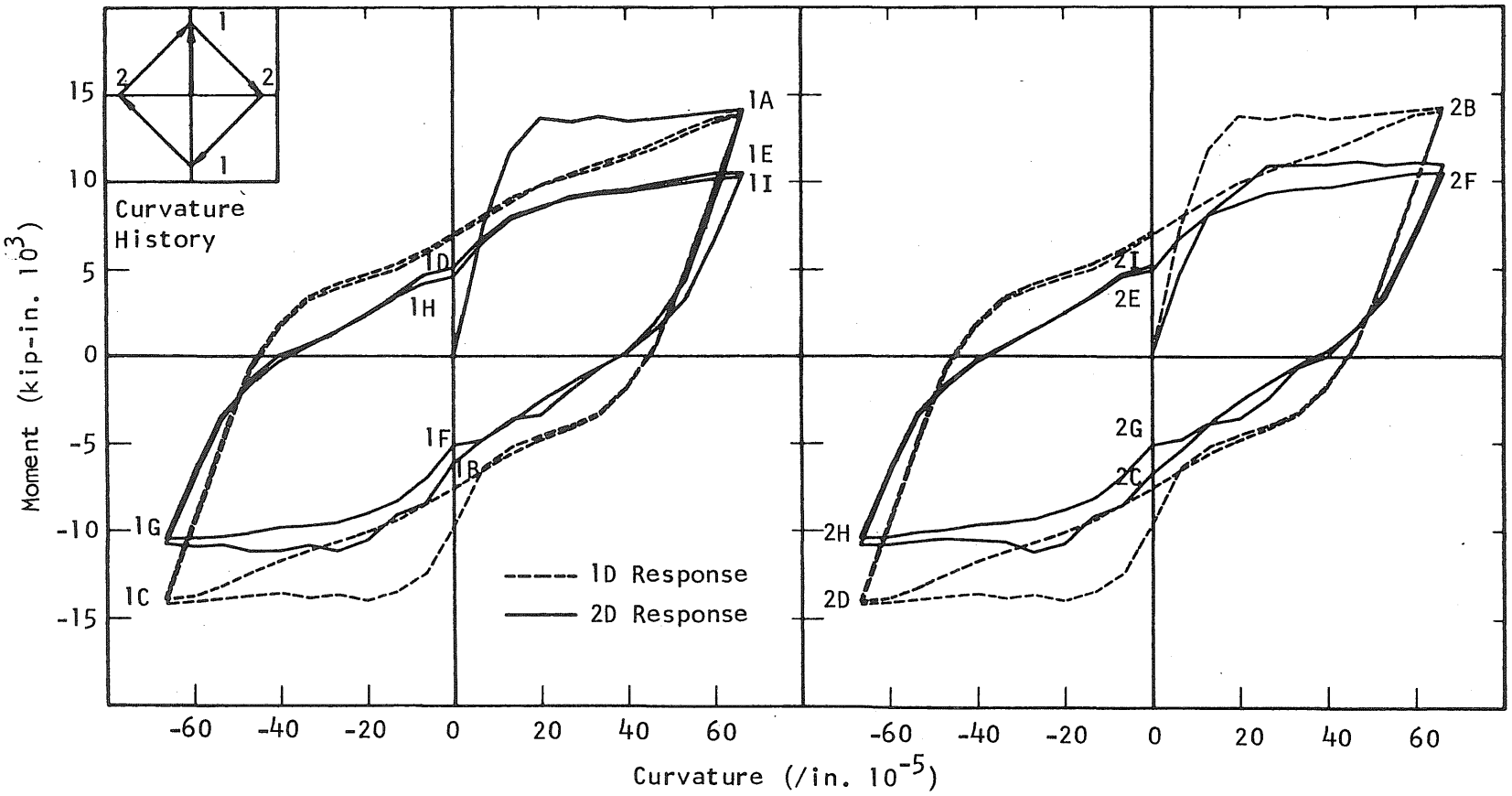

(a) First Direction (b) Second Direction

Fig. 3.10 1D and 2D Moment-Curvature Responses

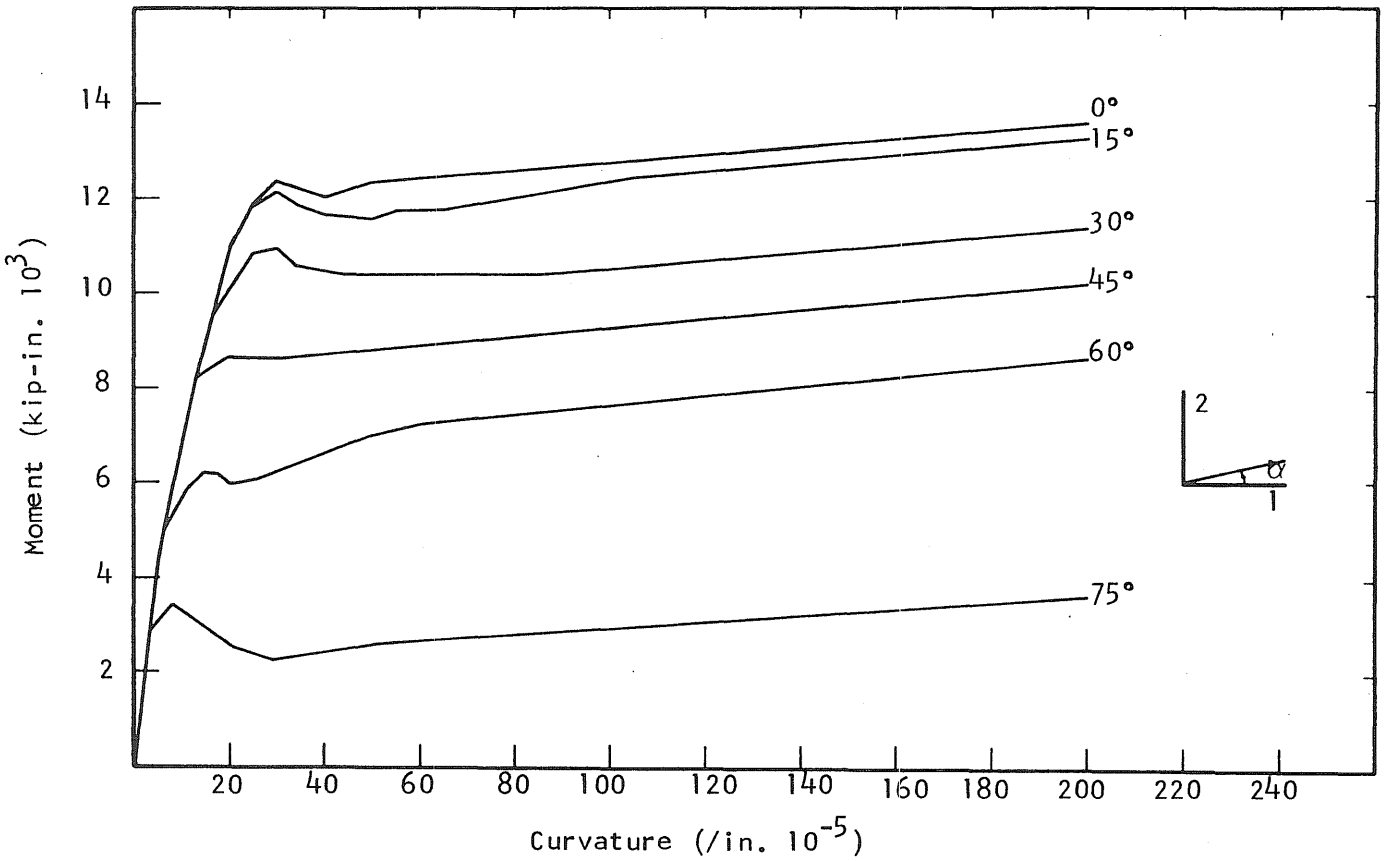

Fig. 3.11 Primary Curves for First Direction

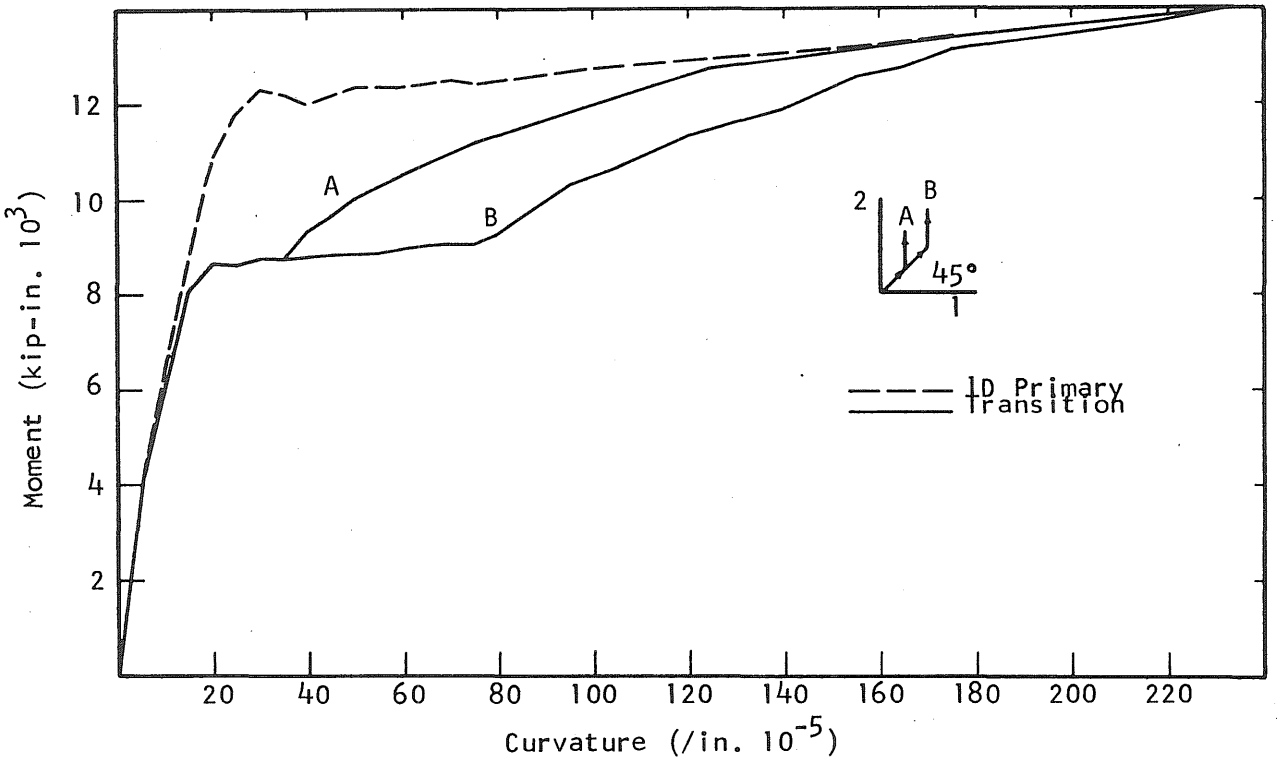

Fig. 3.12 Second Direction Transition from 45° Primary Curve to 0° Primary Curve

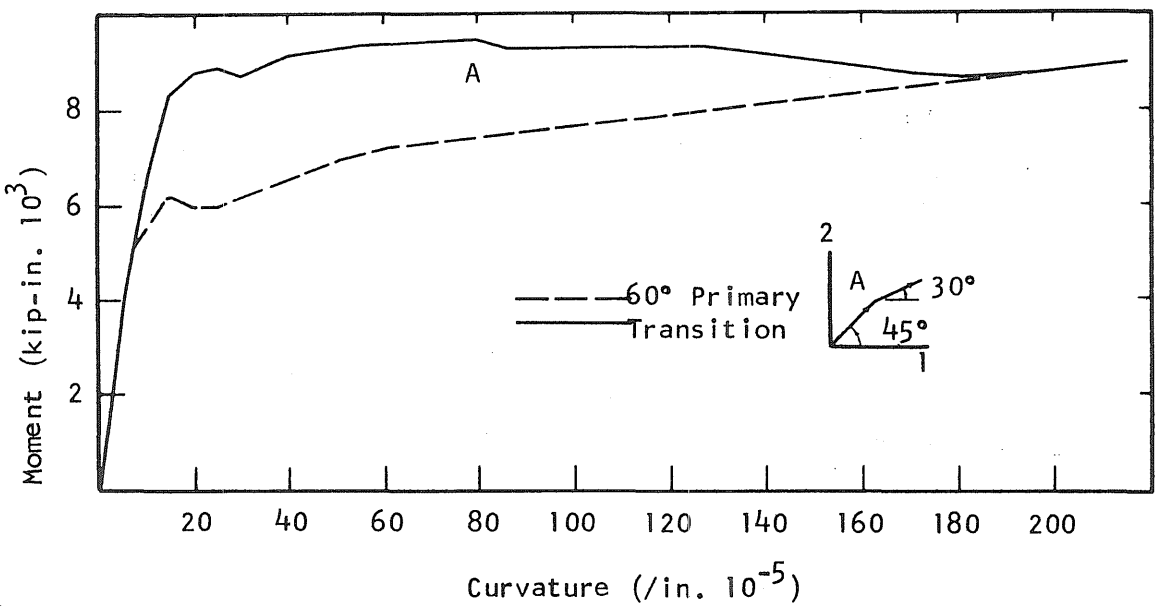

Fig. 3.13 Second Direction Transition from 45° Primary Curve to 60° Primary Curve

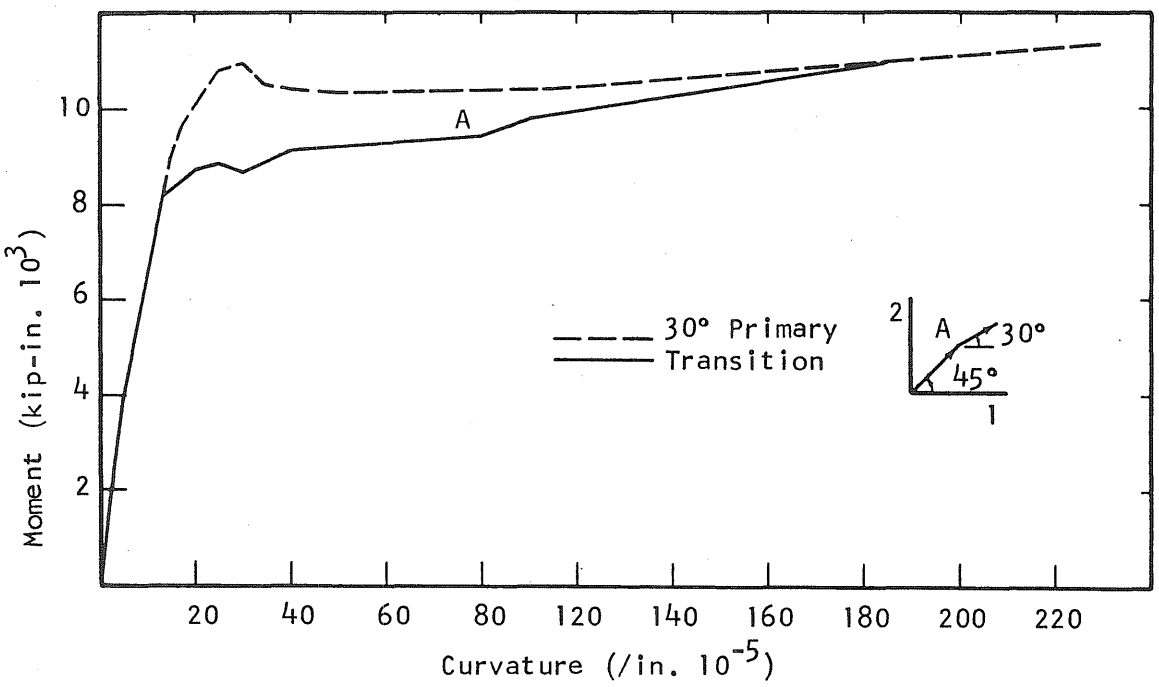

Fig. 3.14 First Direction Transition from 45° Primary Curve to 30° Primary Curve

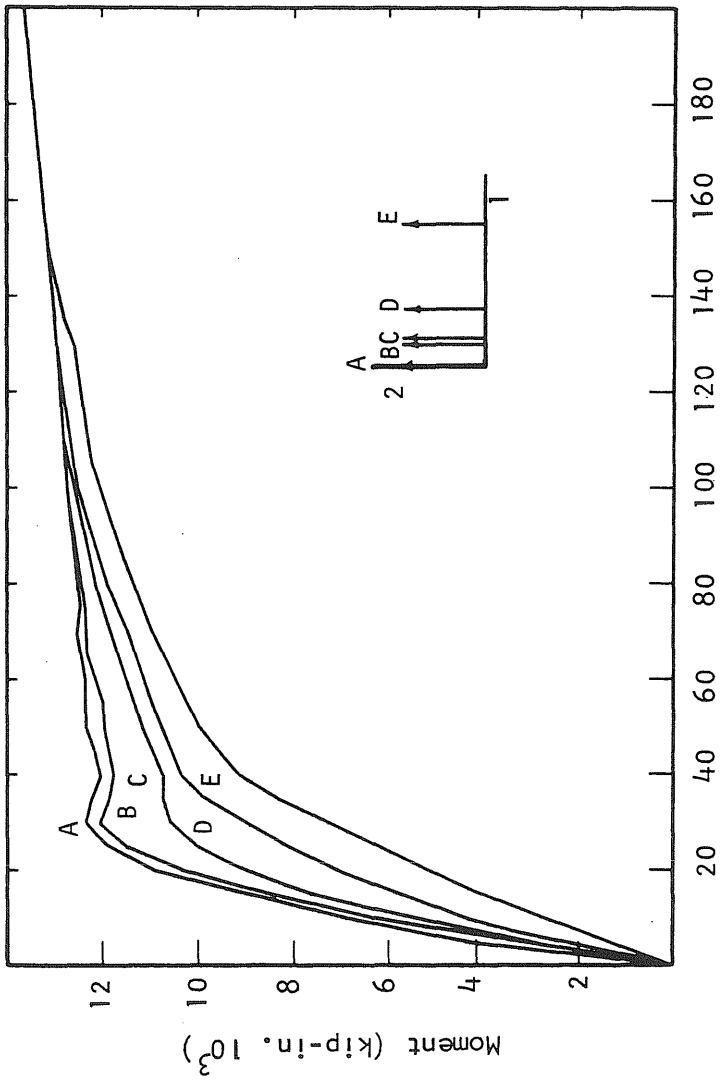

Fig. 3.15 Transition To 0° Primary Curve

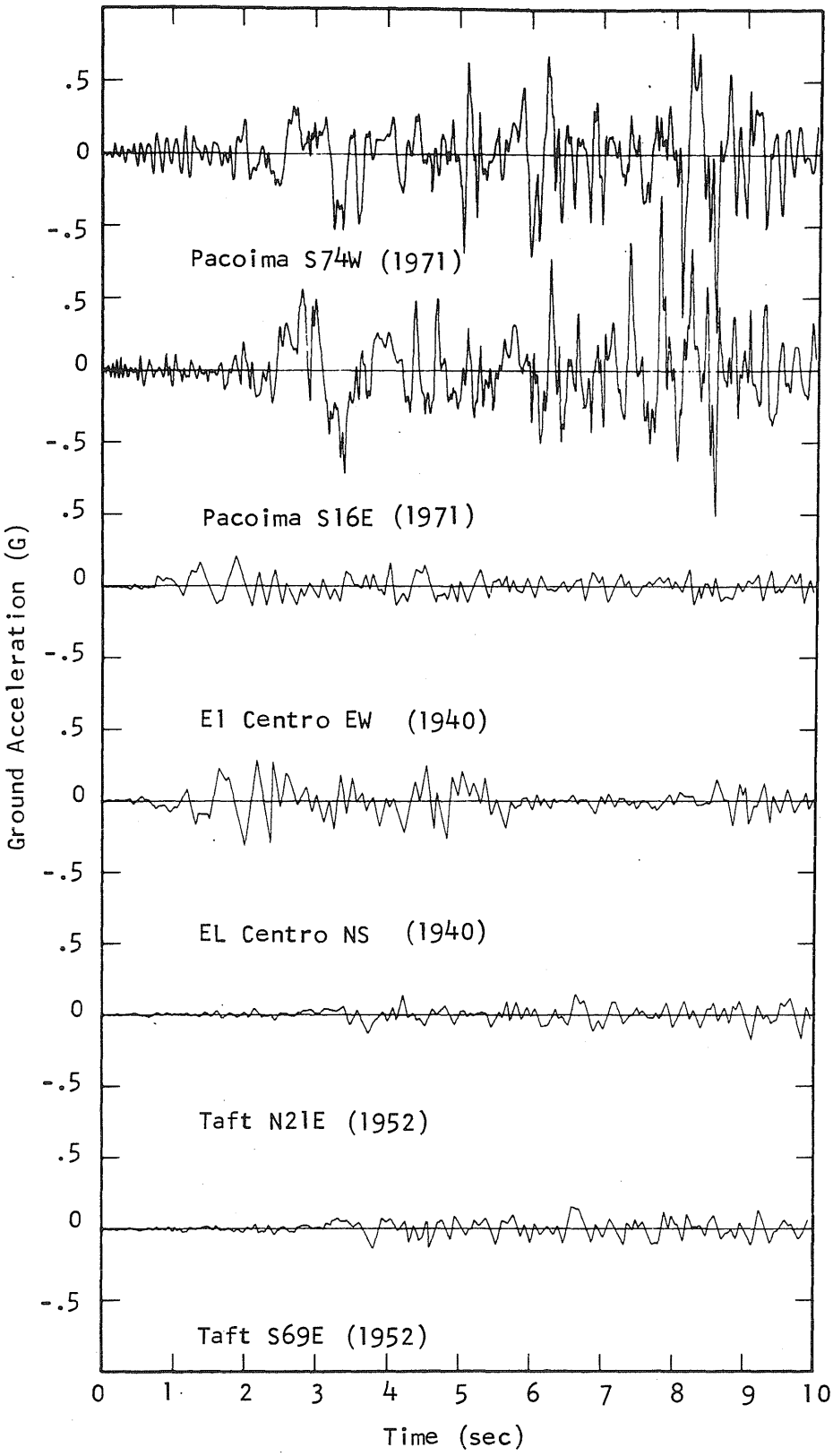

Fig. 4.1 Ground Acceleration-Time Histories, 1971 Pacoima, 1940 El Centro, and 1952 Taft Records (First ten sec.)

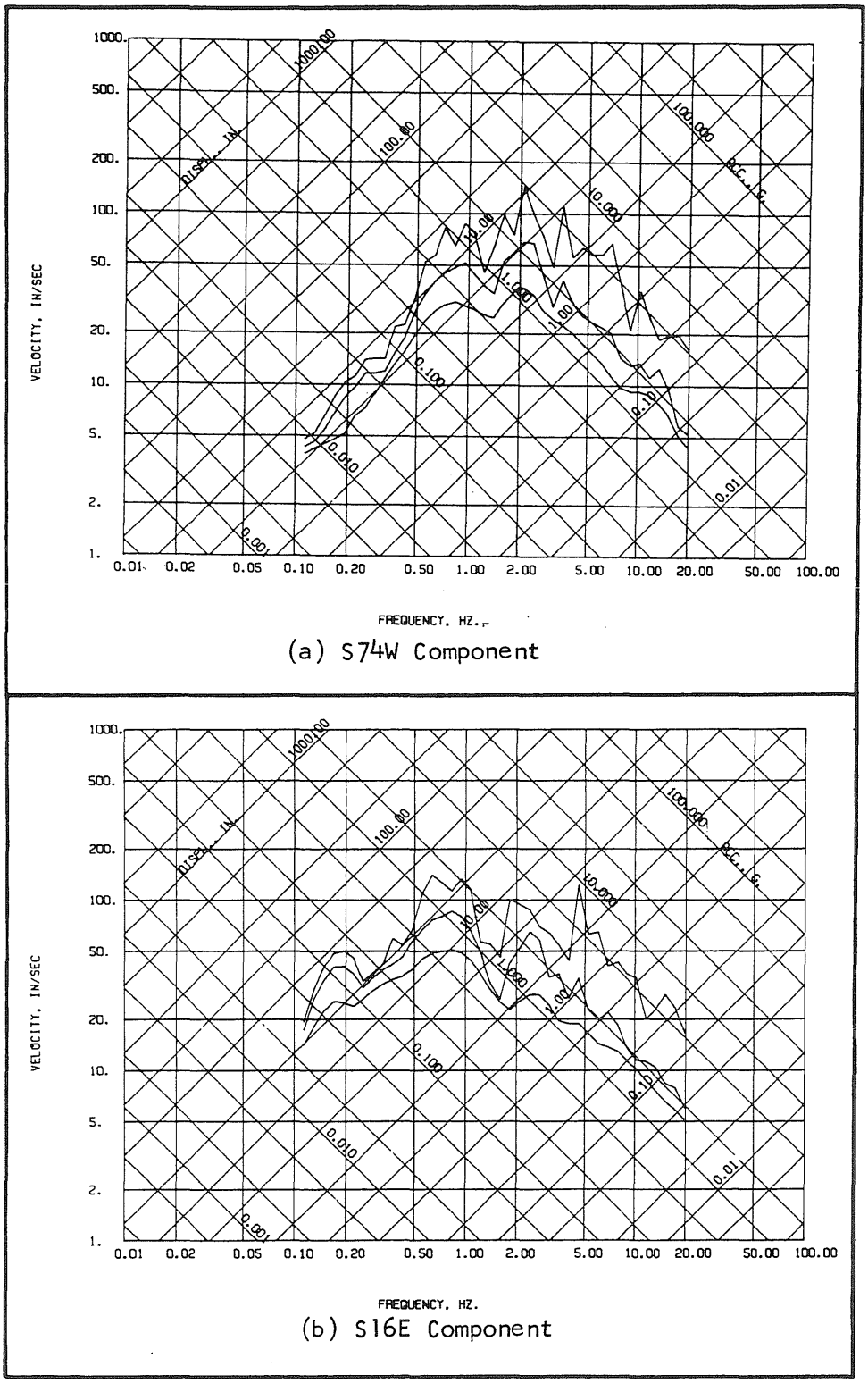

(a) S74W Component

(b) S16E Component

Fig. 4.2 10 Second Elastic Response Spectra, 1971 Pacoima Record, 0%, 5%, and 20% Damping

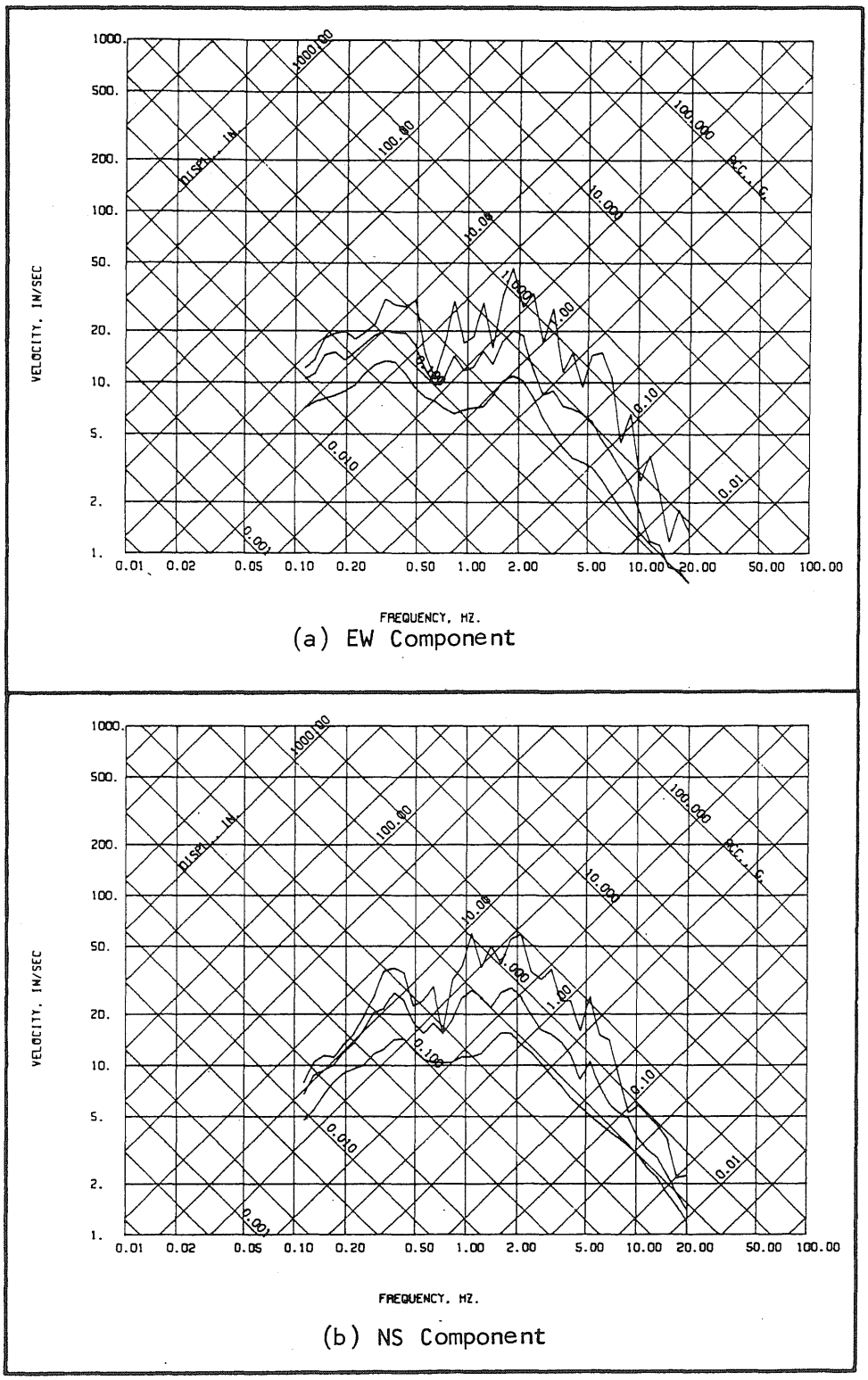

Fig. 4.3 10 Second Elastic Response Spectra, 1940 El Centro Record, 0%, 5%, and 20% Damping

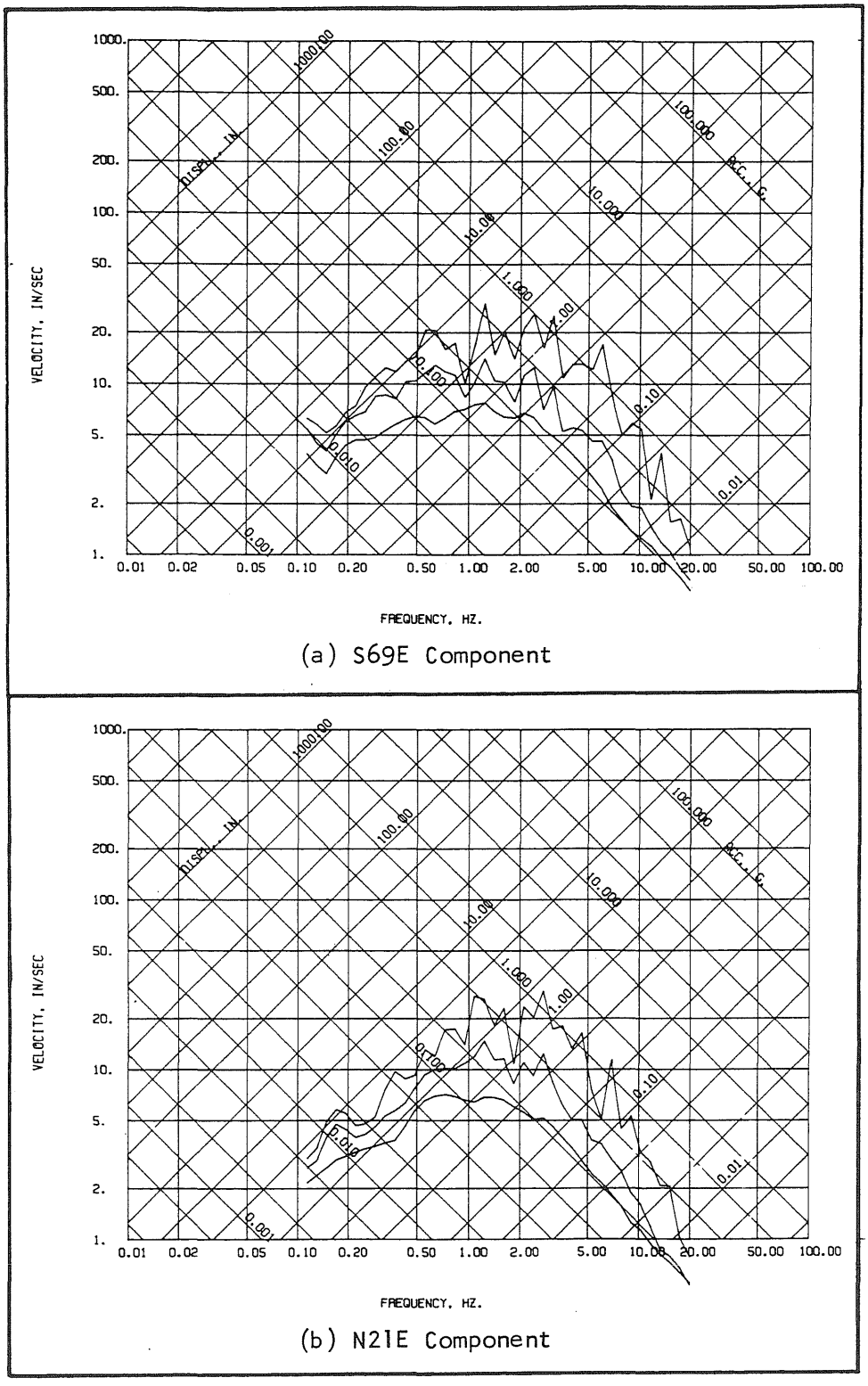

(a) S69E Component

(b) N21E Component

Fig. 4.4 10 Second Elastic Response Spectra, 1952 Taft Record, 0%, 5%, and 20% Damping

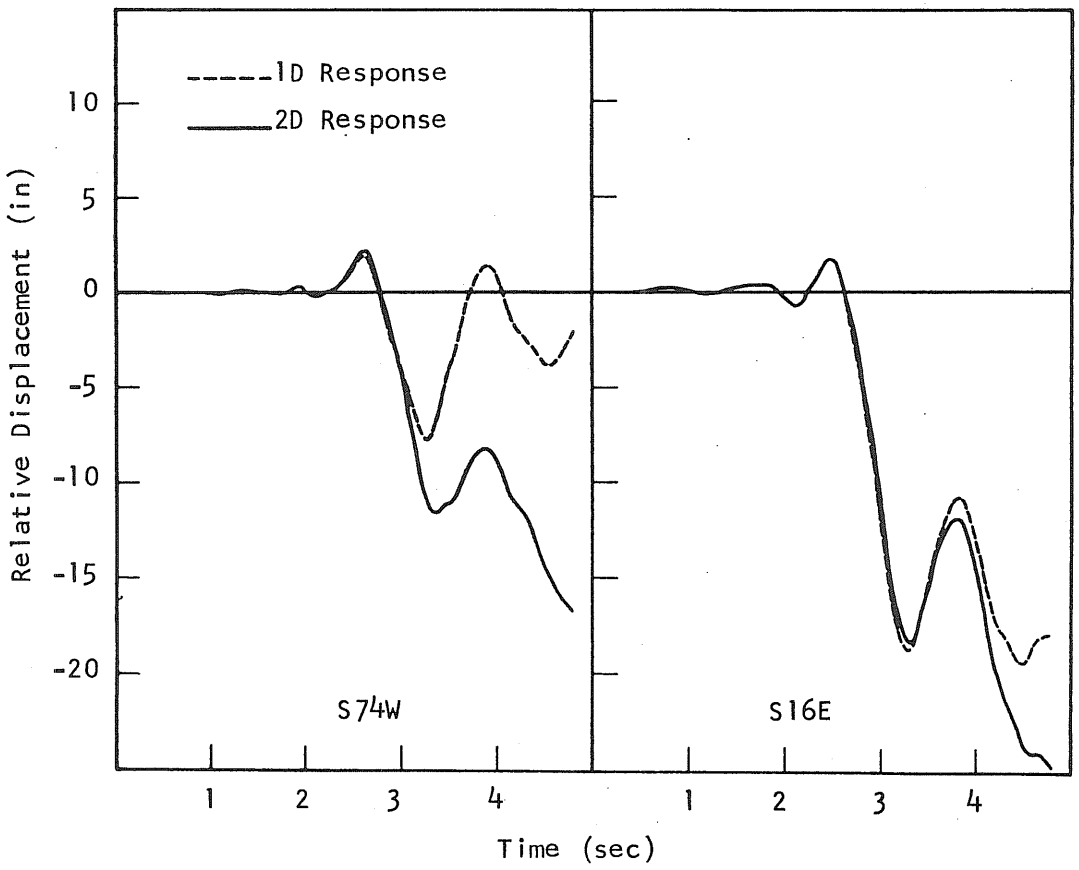

Fig. 4.5 Relative Displacement-Time Histories, Pacoima Record, Initial Period 0.7 Seconds

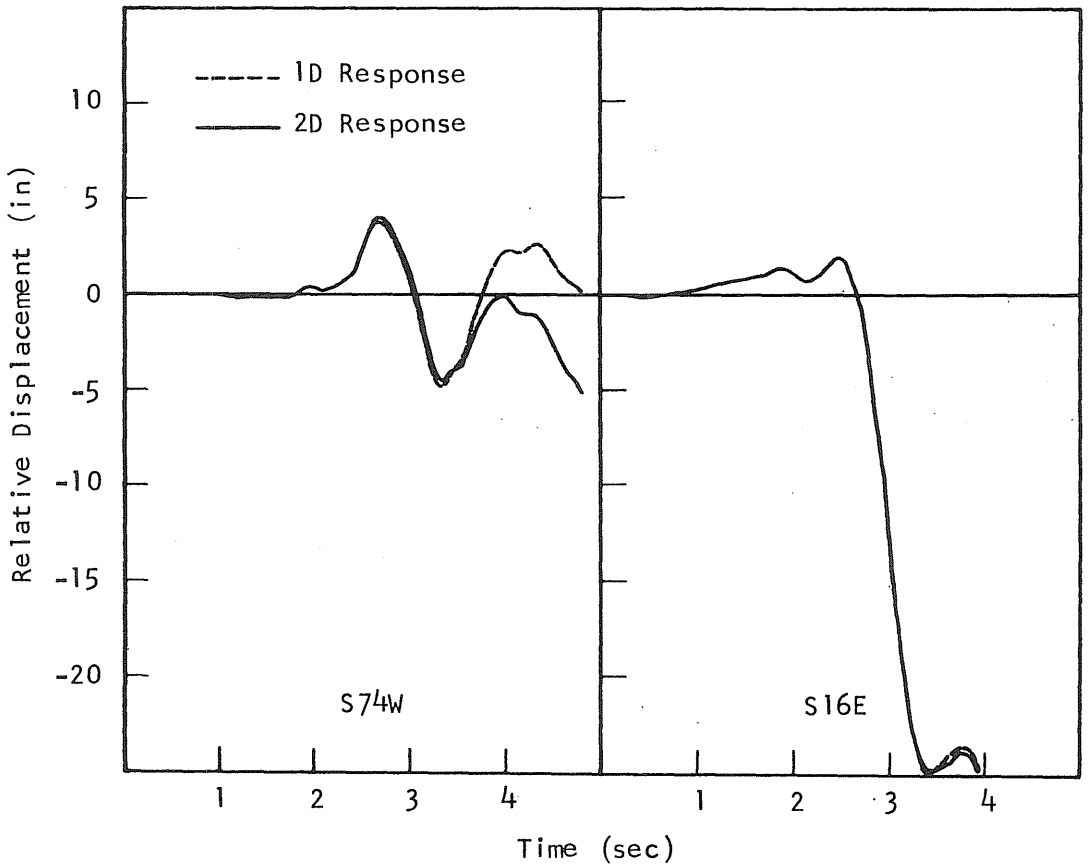

Fig. 4.6 Relative Displacement-Time Histories, Pacoima Record, Initial Period 1.5 Seconds

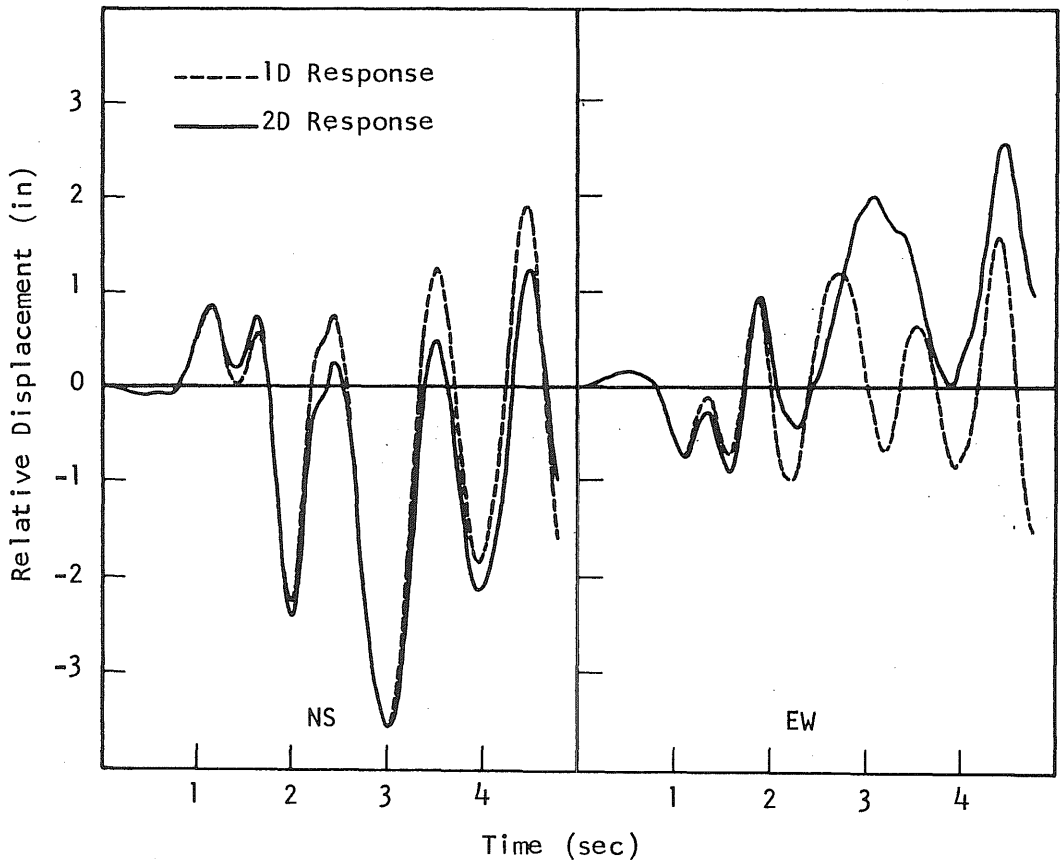

Fig. 4.7 Relative Displacement-Time Histories, El Centro Record, Initial Period 0.7 Seconds

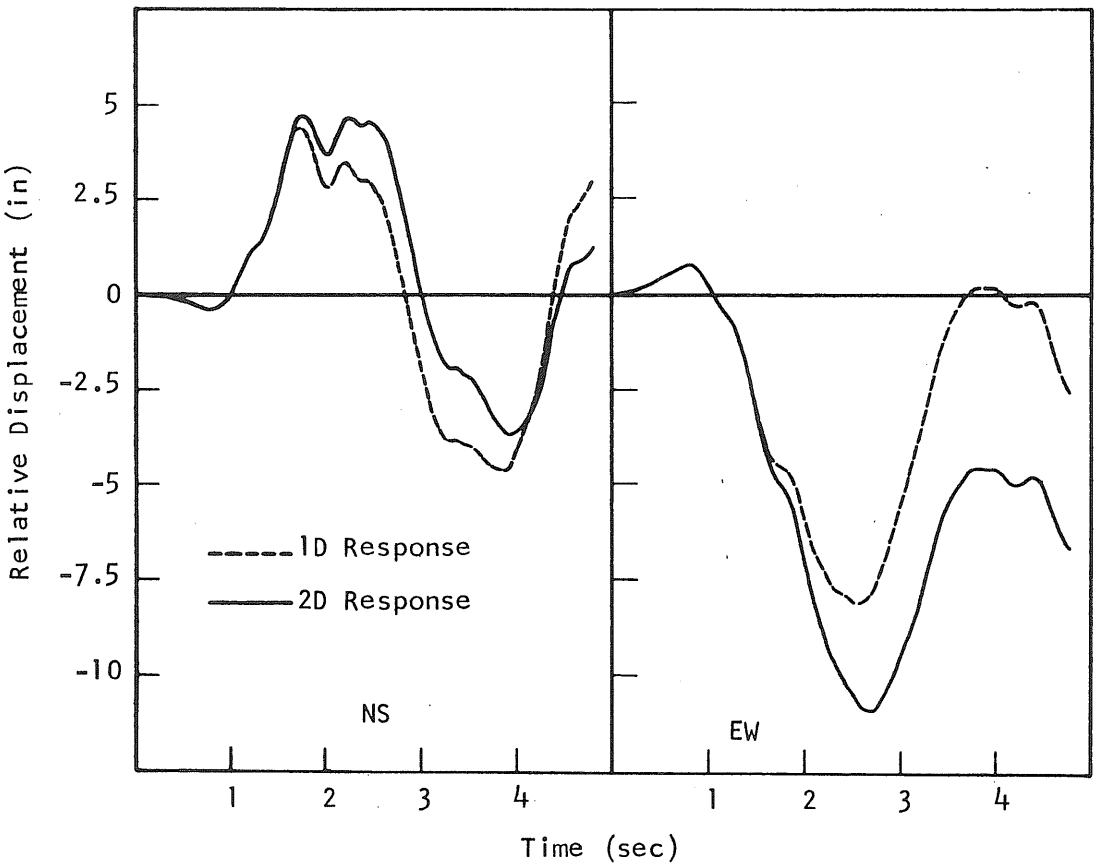

Fig. 4.8 Relative Displacement-Time Histories, El Centro Record, Initial Period 1.5 Seconds

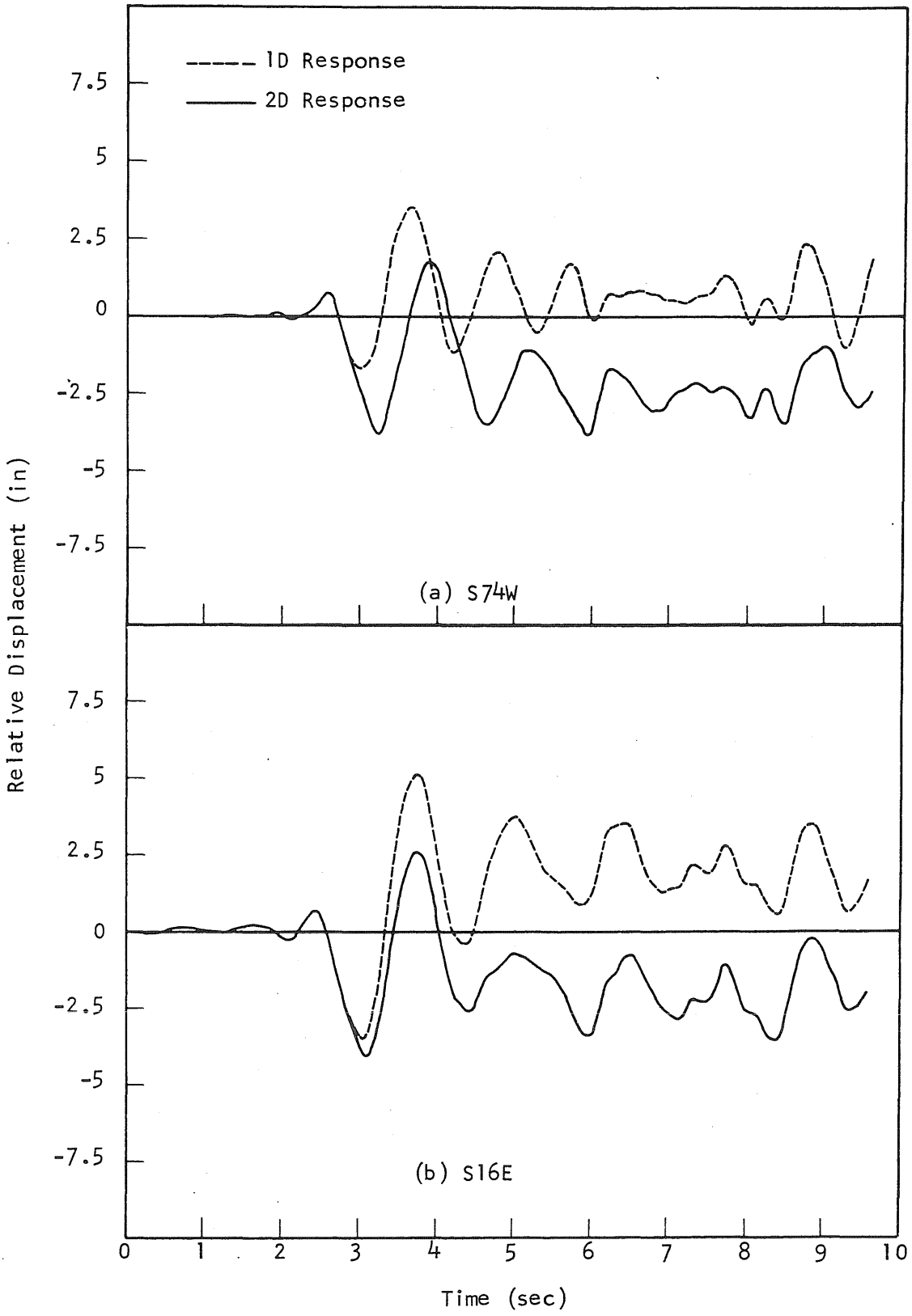

Fig. 4.9 Relative Displacement-Time Histories, Pacoima Record, Relative Intensity 4, Initial Period 0.7 Seconds

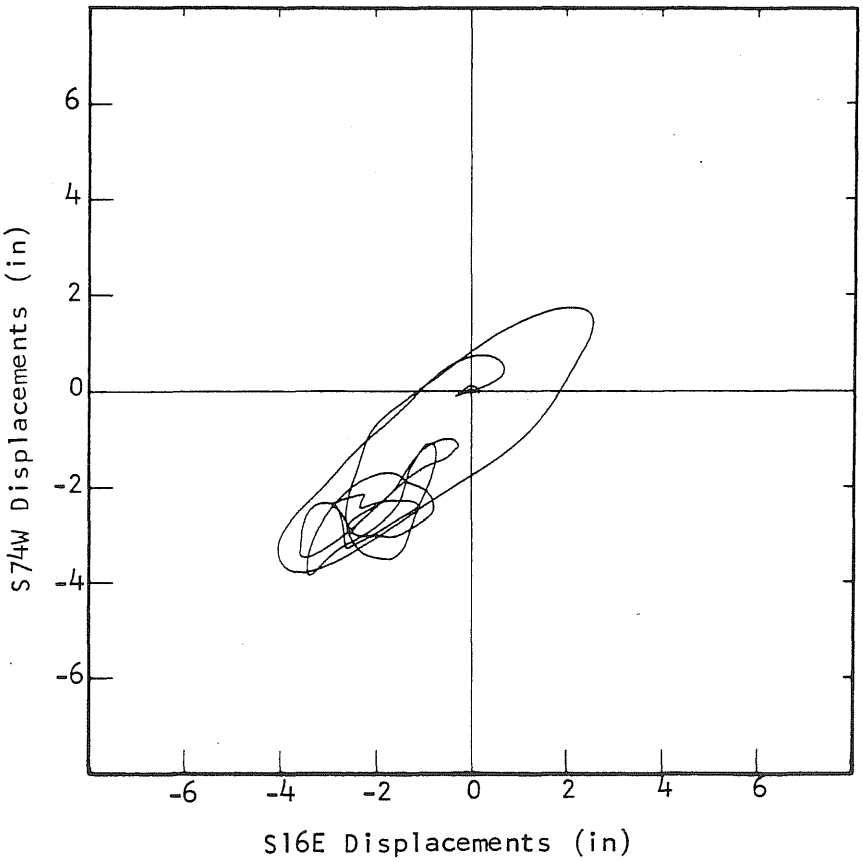

Fig. 4.10 2D Column Top Displacements, Pacoima Record, Relative Intensity 4, Initial Period 0.7 Seconds

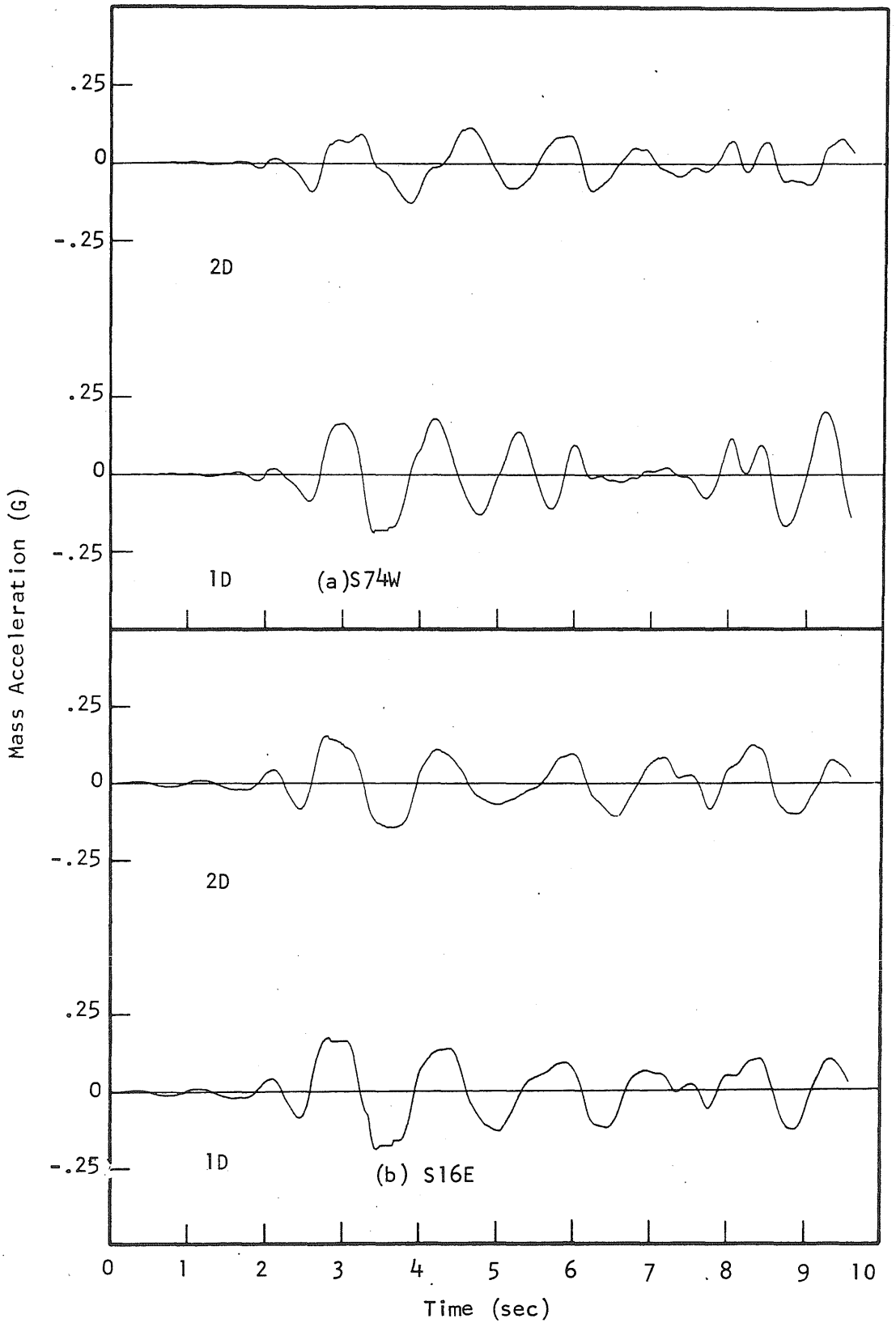

Fig. 4.11 Mass Acceleration-Time Histories, Pacoima Record, Relative Intensity 4, Initial Period 0.7 Seconds

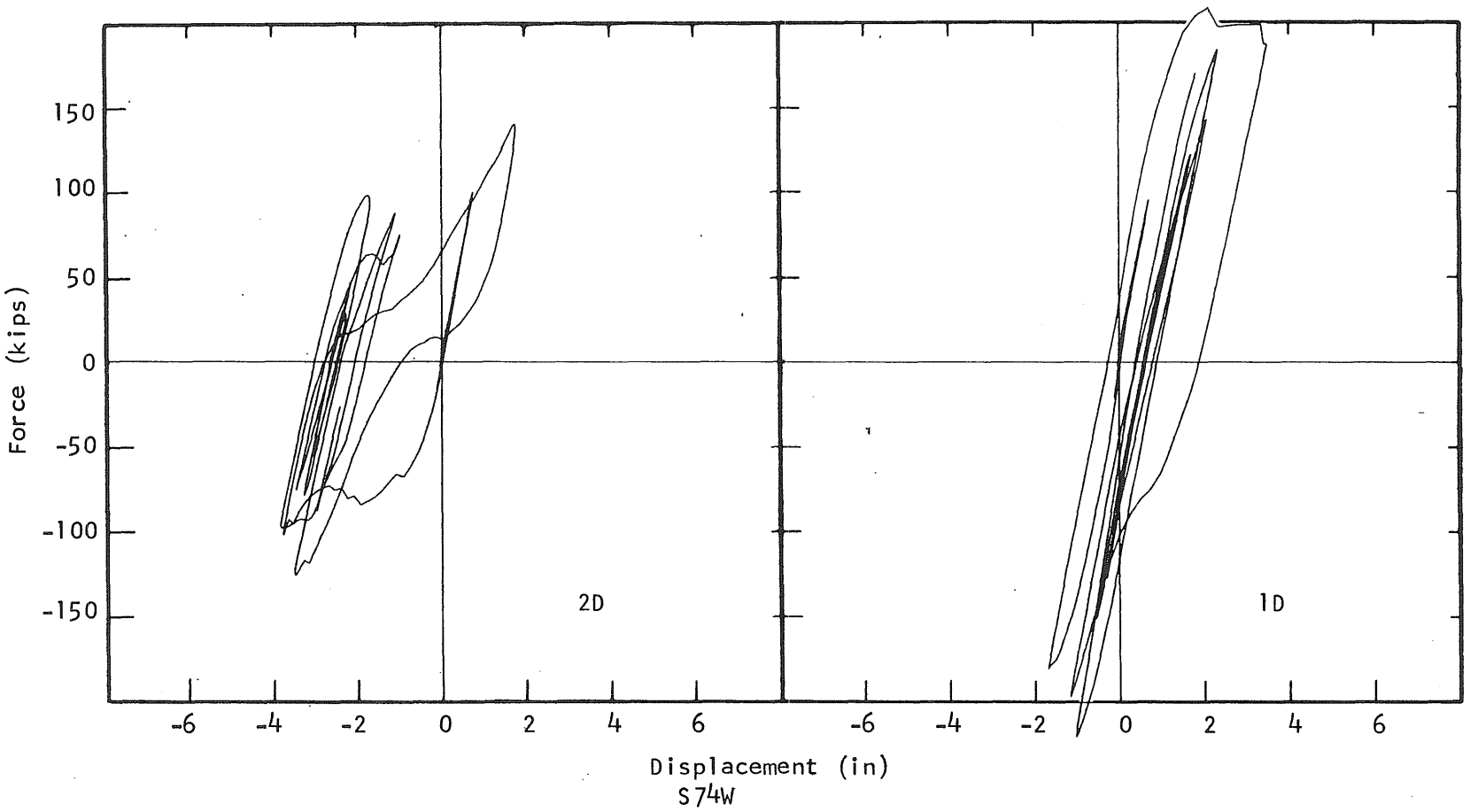

Fig. 4.12 Force-Displacement Responses, Pacoima Record, Relative Intensity 4, Initial Period 0.7 Seconds

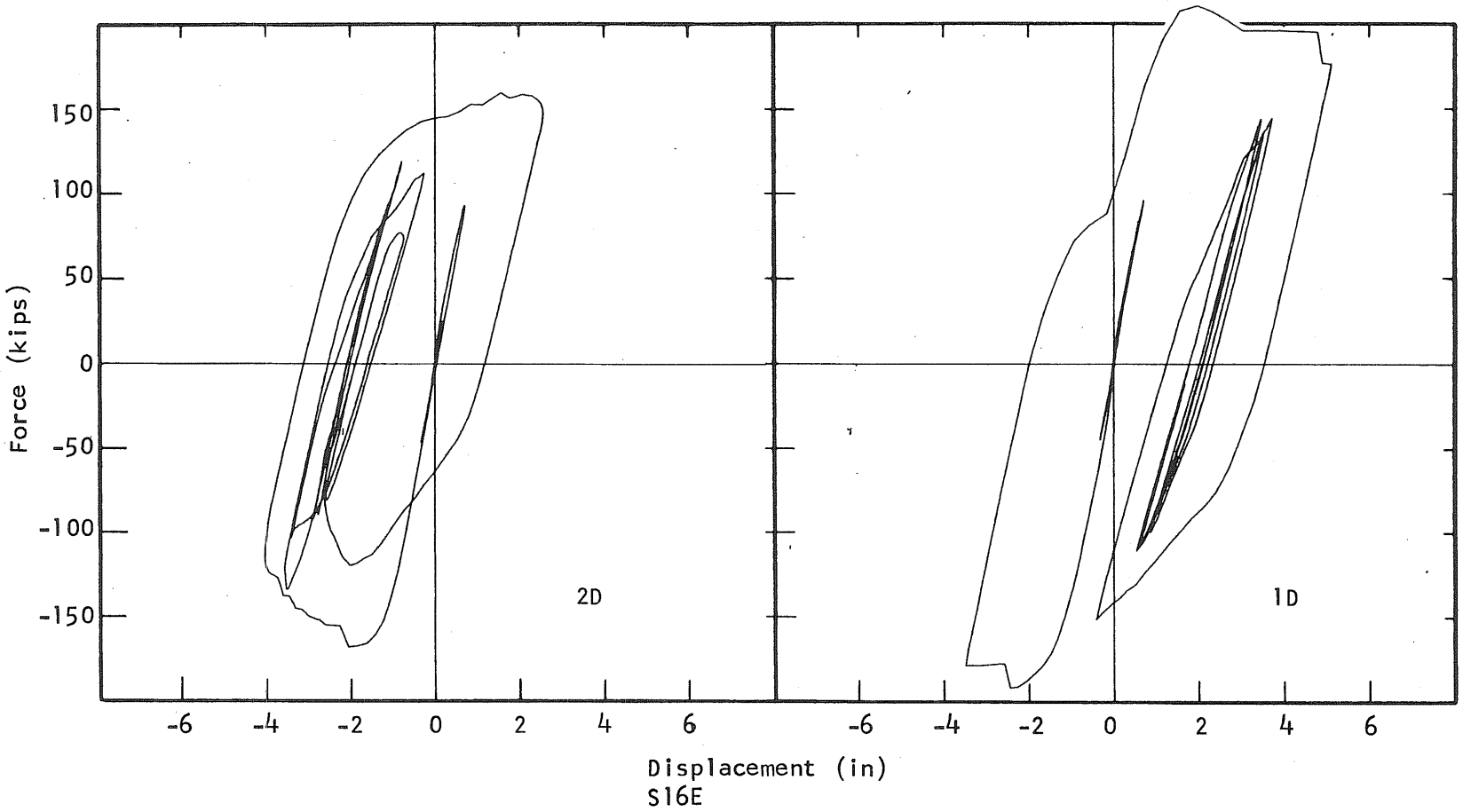

Fig. 4.13 Force-Displacement Responses, Pacoima Record, Relative Intensity 4, Initial Period 0.7 Seconds

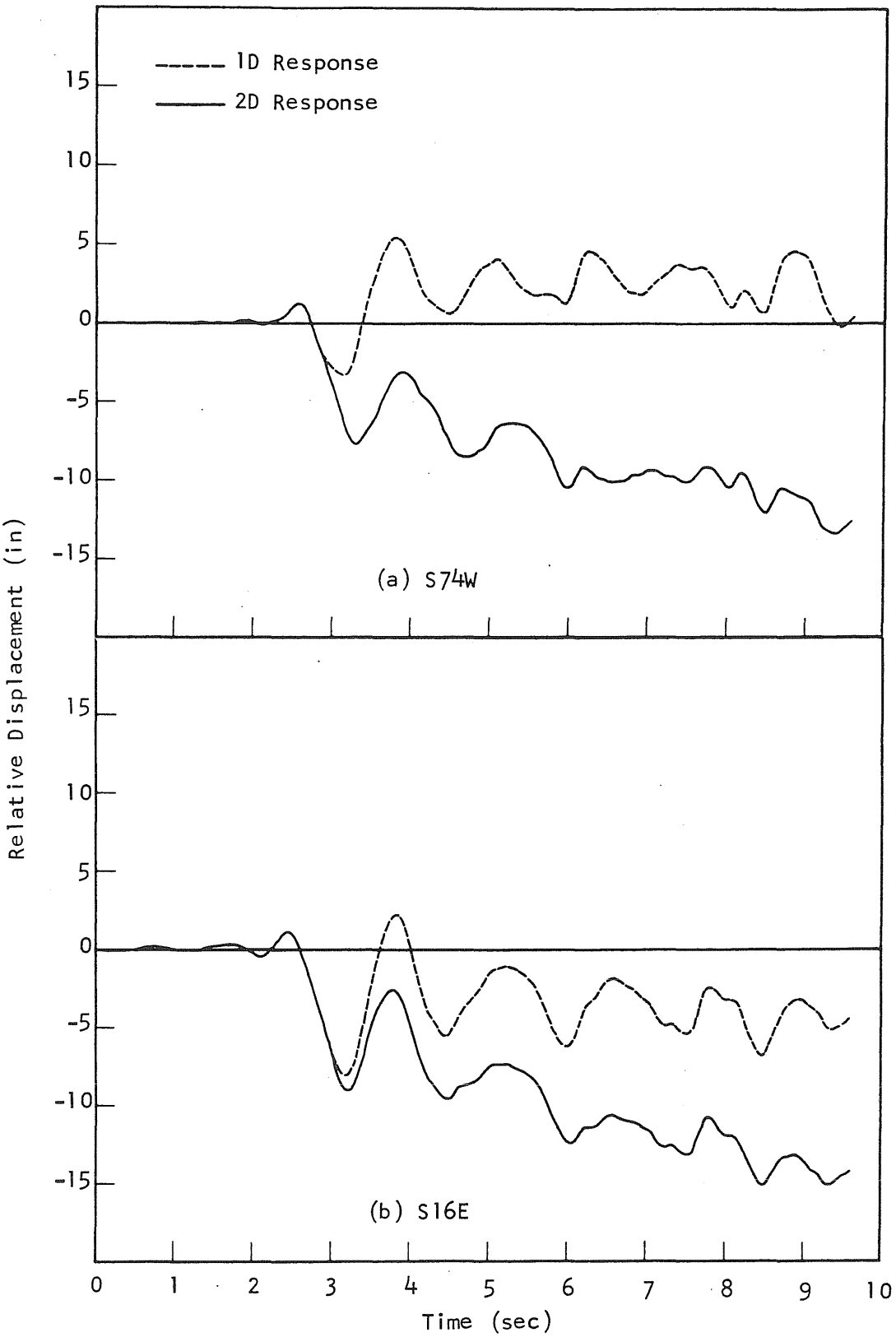

Fig. 4.14 Relative Displacement-Time Histories, Pacoima Record, Relative Intensity 6, Initial Period 0.7 Seconds

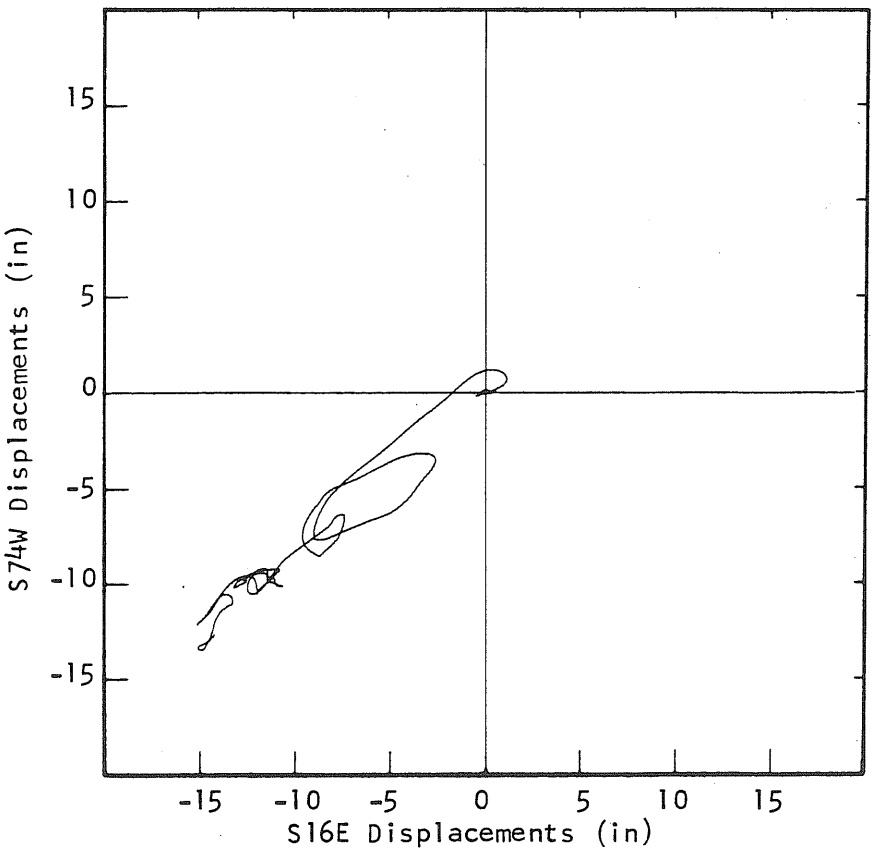

Fig. 4.15 2D Column Top Displacements, Pacoima Record, Relative Intensity 6, Initial Period 0.7 Seconds

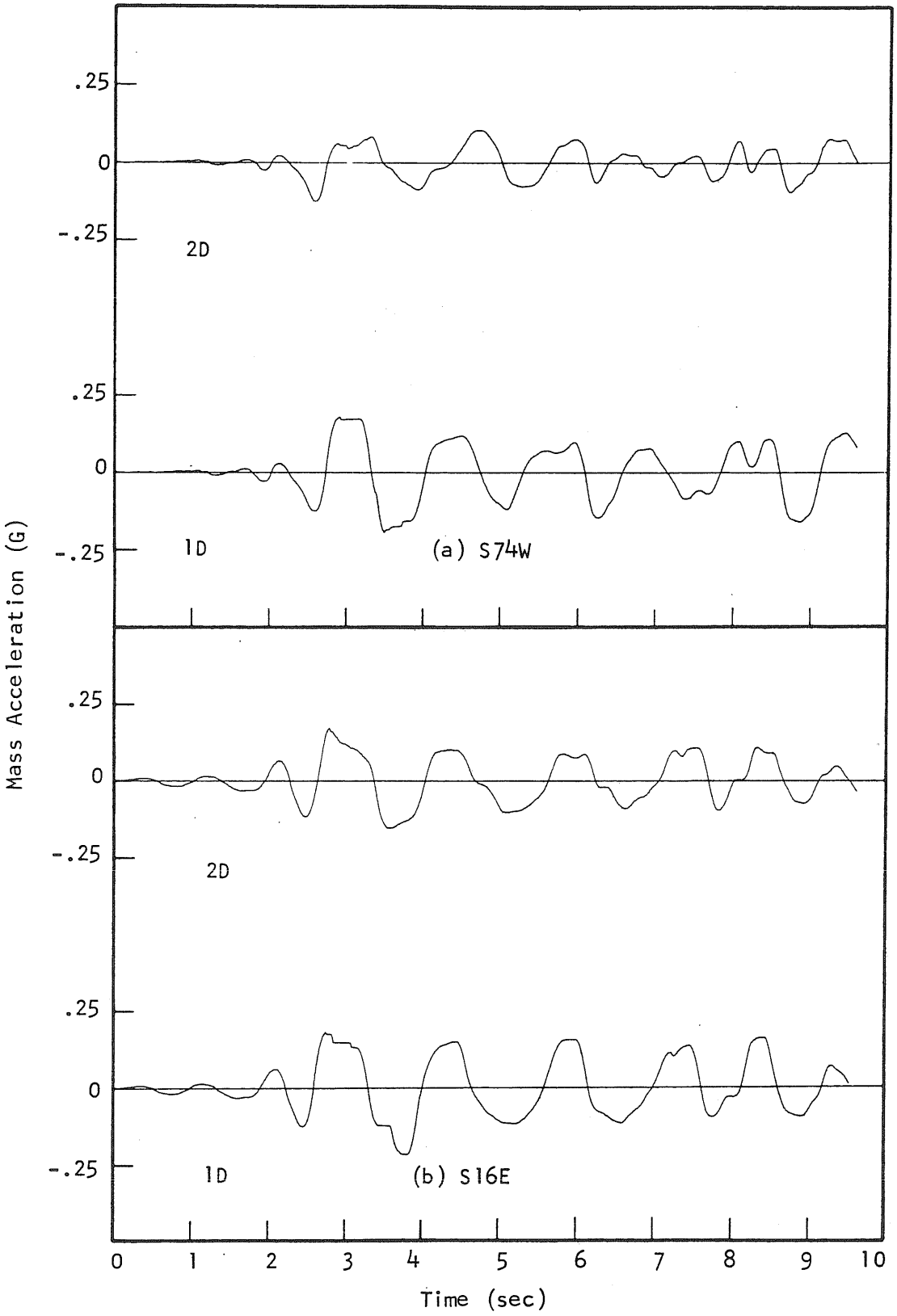

Fig. 4.16 Mass Acceleration-Time Histories, Pacoima Record, Relative Intensity 6, Initial Period 0.7 Seconds

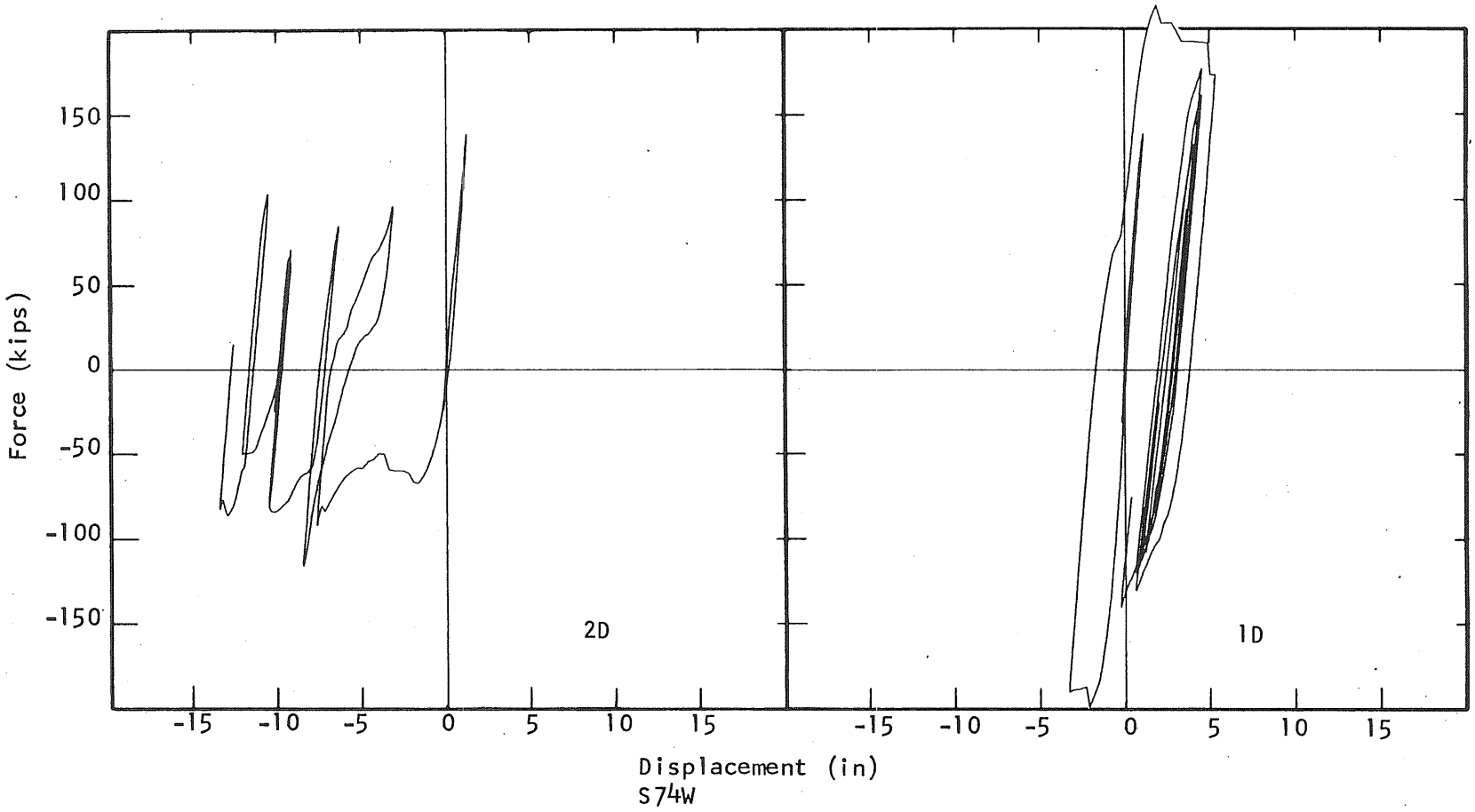

Fig. 4.17 Force-Displacement Responses, Pacoima Record, Relative Intensity 6, Initial Period 0.7 Seconds

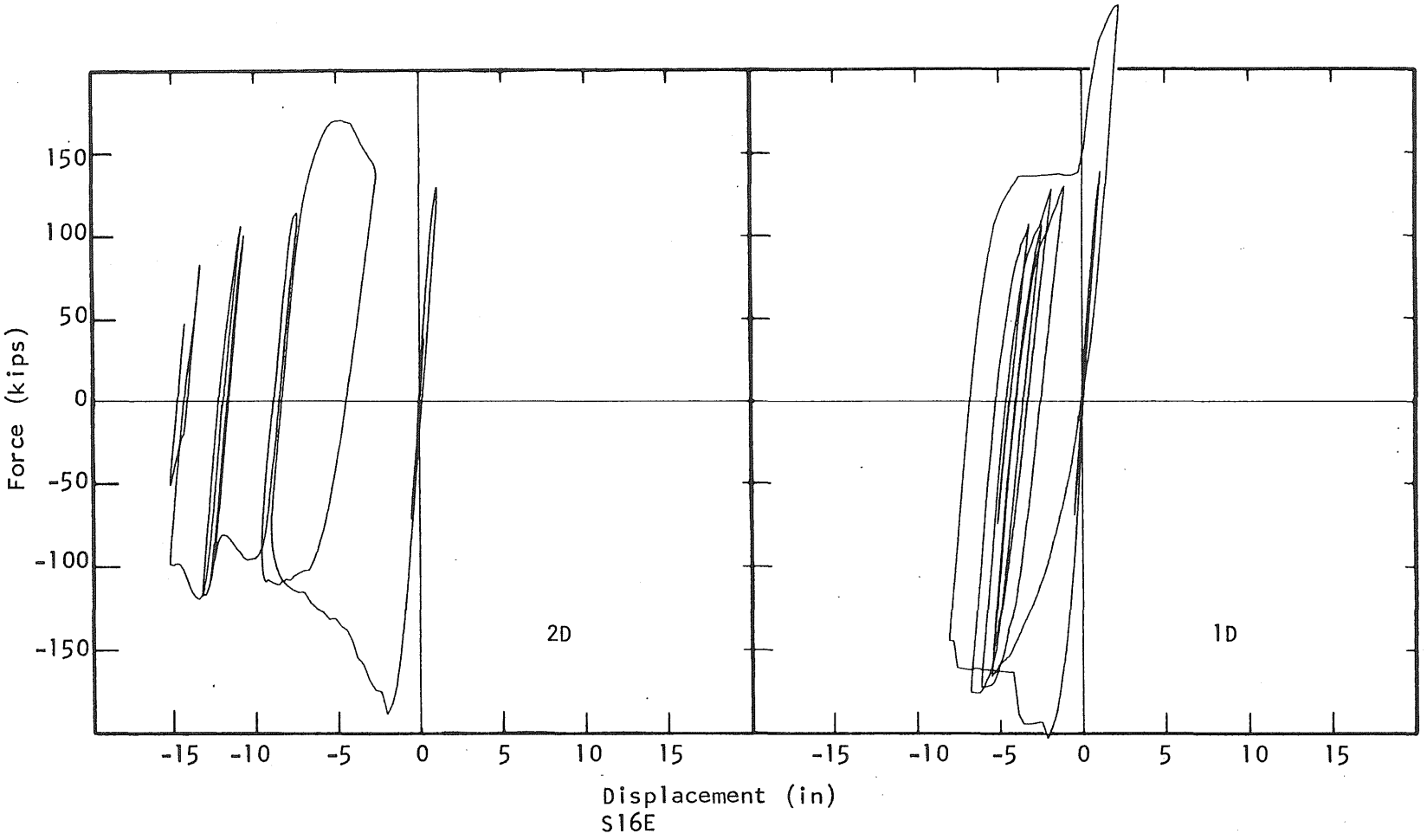

Fig. 4.18 Force-Displacement Responses, Pacoima Record, Relative Intensity 6, Initial Period 0.7 Seconds

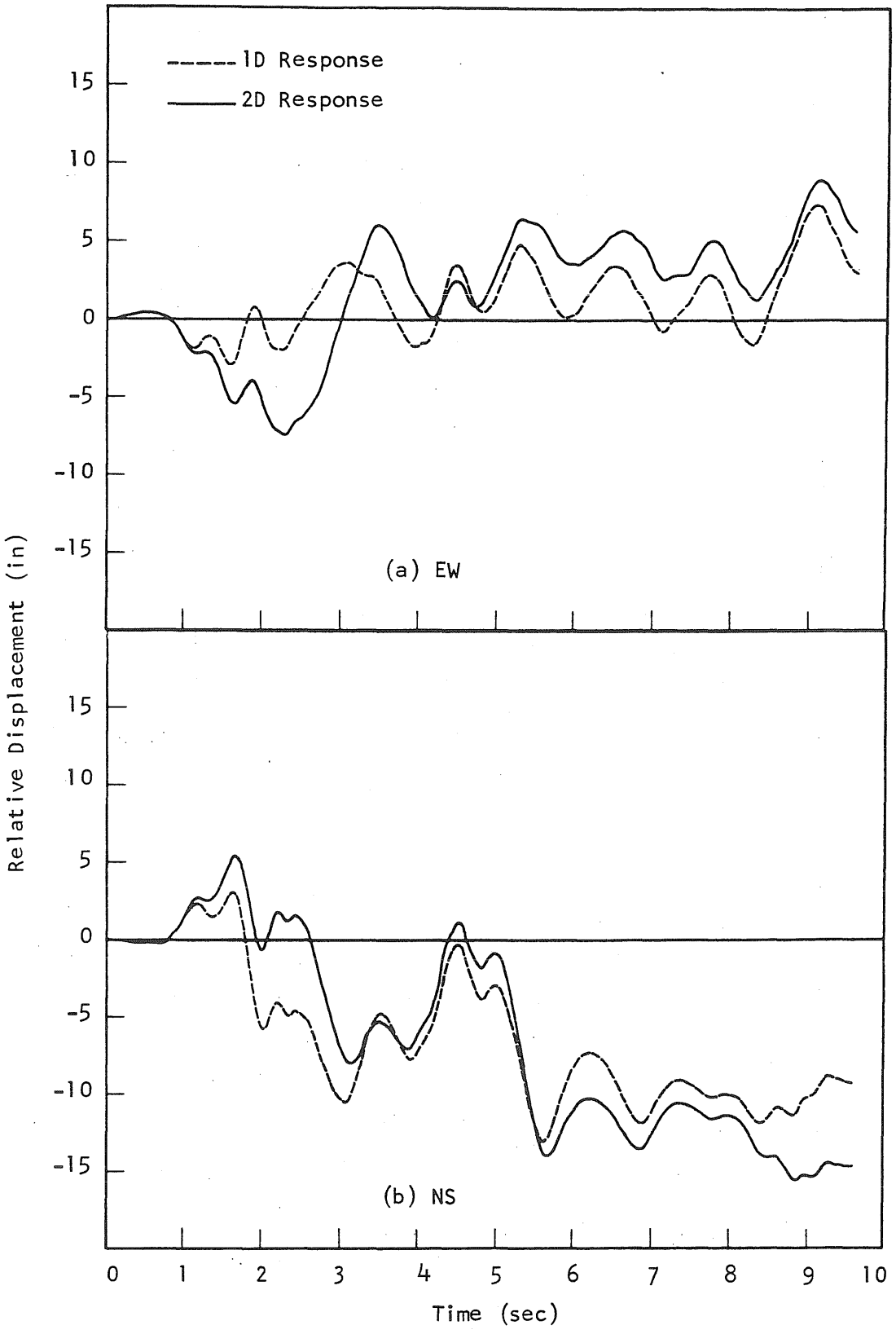

Fig. 4.19 Relative Displacement-Time Histories, El Centro Record, Relative Intensity 6, Initial Period 0.7 Seconds

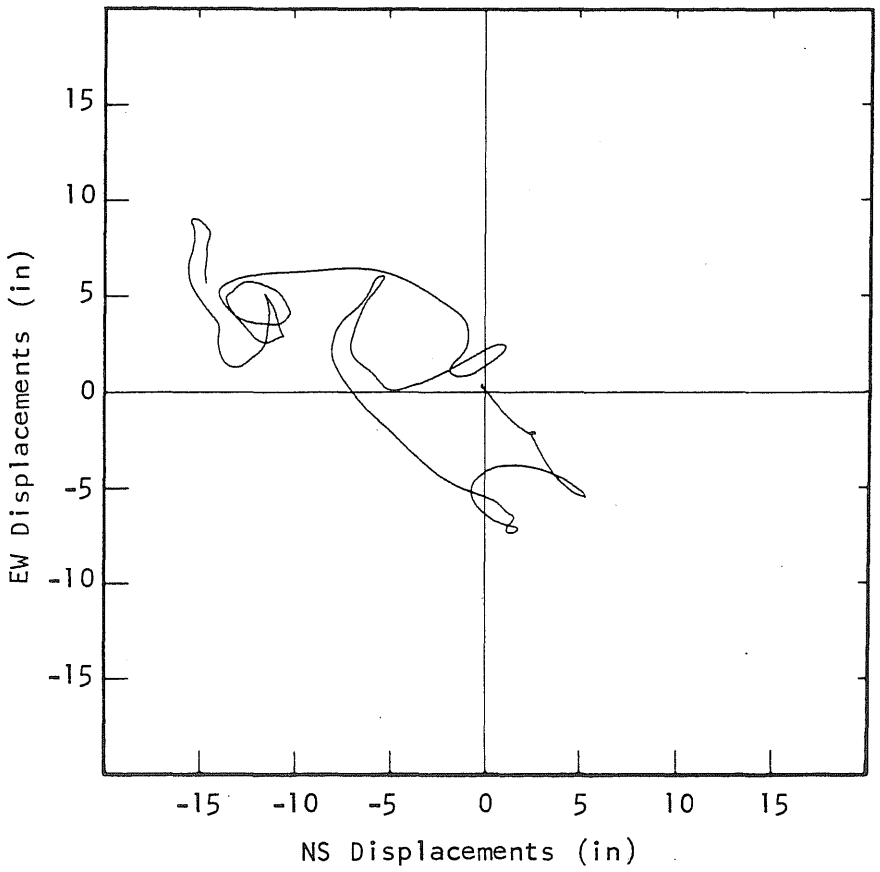

Fig. 4.20 2D Column Top Displacements, El Centro Record, Relative Intensity 6, Initial Period 0.7 Seconds

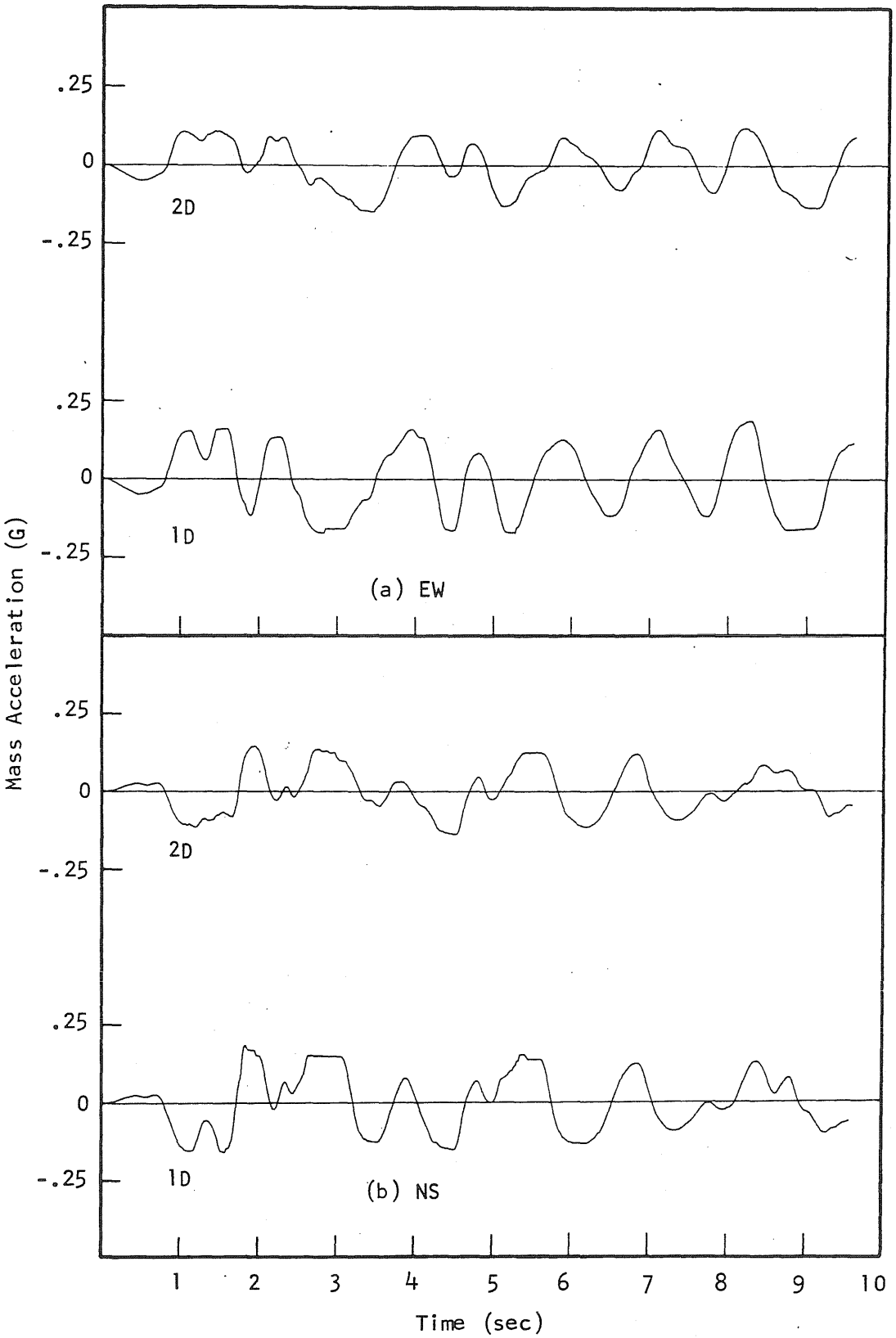

Fig. 4.21 Mass Acceleration-Time Histories, El Centro Record, Relative Intensity 6, Initial Period 0.7 Seconds

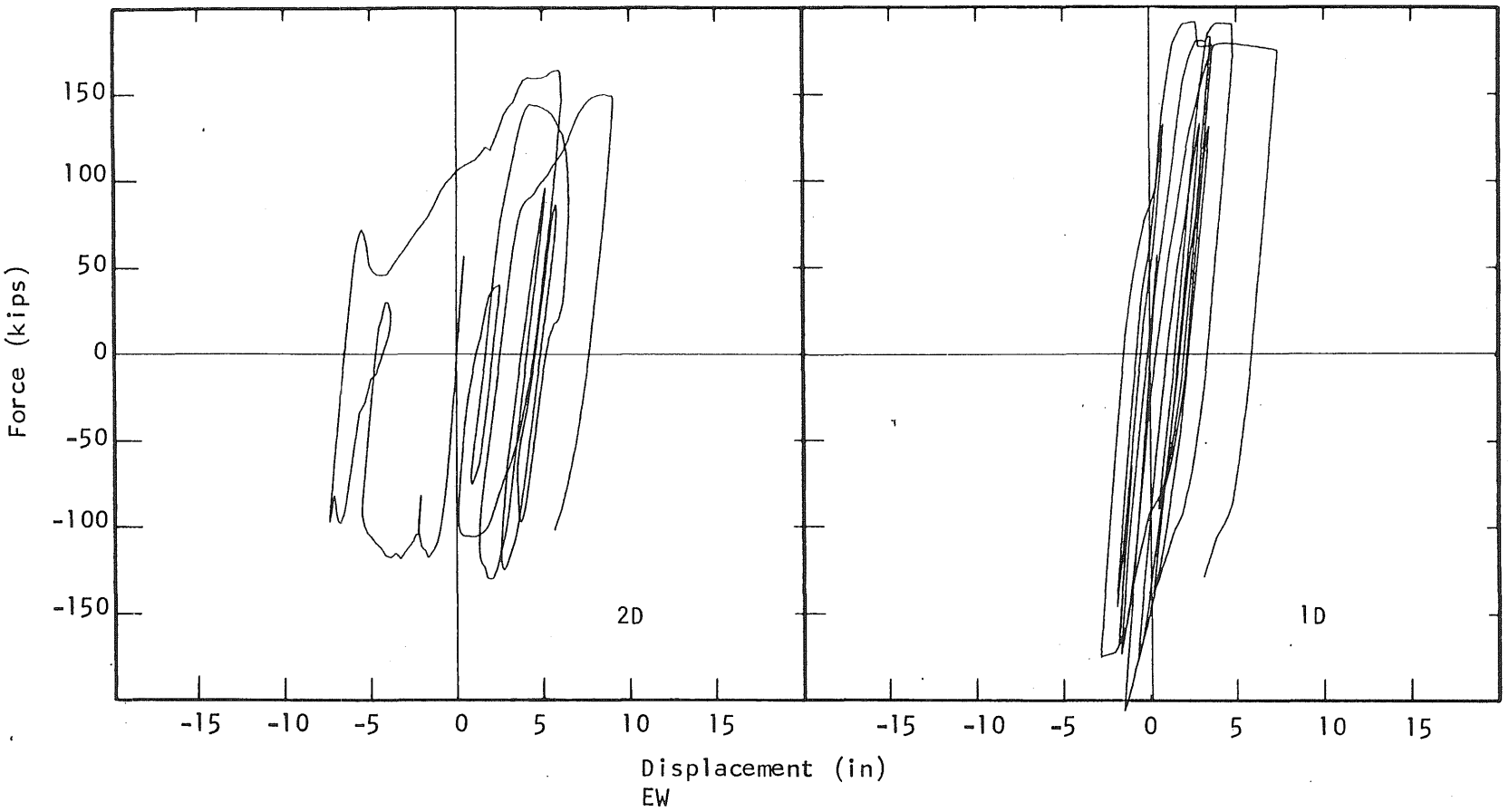

Fig. 4.22 Force-Displacement Responses, El Centro Record, Relative Intensity 6, Initial Period 0.7 Seconds

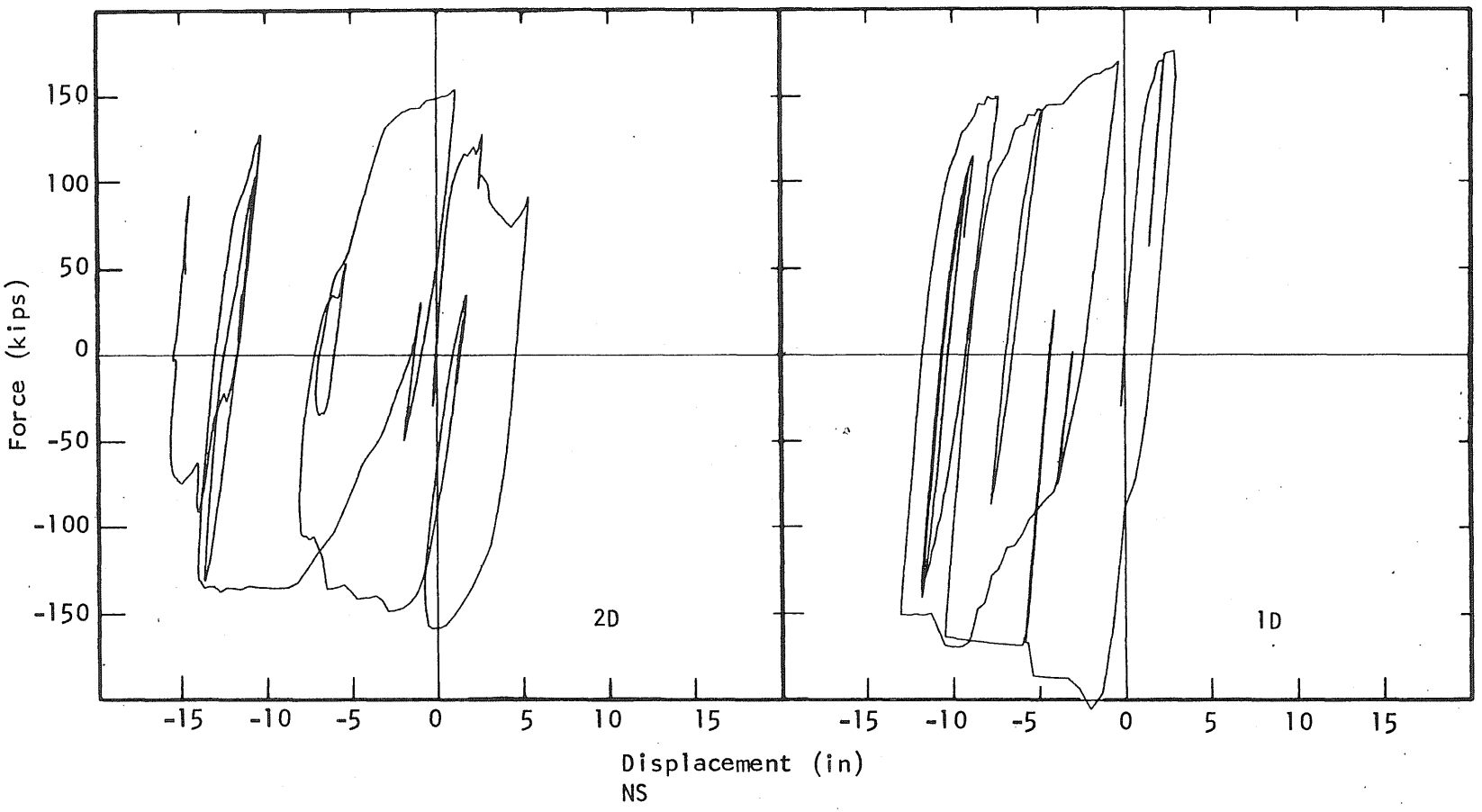

Fig. 4.23 Force-Displacement Responses, El Centro Record, Relative Intensity 6, Initial Period 0.7 Seconds

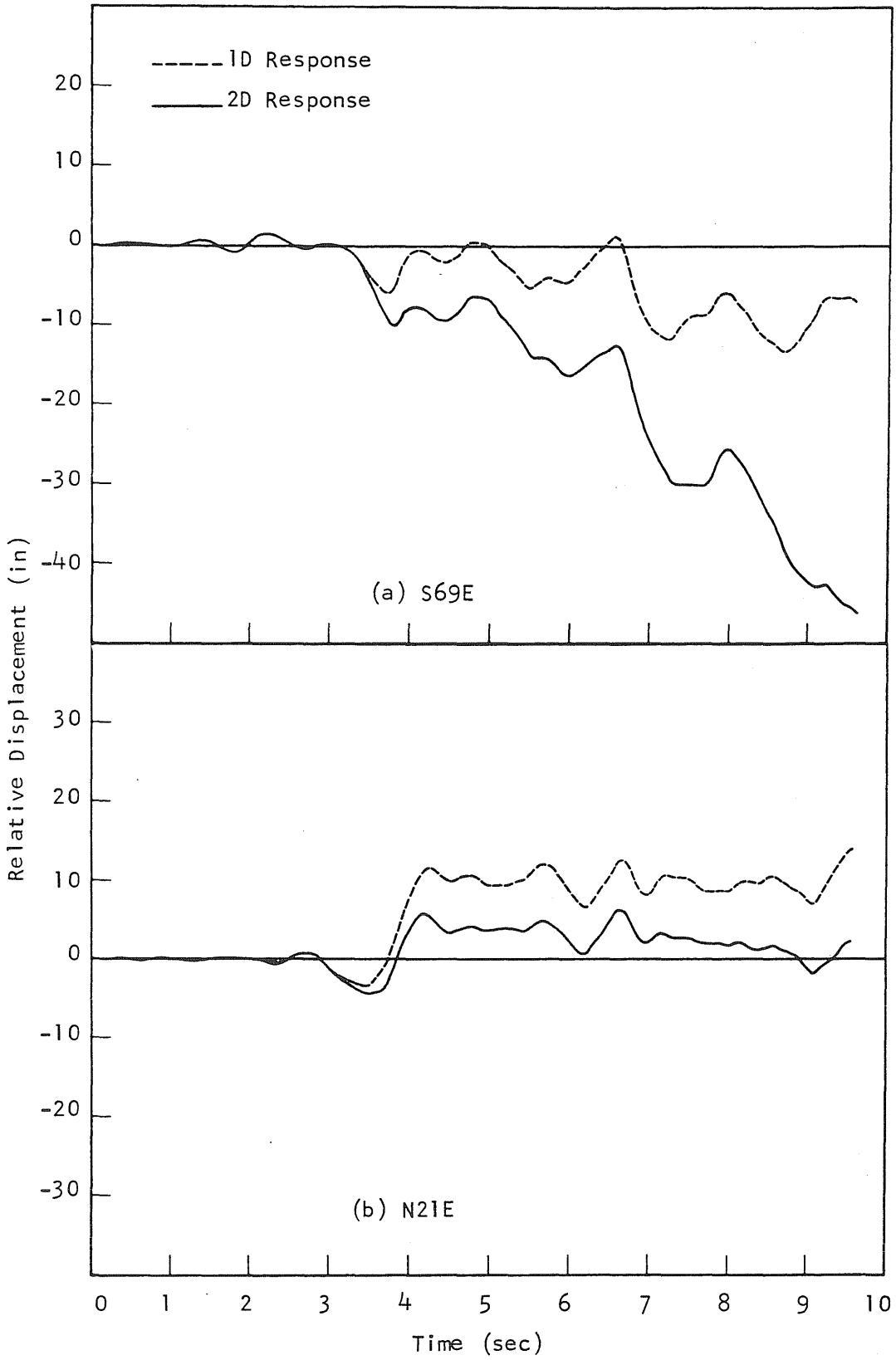

Fig. 4.24 Relative Displacement-Time Histories, Taft Record, Relative Intensity 6, Initial Period 0.7 Seconds

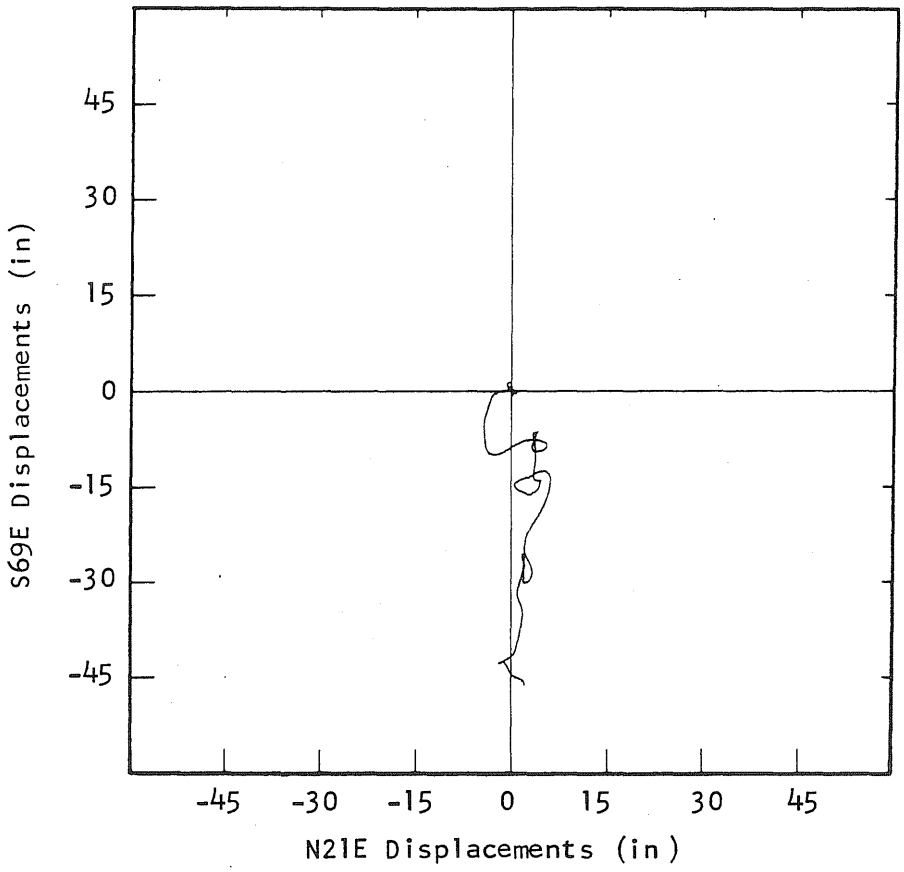

Fig. 4.25 2D Column Top Displacements, Taft Record, Relative Intensity 6, Initial Period 0.7 Seconds

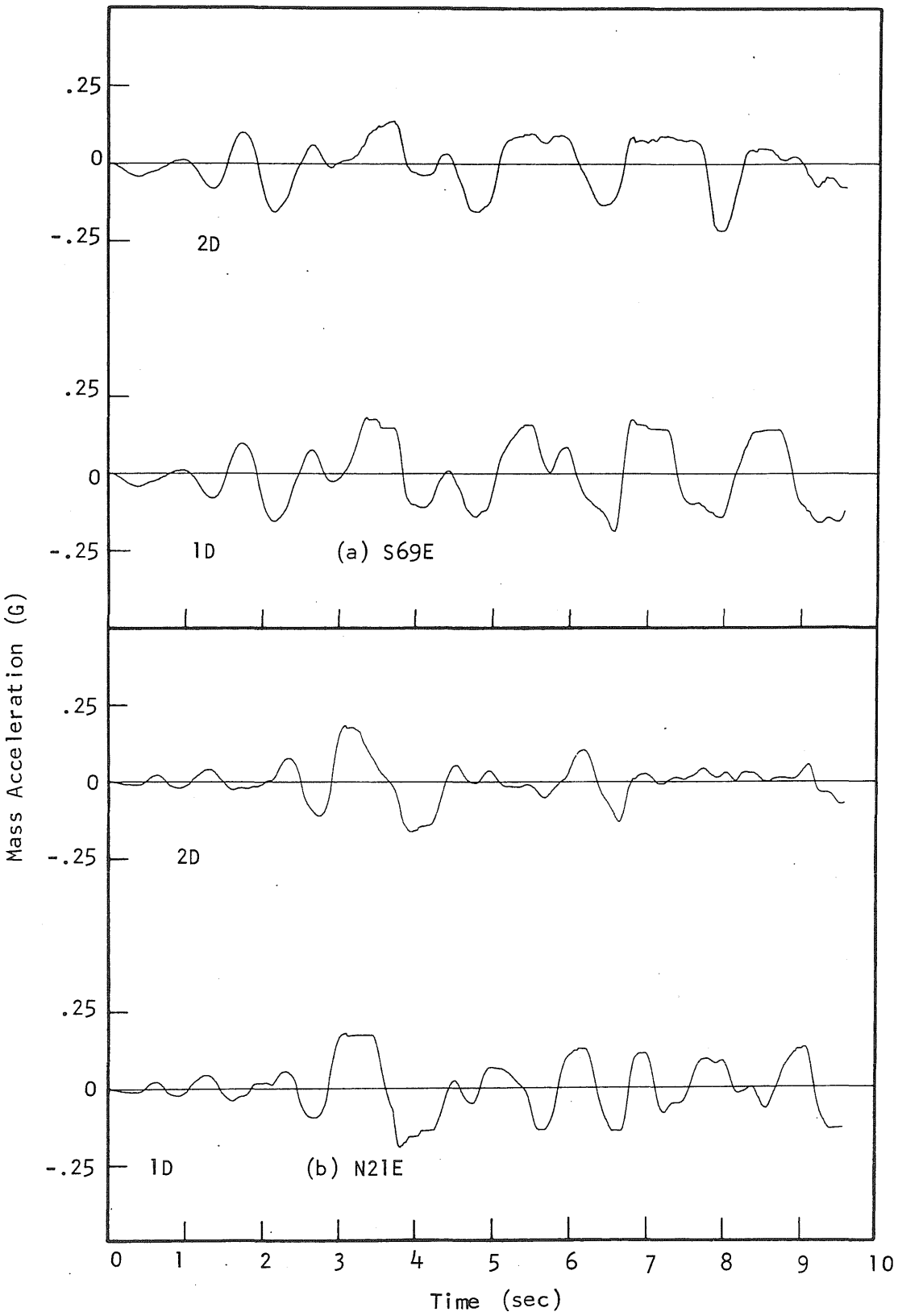

Fig. 4.26 Mass Acceleration-Time Histories, Taft Record, Relative Intensity 6, Initial Period 0.7 Seconds

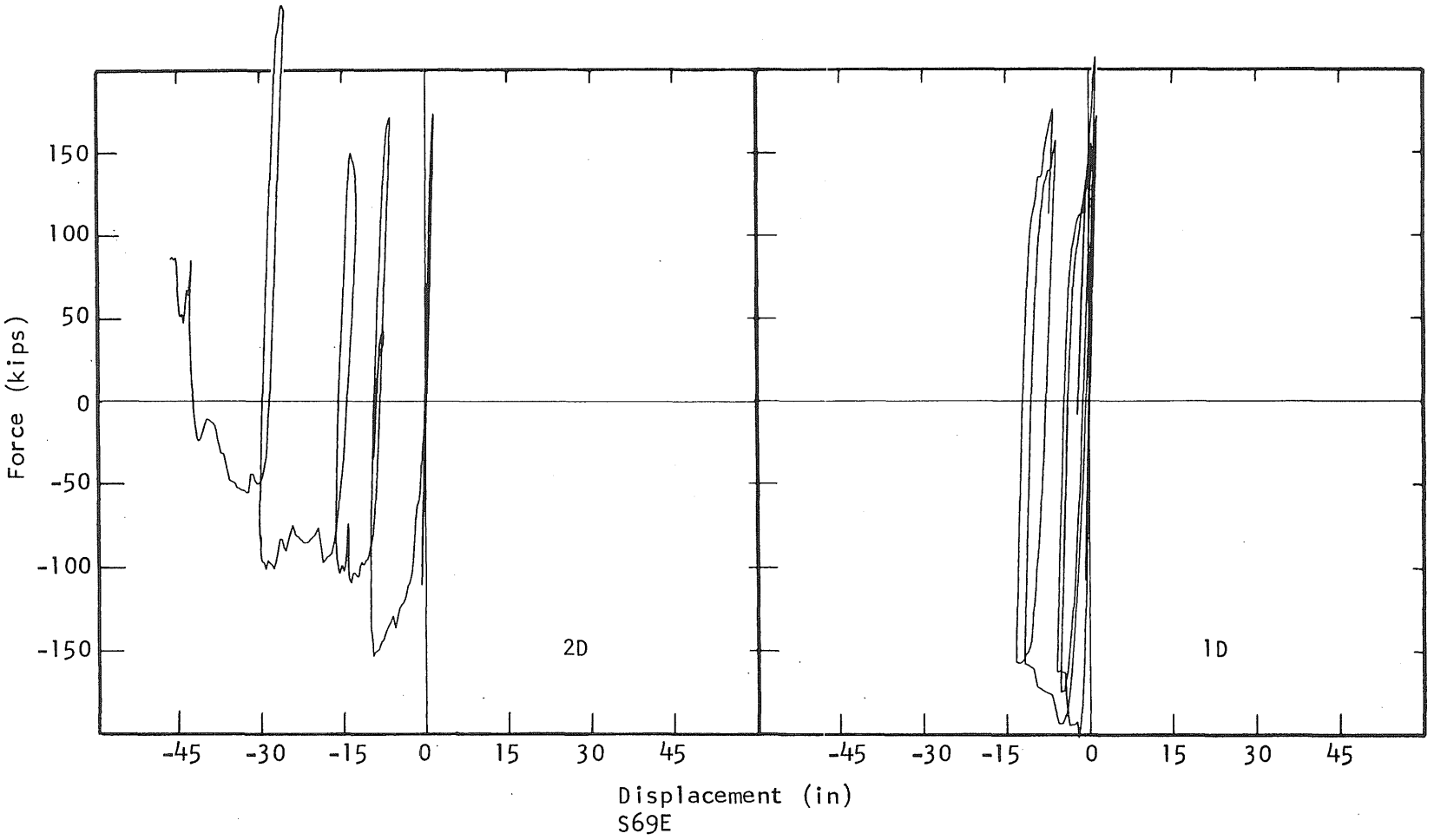

Fig. 4.27 Force-Displacement Responses, Taft Record, Relative Intensity 6, Initial Period 0.7 Seconds

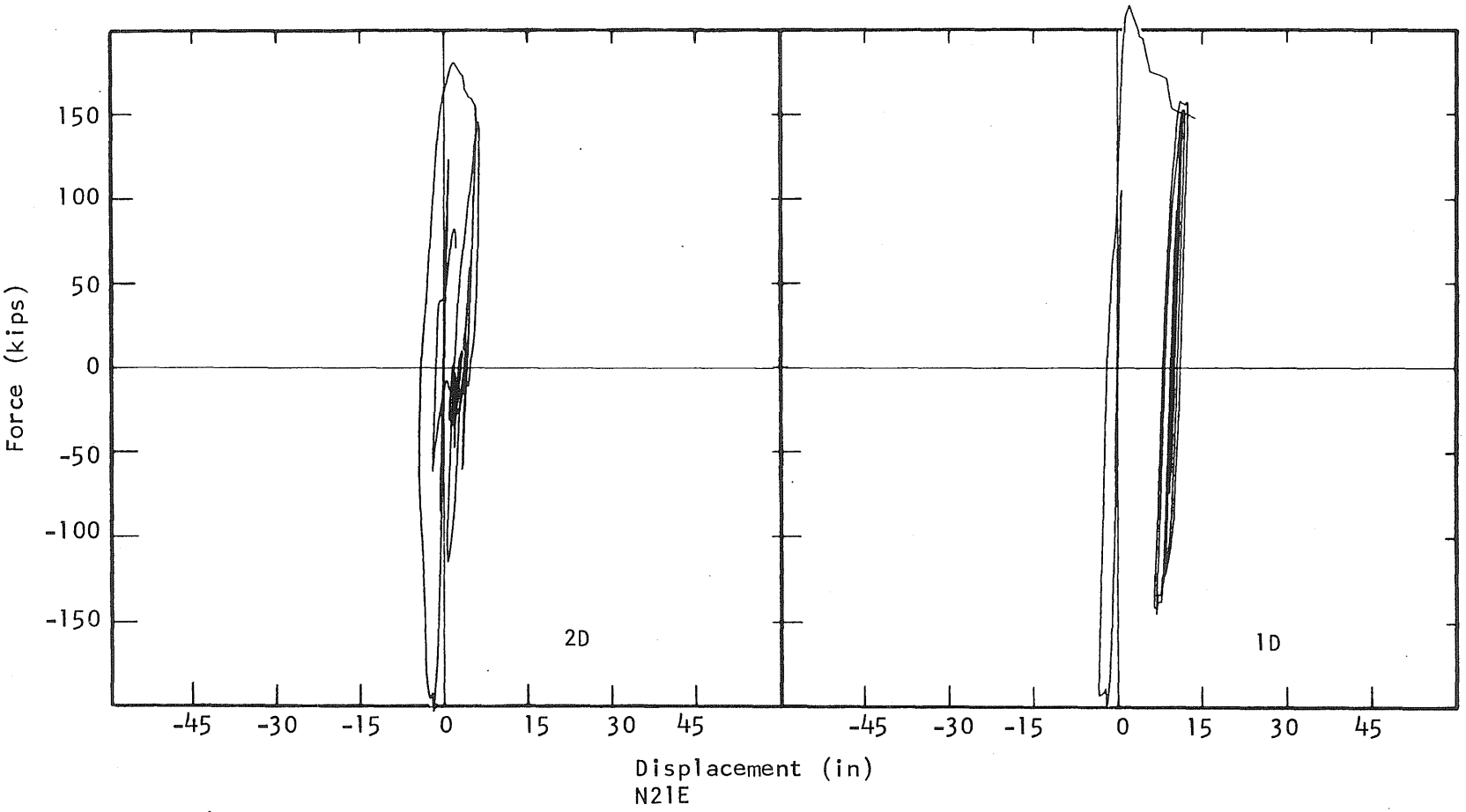

Fig. 4.28 Force-Displacement Responses, Taft Record, Relative Intensity 6, Initial Period 0.7 Seconds

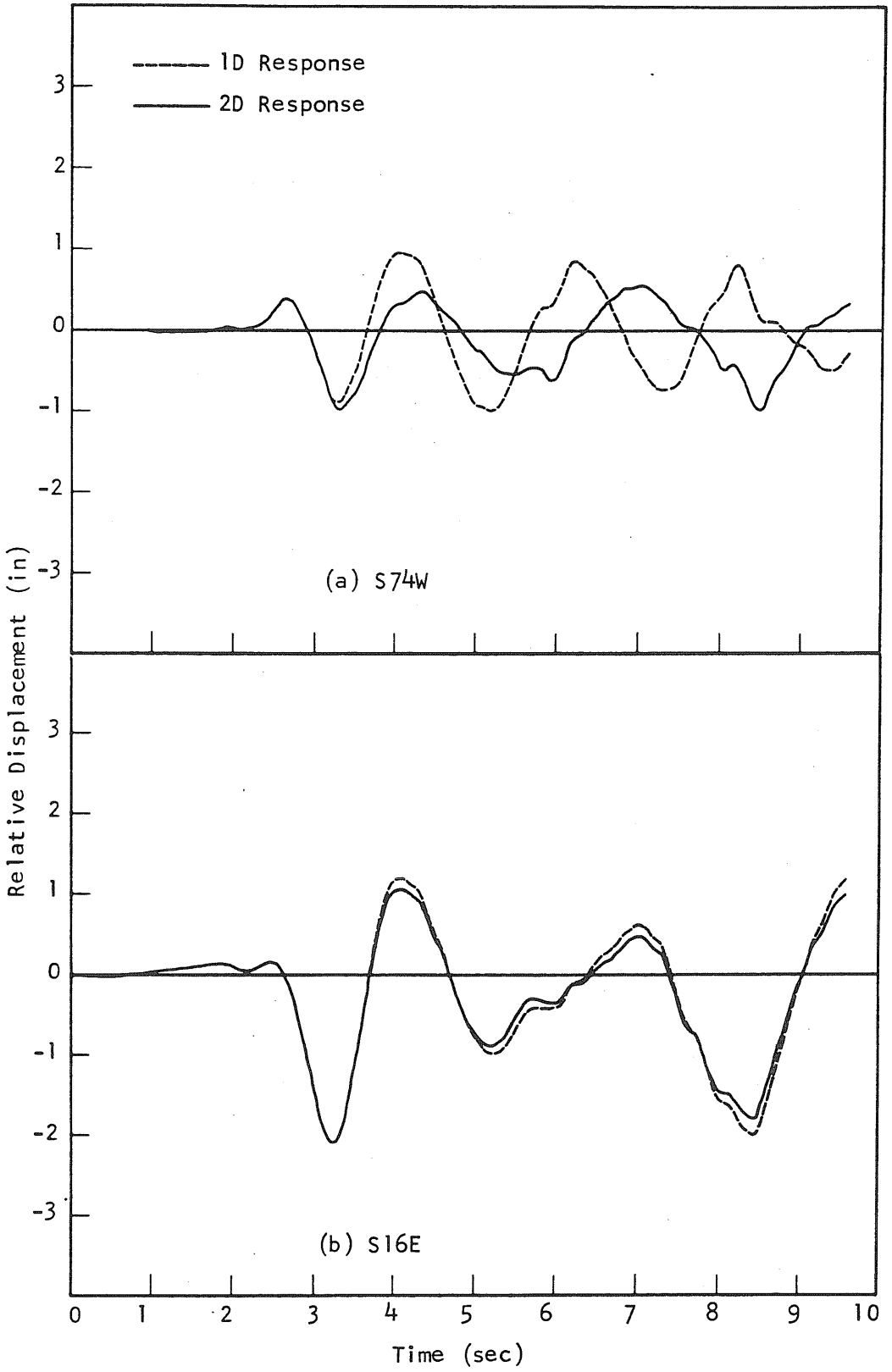

Fig. 4.29 Relative Displacement-Time Histories, Pacoima Record, Relative Intensity 6, Initial Period 1.5 Seconds

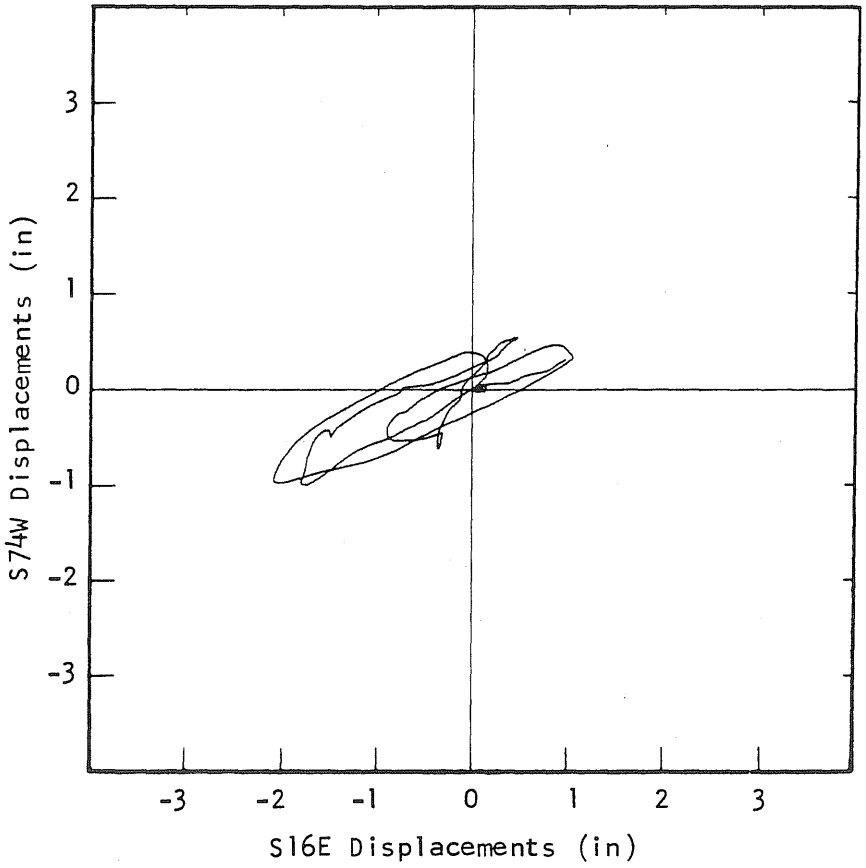

Fig. 4.30 2D Column Top Displacements, Pacoima Record, Relative Intensity 6, Initial Period 1.5 Seconds

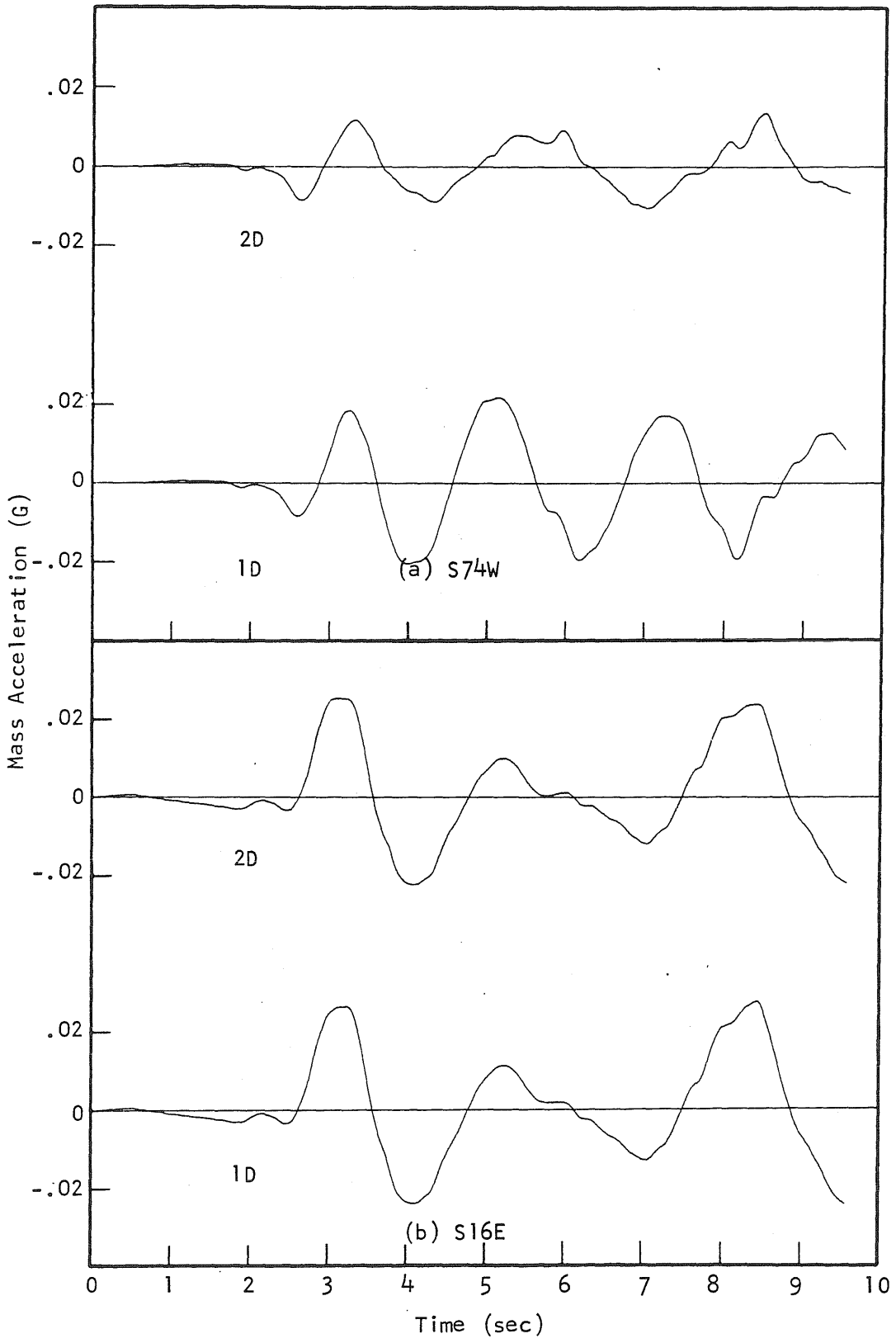

Fig. 4.31 Mass Acceleration-Time Histories, Pacoima Record, Relative Intensity 6, Initial Period 1.5 Seconds

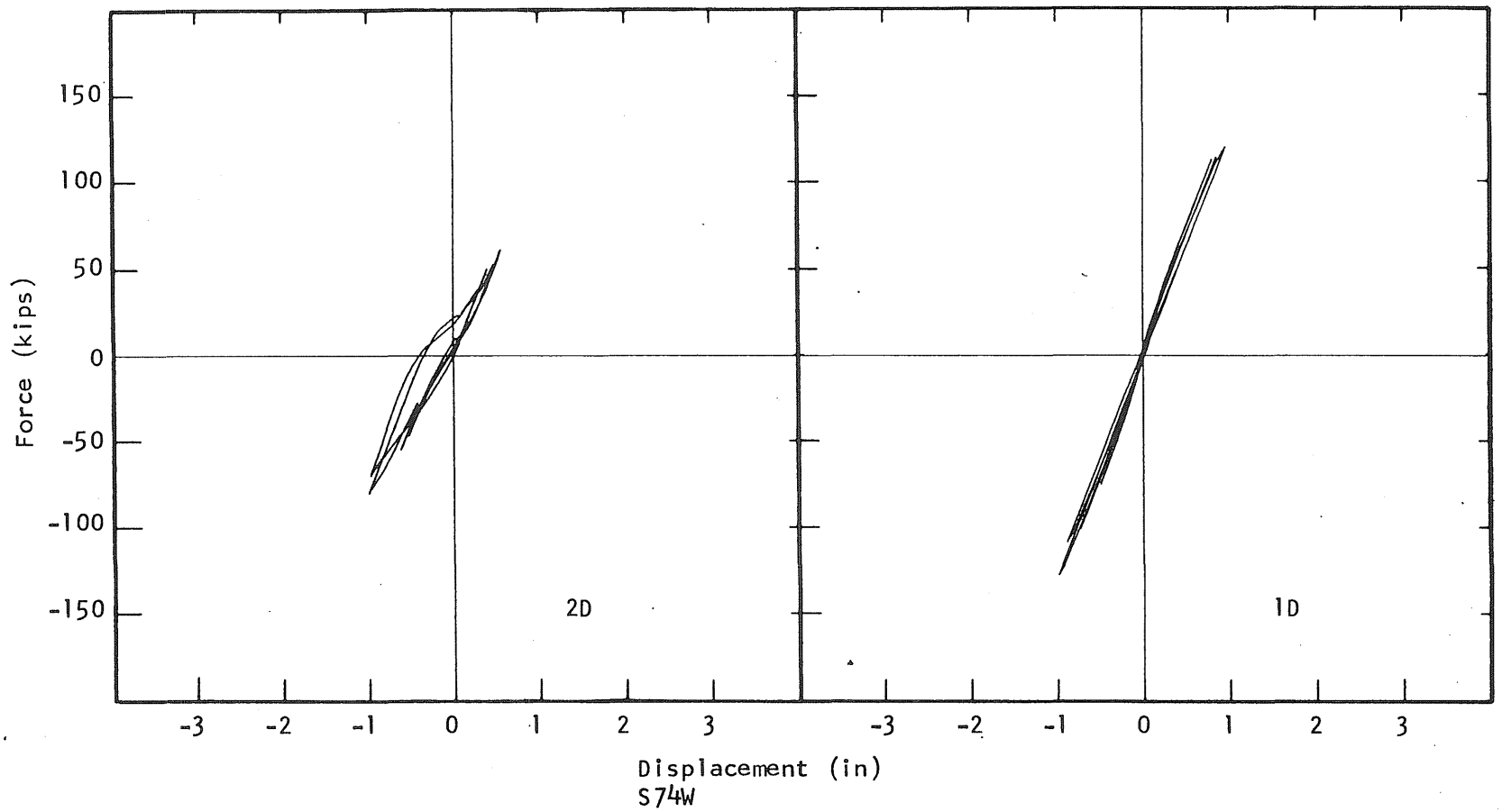

Fig. 4.32 Force-Displacement Responses, Pacoima Record, Relative Intensity 6, Initial Period 1.5 Seconds

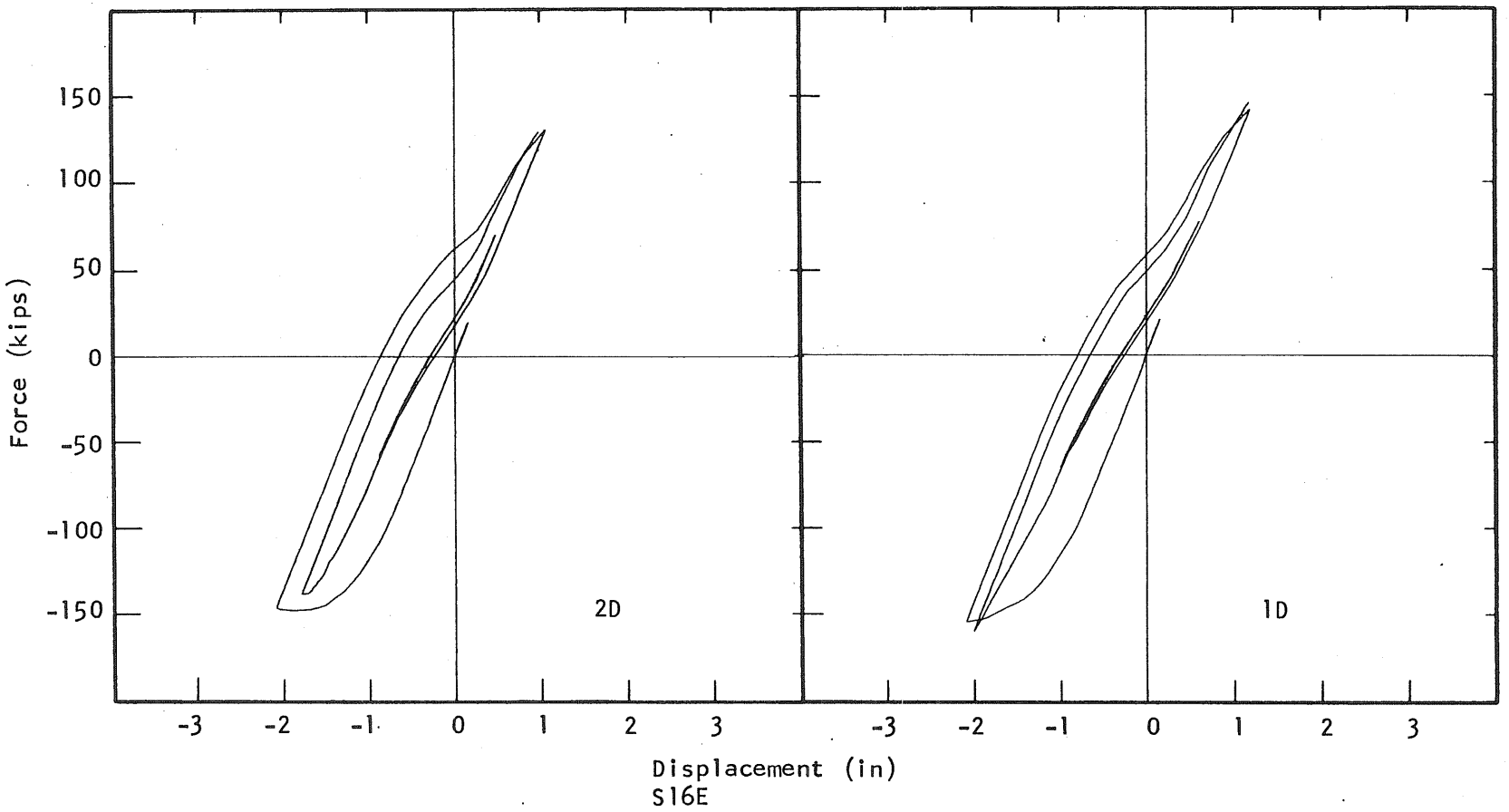

Fig. 4.33 Force-Displacement Responses, Pacoima Record, Relative Intensity 6, Initial Period 1.5 Seconds

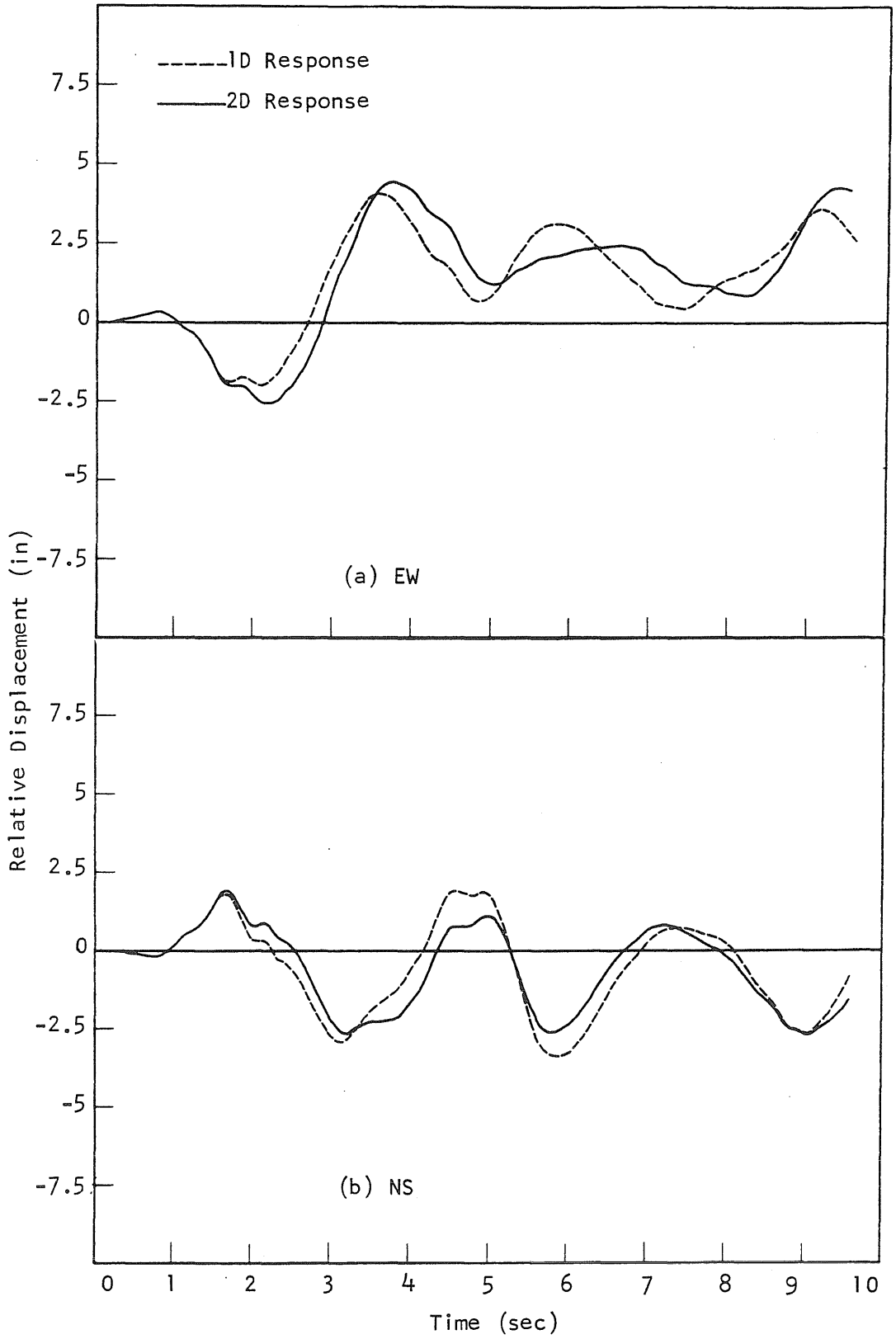

Fig. 4.34 Relative Displacement-Time Histories, El Centro Record, Relative Intensity 6, Initial Period 1.5 Seconds

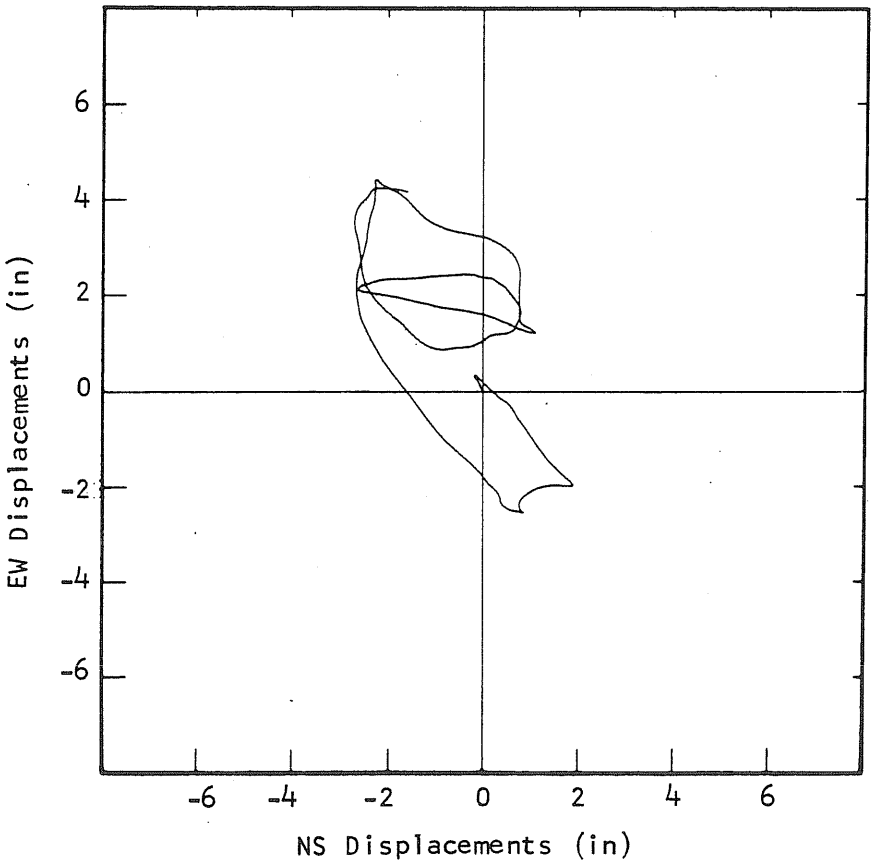

Fig. 4.35 2D Column Top Displacements, El Centro Record, Relative Intensity 6, Initial Period 1.5 Seconds

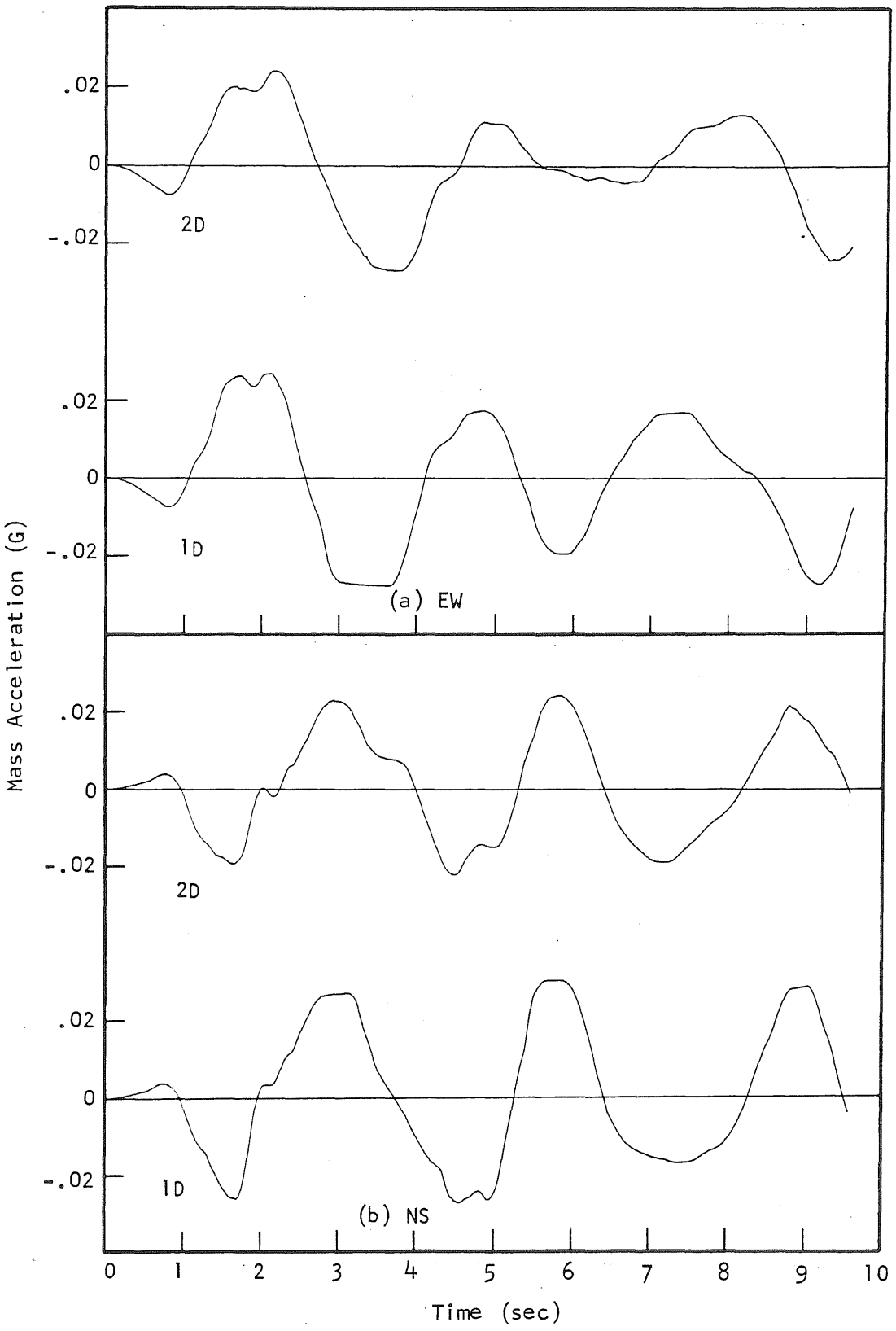

Fig. 4.36 Mass Acceleration-Time Histories, El Centro Record, Relative Intensity 6, Initial Period 1.5 Seconds

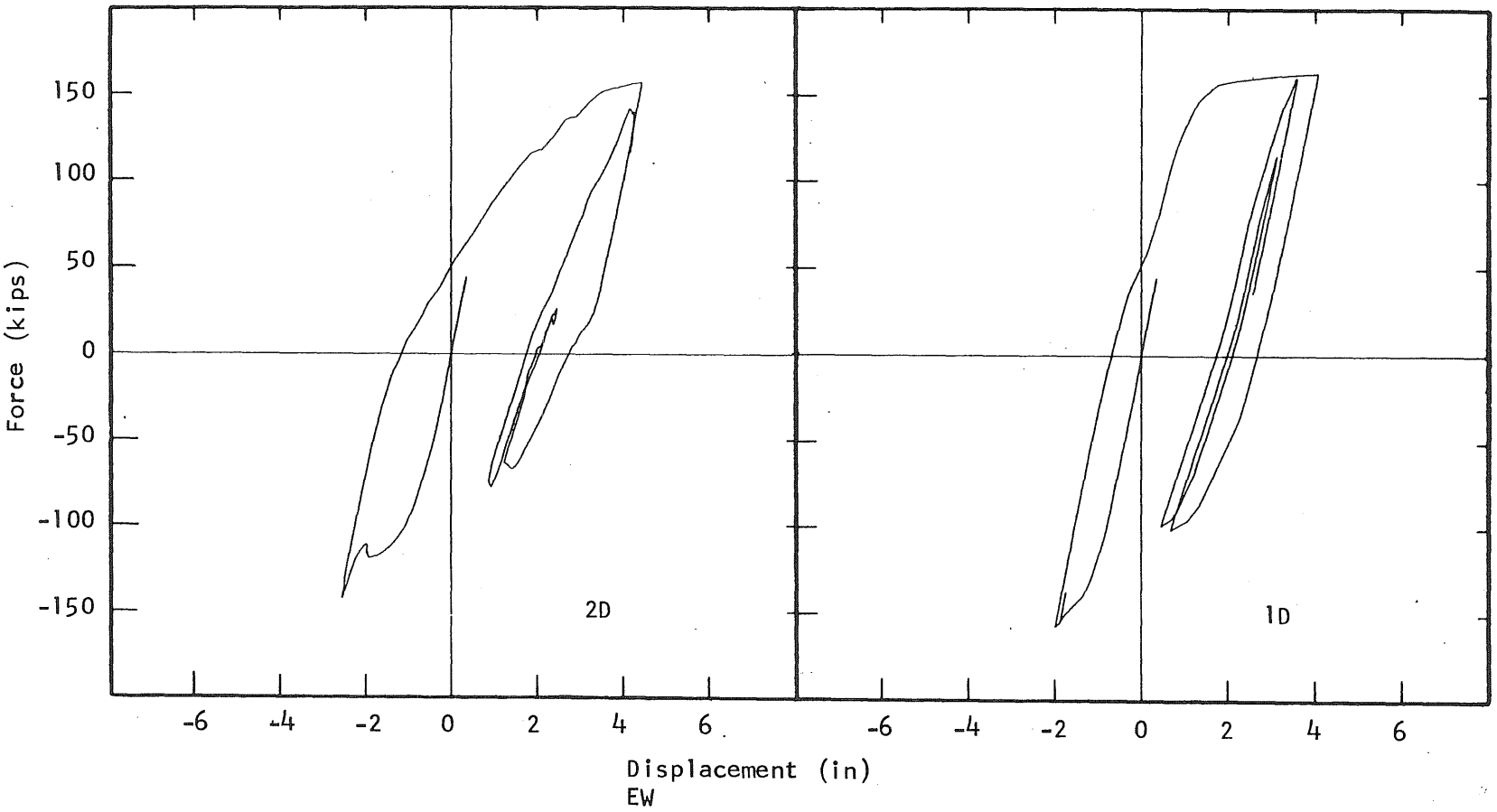

Fig. 4.37 Force-Displacement Responses, El Centro Record, Relative Intensity 6, Initial Period 1.5 Seconds

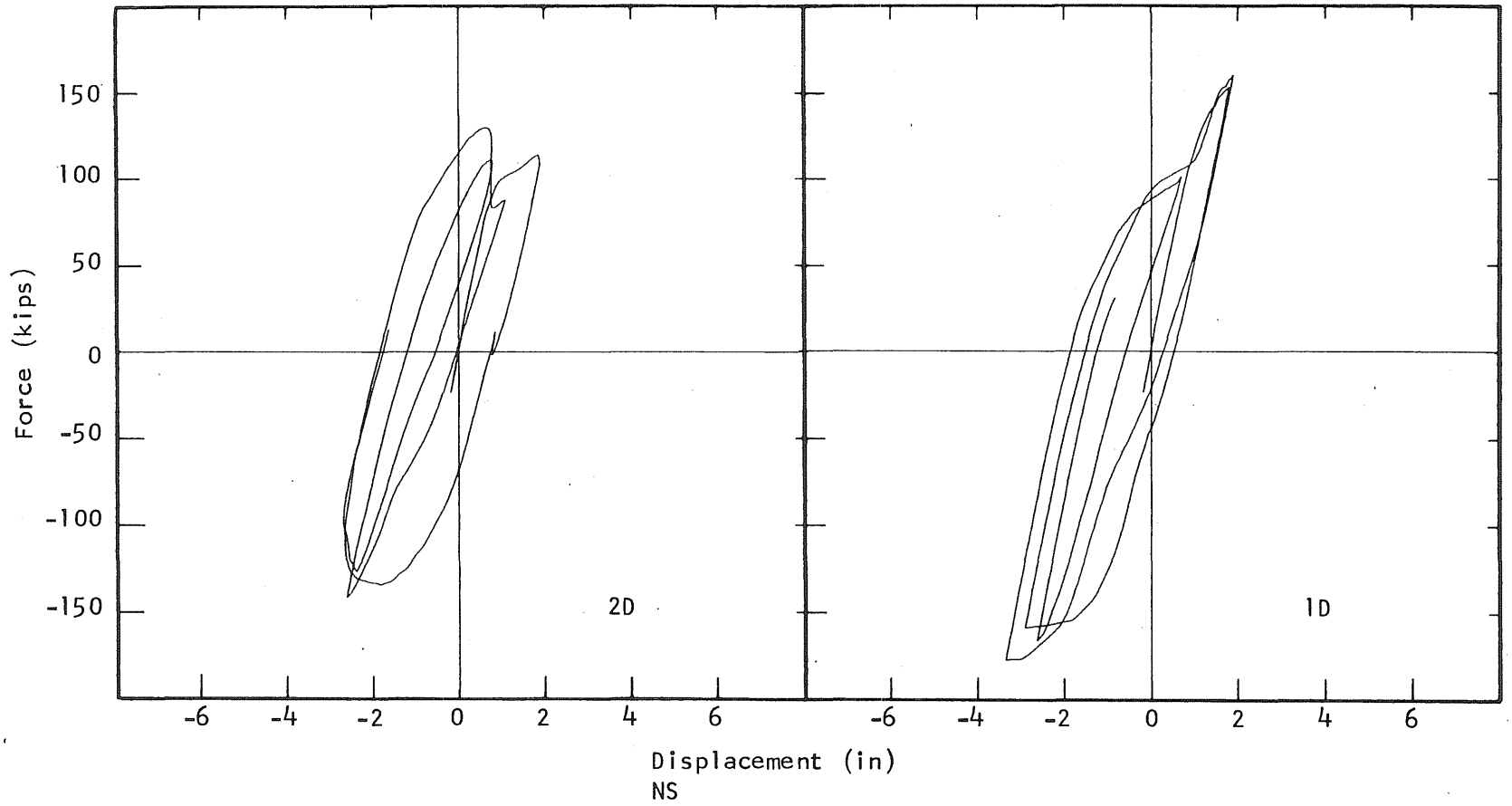

Fig. 4.38 Force-Displacement Responses, El Centro Record, Relative Intensity 6, Initial Period 1.5 Seconds

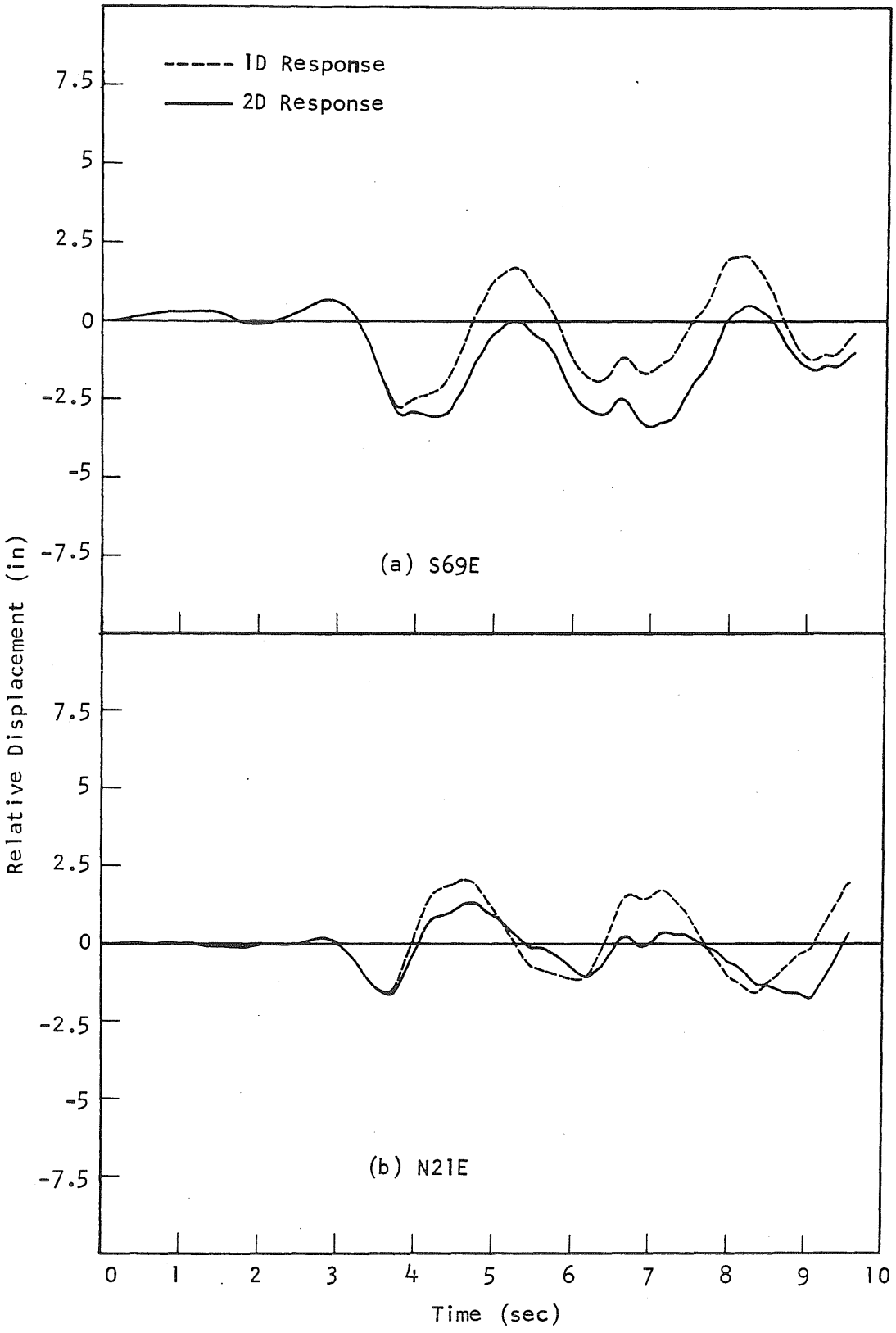

Fig. 4.39 Relative Displacement-Time Histories, Taft Record, Relative Intensity 6, Initial Period 1.5 Seconds

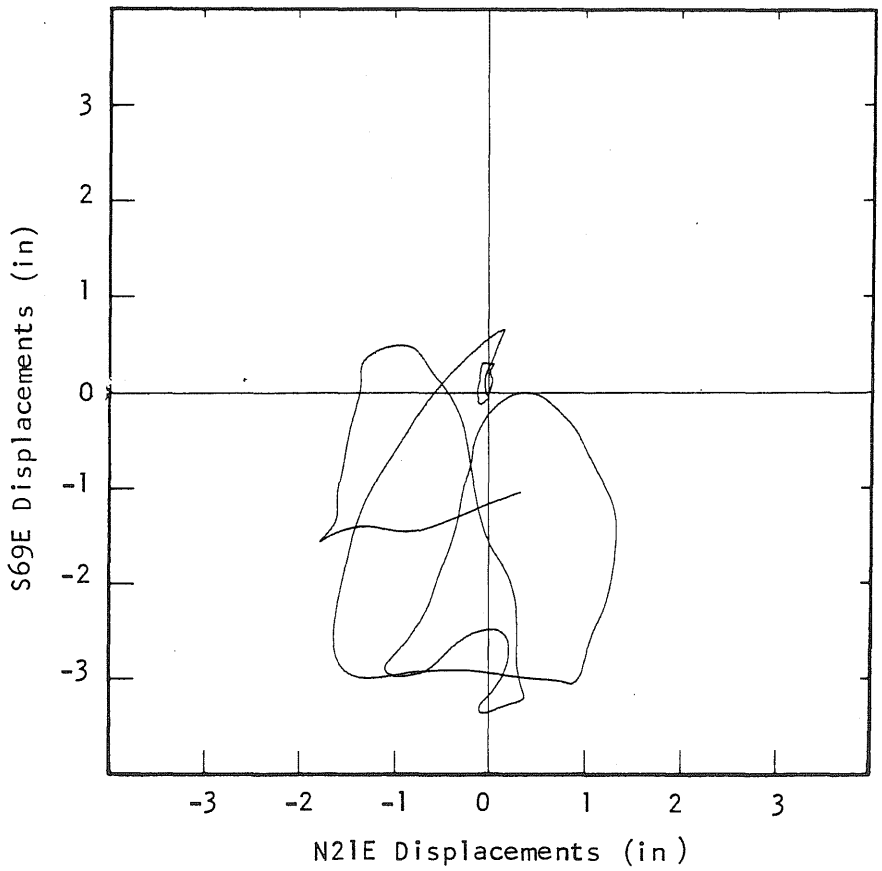

Fig. 4.40 2D Column Top Displacements, Taft Record, Relative Intensity 6, Initial Period 1.5 Seconds

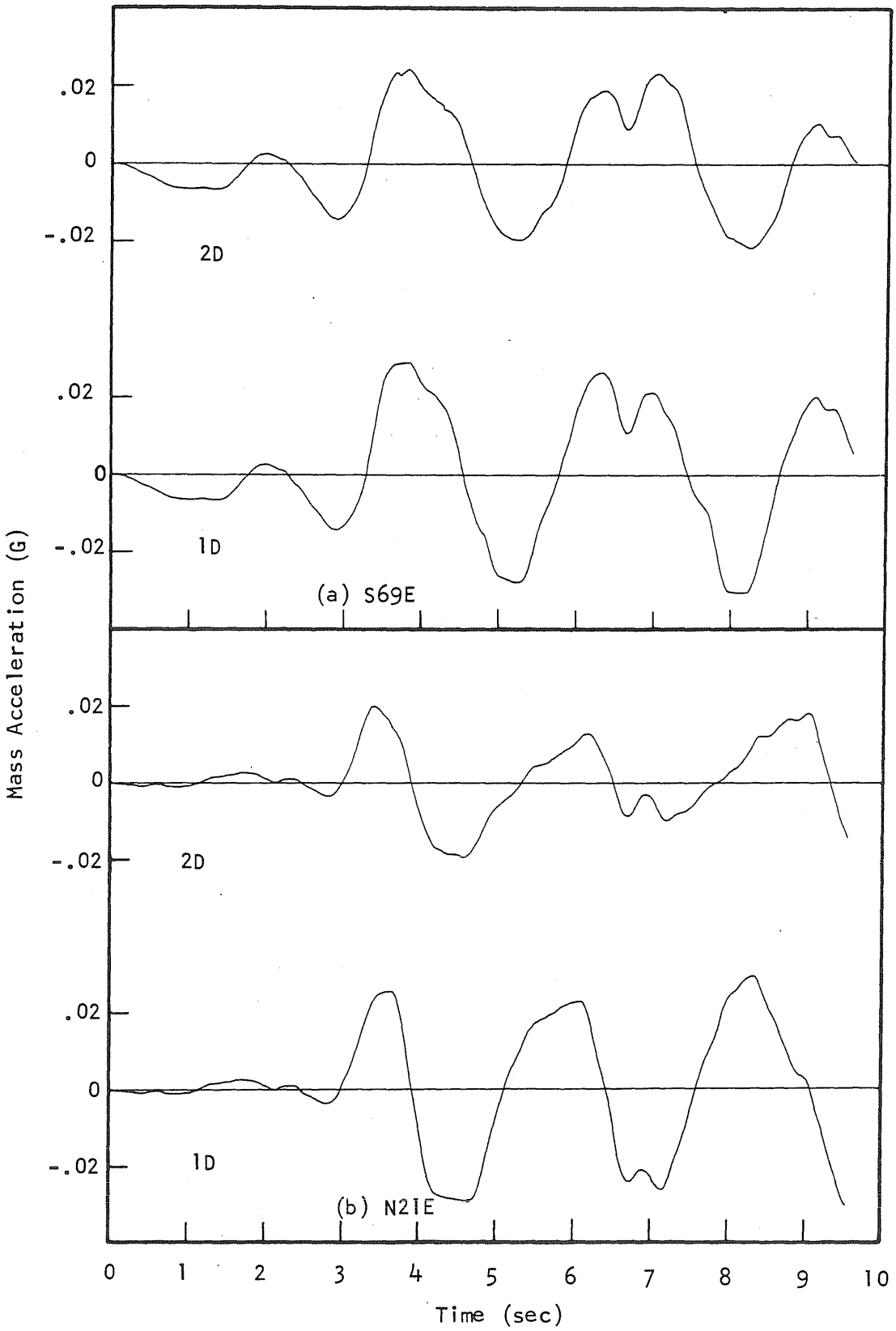

Fig. 4.41 Mass Acceleration-Time Histories, Taft Record, Relative Intensity 6, Initial Period 1.5 Seconds

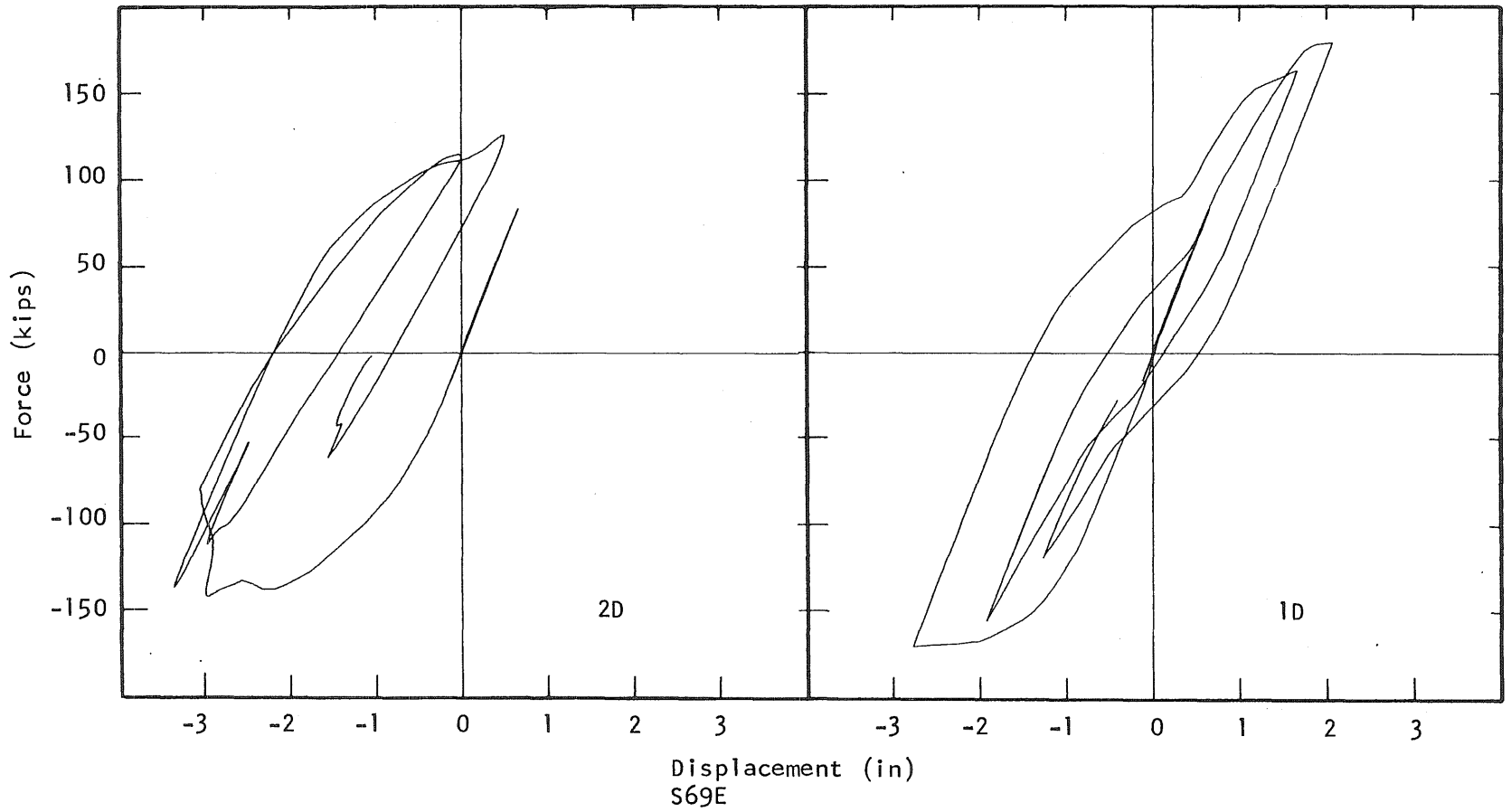

Fig. 4.42 Force-Displacement Responses, Taft Record, Relative Intensity 6, Initial Period 1.5 Seconds

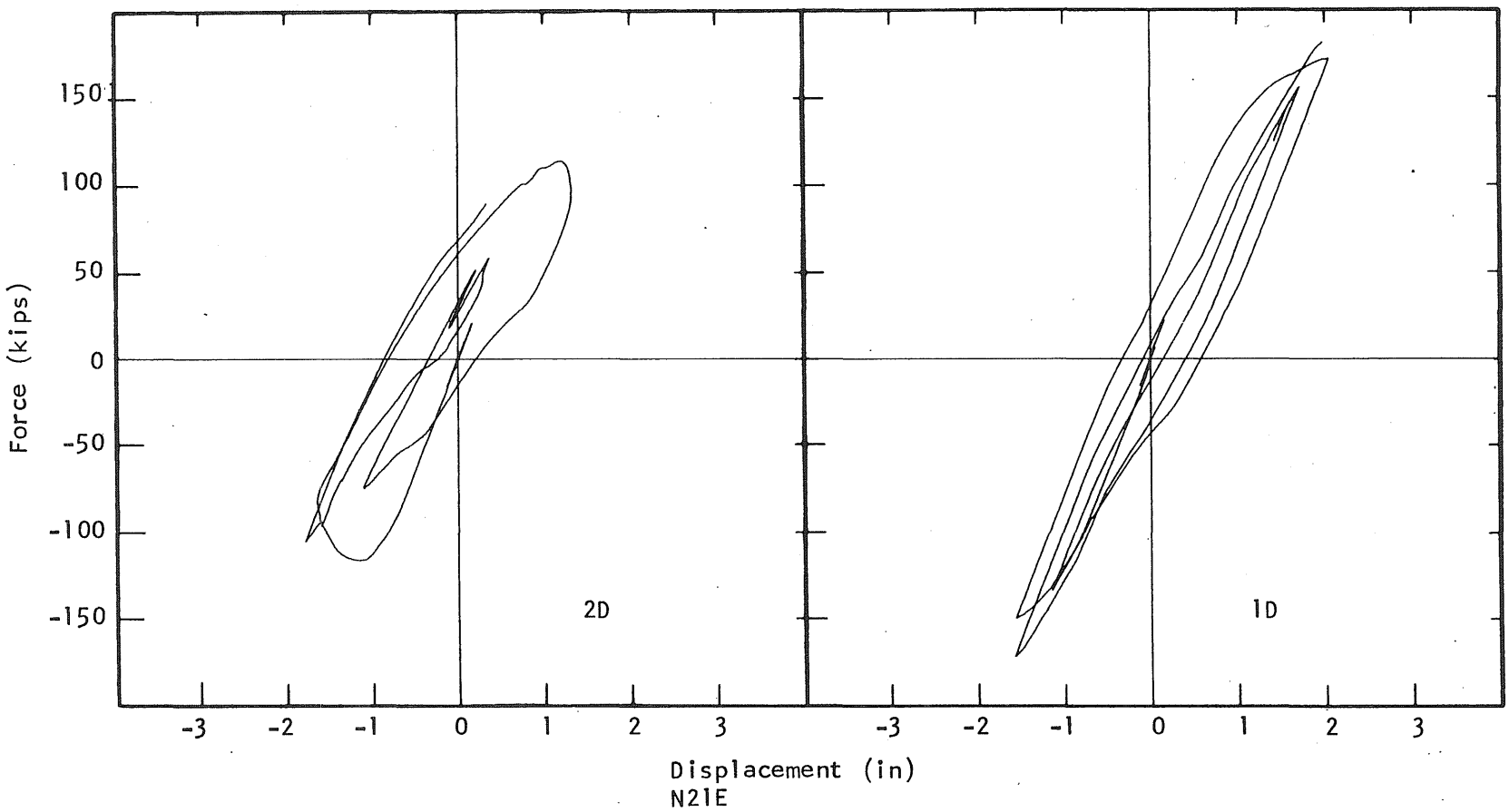

Fig. 4.43 Force-Displacement Responses, Taft Record, Relative Intensity 6, Initial Period 1.5 Seconds

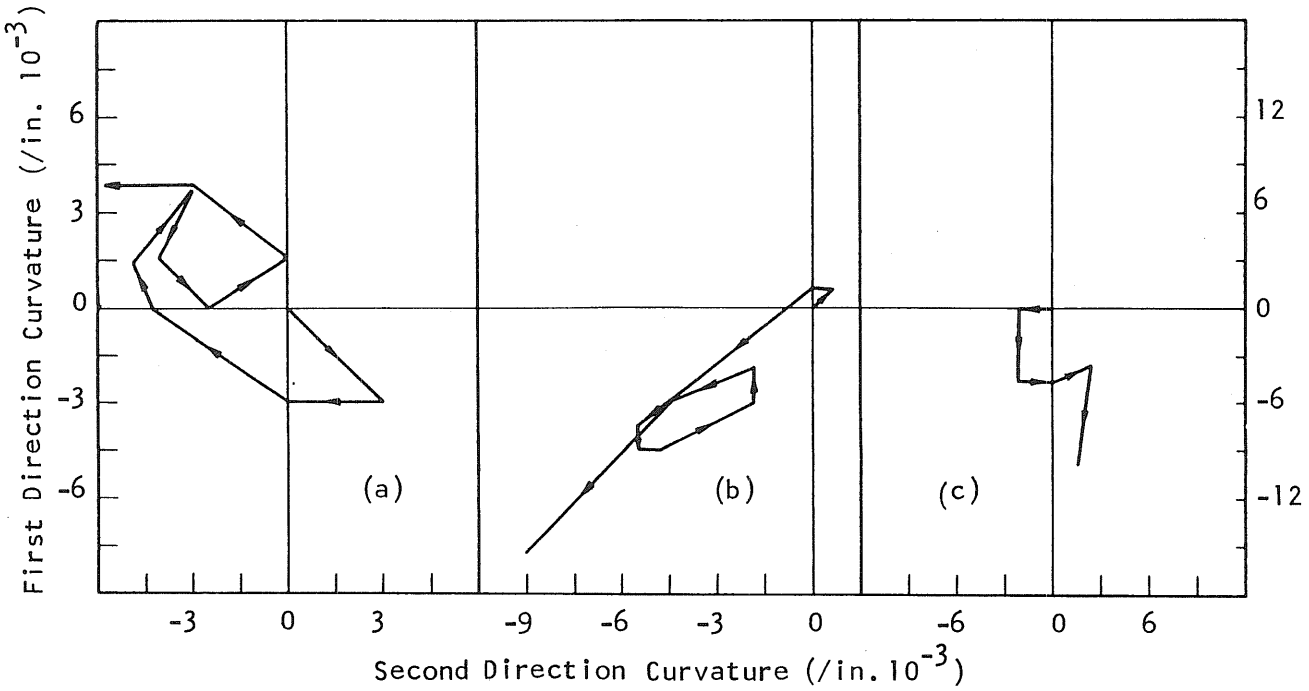

Fig. 4.44 Curvature History Representations of 2D Column Top Displacements

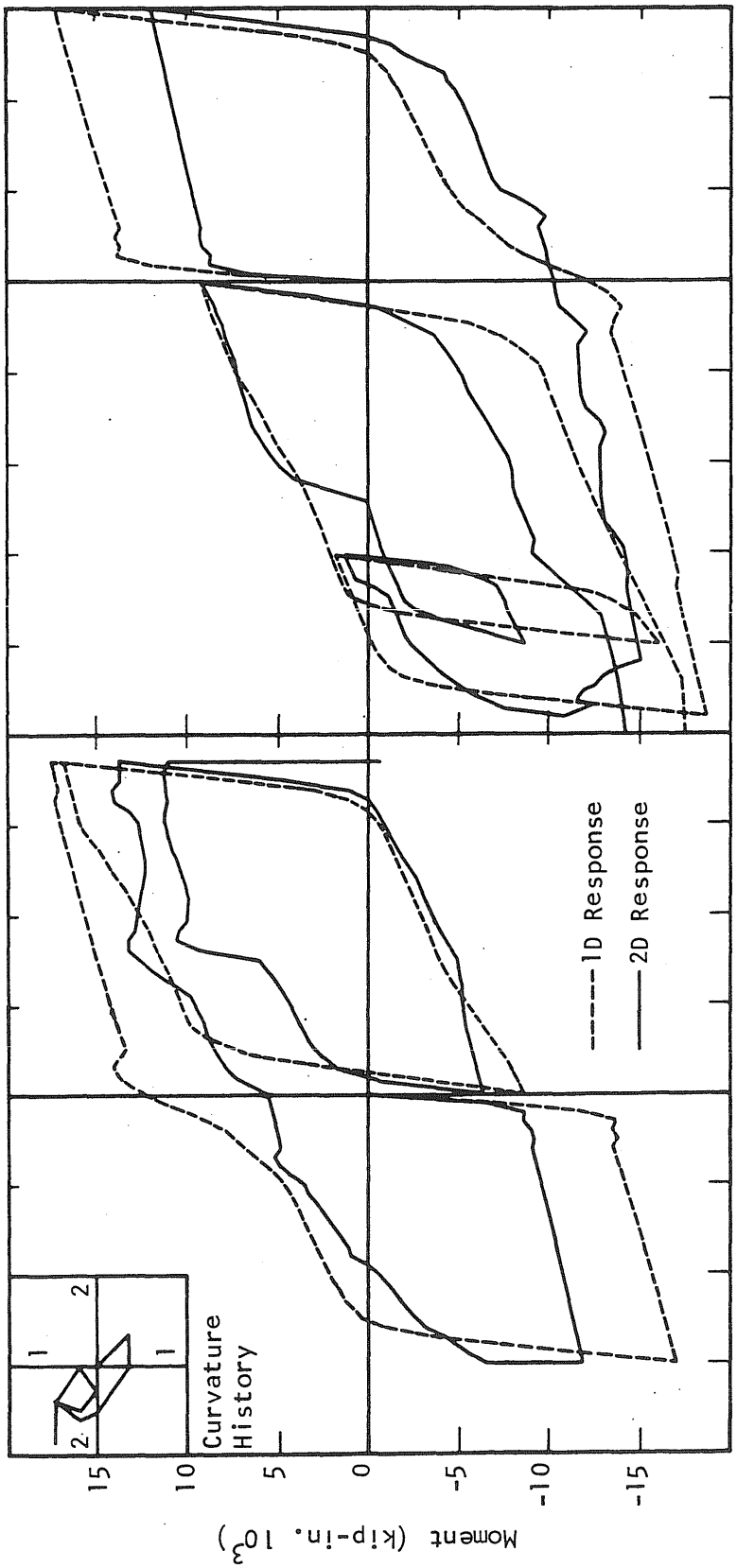

(a) First Direction (b) Second Direction

Fig. 4.45 1D and 2D Moment-Curvature Responses

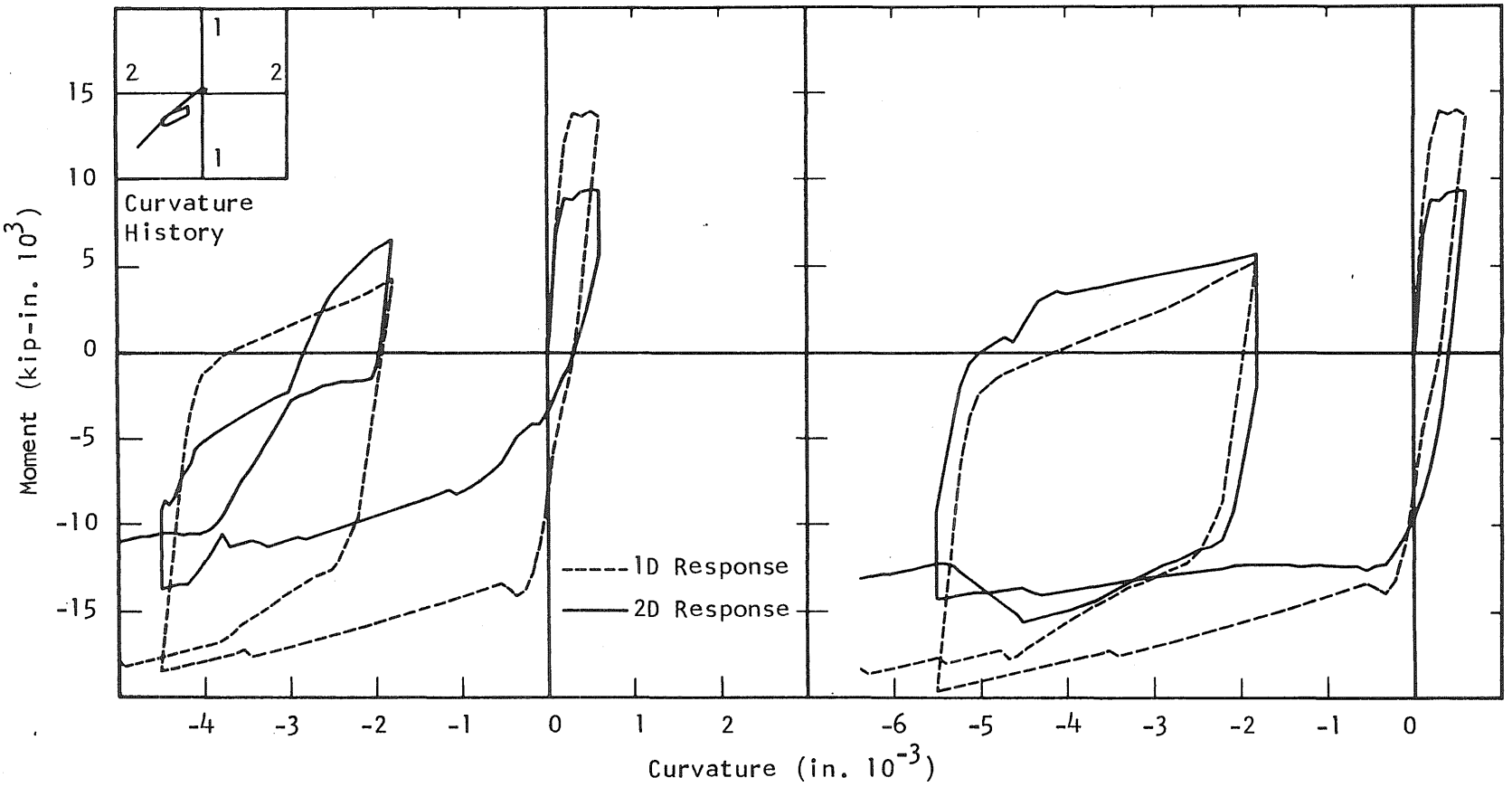

Fig. 4.46 1D and 2D Moment-Curvature Responses

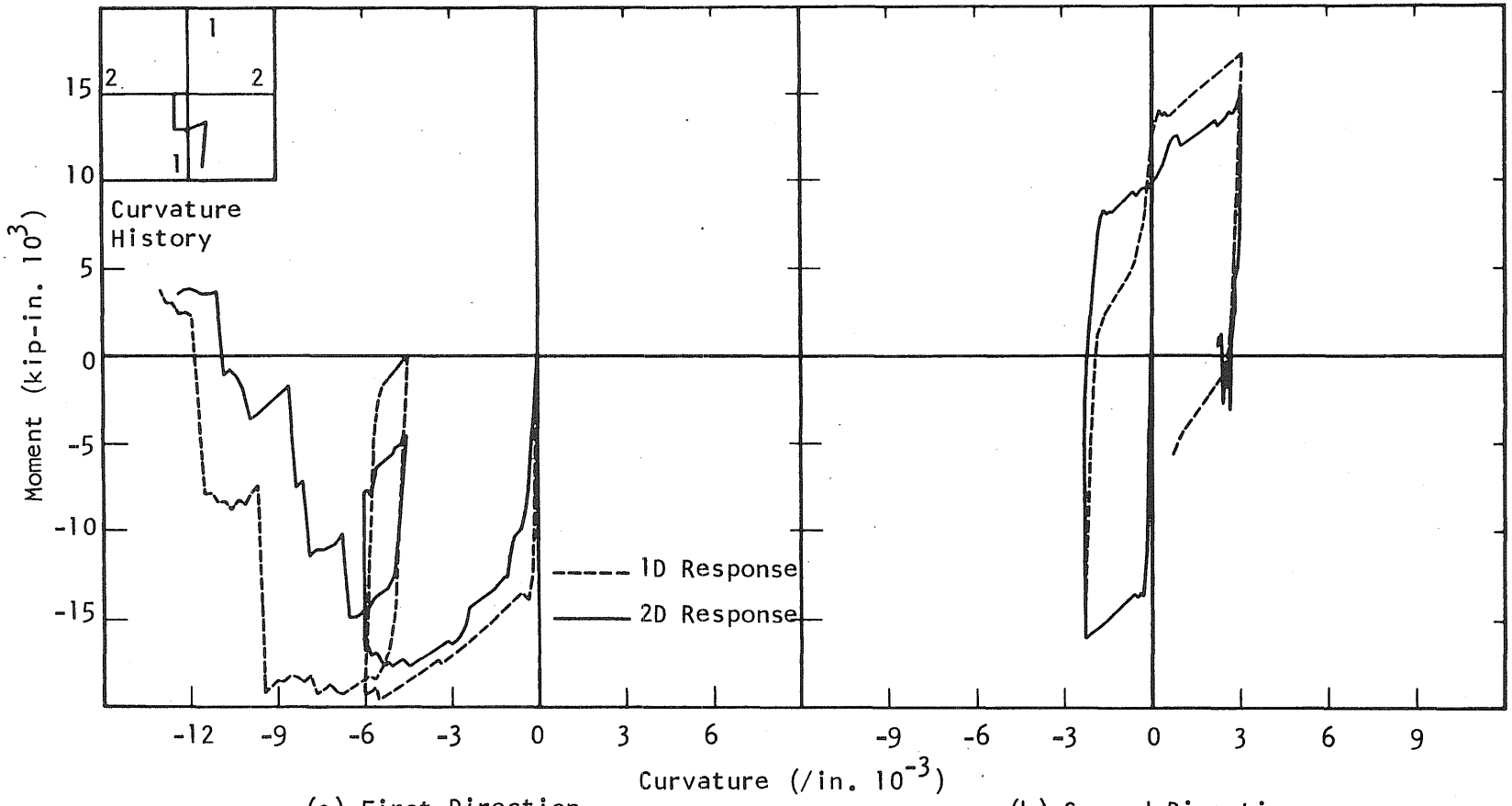

(a) First Direction (b) Second Direction

Fig. 4.47 1D and 2D Moment-Curvature Responses

APPENDIX A

THE PROPERTIES OF A REINFORCED CONCRETE SECTION

A.1 Introductory Comments

A column segment is visualized to consist of a number of solid tubes along its long axis (Fig. A.1), of cross sectional area A_i. These tubes are defined as finite-filaments. Together, they form the column segment which is considered as the finite element in this study. Each finite-filament is assumed to be uniaxially stressed and has prescribed stress-strain characteristics. The strain history of a finite filament varies along its long axis. A number of check sections are assigned along a column segment to keep track of the strain histories at the centroid of the finite-filaments. These check sections are termed checkpoints. It is assumed that the stress within a filament at a checkpoint can be obtained from the strain history at the centroid of the filament at that checkpoint. The column segment, checkpoints and filaments are shown in Fig. 2.1.

A.2 Relation Between Total Moments and Curvatures

Assuming the section remains plane after deformation, the strain at the centroid of a finite-filament A_i (Fig. A.1) is:

$$\epsilon = \epsilon_o - z K_1 + y K_2 \qquad (A.1)$$

where ϵ_o, K_1 and K_2 are strain and curvatures at the centroid of the section, z and y are the coordinates of the filament centroid. Assume that the stress-strain relation shown in Fig. A.2 represents the stress-strain relation prescribed for the filament A_i. Knowing the previous strain history, the stress corresponding to a strain change can be obtained using one of the following relations:

$$\sigma_i = C_o \varepsilon_i \tag{A.2}$$

$$\Delta\sigma = C_s \Delta\varepsilon \tag{A.3}$$

$$\partial\sigma = C_t \partial\varepsilon \tag{A.4}$$

where σ_i is the total stress at ε_i obtained by the initial secant C_o, $\Delta\sigma$ is the stress increment between the present and previous strain states obtained by the intermediate secant C_s and $\partial\sigma$ is the tangential change in stress obtained by the tangent C_t at the previous strain state. If the tangent C_t is used to approximate the stress at ε_i, an error defined as σ_r is introduced as shown in Fig. A.2. This residual stress at ε_i is given by:

$$\sigma_r = (C_t - C_s)\, \partial\varepsilon \tag{A.5}$$

The stress resultants on the section are defined by:

$$N = \sum_{i=1}^{n} \left(\int_{A_i} \sigma_i \, dA \right)$$

$$M_1 = \sum_{i=1}^{n} \left(- \int_{A_i} z \, \sigma_i \, dA \right)$$

$$M_2 = \sum_{i=1}^{n} \left(\int_{A_i} y \, \sigma_i \, dA \right) \tag{A.6}$$

Where the stresses, strains and N are positive in compression.

Substitution of the expressions (A.1) and (A.2) in (A.6) yields the following relation between the section forces and strains:

$$\begin{bmatrix} N \\ M_1 \\ M_2 \end{bmatrix} = \left(\sum_{i=1}^{n} C_{oi} \, [G_i] \right) \begin{bmatrix} \epsilon_o \\ K_1 \\ K_2 \end{bmatrix} \tag{A.7}$$

where $[G_i]$ contains geometric quantities of the filament A_i,

$$[G_i] = \begin{bmatrix} A_i & -Z_i & Y_i \\ & I_{zzi} & -I_{zyi} \\ \text{Symmetric} & & I_{yyi} \end{bmatrix} \tag{A.8}$$

A_i, Z_i, Y_i are the area and section moduli of the filament along the z and y axes. I_{zz} and I_{yy} are the moments of inertia along the z and y axes and I_{zy} is the product of inertia. Defining the moments by [m], curvatures by [k] and the relating matrix in expression (A.7) by [D], expression (A.7) becomes

$$\begin{bmatrix} \frac{N}{m} \end{bmatrix} = [D] \begin{bmatrix} \frac{\epsilon_o}{k} \end{bmatrix} \tag{A.9}$$

Defining the section forces by $[\sigma]$ and the strains by $[\epsilon]$ one obtains:

$$[\sigma] = [D] \, [\epsilon] \tag{A.10}$$

Expressions (A.7), (A.9), and (A.10) express the total section forces in terms of the total section strains. If a curvature history for the section is prescribed and the axial load is known, this curvature history

can be followed in small increments and the moments at each increment can be found. Assuming ε_o, evaluating the [D] matrix and checking if the correct axial load is obtained, ε_o at that increment is found by iteration. The correct [D] matrix, corresponding to the previous strain histories and the occurring strain of the filaments, obtained from expression (A.1), is then evaluated to compute the section moments.

A.3 Relation Between Incremental and Tangential Moments and Curvatures

For the purposes of constructing the force-displacement relation of the finite element, which is required in incremental dynamic analysis, the relation between tangential stress and strain increments of the section are used. Proceeding in the same manner as in section A.1, the following relation can be obtained for incremental section stresses and strains:

$$\begin{bmatrix} \Delta N \\ \Delta M_1 \\ \Delta M_2 \end{bmatrix} = \left(\sum_{i=1}^{n} C_{si} [G_i] \right) \begin{bmatrix} \Delta \varepsilon_o \\ \Delta K_1 \\ \Delta K_2 \end{bmatrix} \tag{A.11}$$

Using the tangent C_t instead of C_s (Fig. A.2), the relation between tangential changes in the section stresses and strains can be obtained as:

$$\begin{bmatrix} \partial N \\ \partial M_1 \\ \partial M_2 \end{bmatrix} = \left(\sum_{i=1}^{n} C_{ti} [G_i] \right) \begin{bmatrix} \partial \varepsilon_o \\ \partial K_1 \\ \partial K_2 \end{bmatrix} \tag{A.12}$$

Defining the tangential moment changes by $[\partial m]$, the curvature changes by $[\partial k]$ and the relating matrix by $[D_t]$,

$$\begin{bmatrix} \partial N \\ \partial m \end{bmatrix} = [D_t] \begin{bmatrix} \partial \epsilon_o \\ \partial k \end{bmatrix} \tag{A.13}$$

is obtained. If the axial force is constant, ∂N will vanish.

Rewriting expression (A.13) for vanishing incremental axial force in the following form,

$$\left[\begin{array}{c} 0 \\ \hline \partial m \end{array}\right] = \left[\begin{array}{c|c} D_{t\epsilon\epsilon} & D_{t\epsilon k} \\ \hline D_{tk\epsilon} & D_{tkk} \end{array}\right] \begin{bmatrix} \partial \epsilon_o \\ \partial k \end{bmatrix} \tag{A.14}$$

the relation can be condensed to yield:

$$[\partial m] = [D_t^*] \quad [\partial k] \tag{A.15}$$

where

$$[D_t^*] = [D_{tkk} - D_{tk\epsilon} D_{t\epsilon\epsilon}^{-1} D_{t\epsilon k}]$$

A.4 Residual Section Stresses

In the case of tangential approximations to stresses, the relation between residual stresses and tangential strains can be obtained as:

$$\begin{bmatrix} N_r \\ M_{1r} \\ M_{2r} \end{bmatrix} = \{ \sum_{i=1}^{n} (C_{ti} - C_{si}) [G_i] \} \begin{bmatrix} \partial \epsilon_o \\ \partial K_1 \\ \partial K_2 \end{bmatrix} \tag{A.16}$$

Defining the residual moments by $[m_r]$ and the relating matrix by $[D_r]$,

$$\begin{bmatrix} N_r \\ m_r \end{bmatrix} = [D_r] \begin{bmatrix} \partial \epsilon_o \\ \partial k \end{bmatrix} \tag{A.17}$$

is obtained.

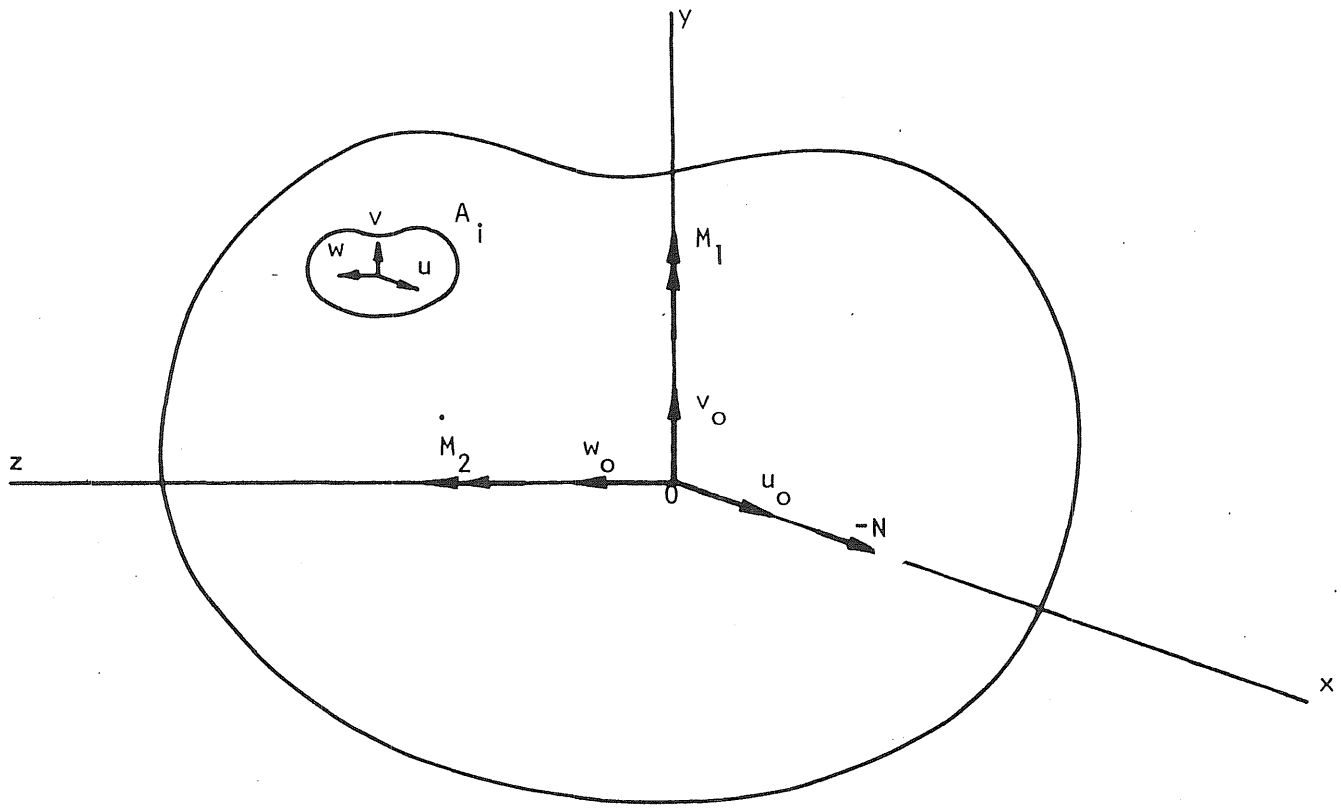

Fig. A.1 Section and Filament Displacements, Section Stress Resultants

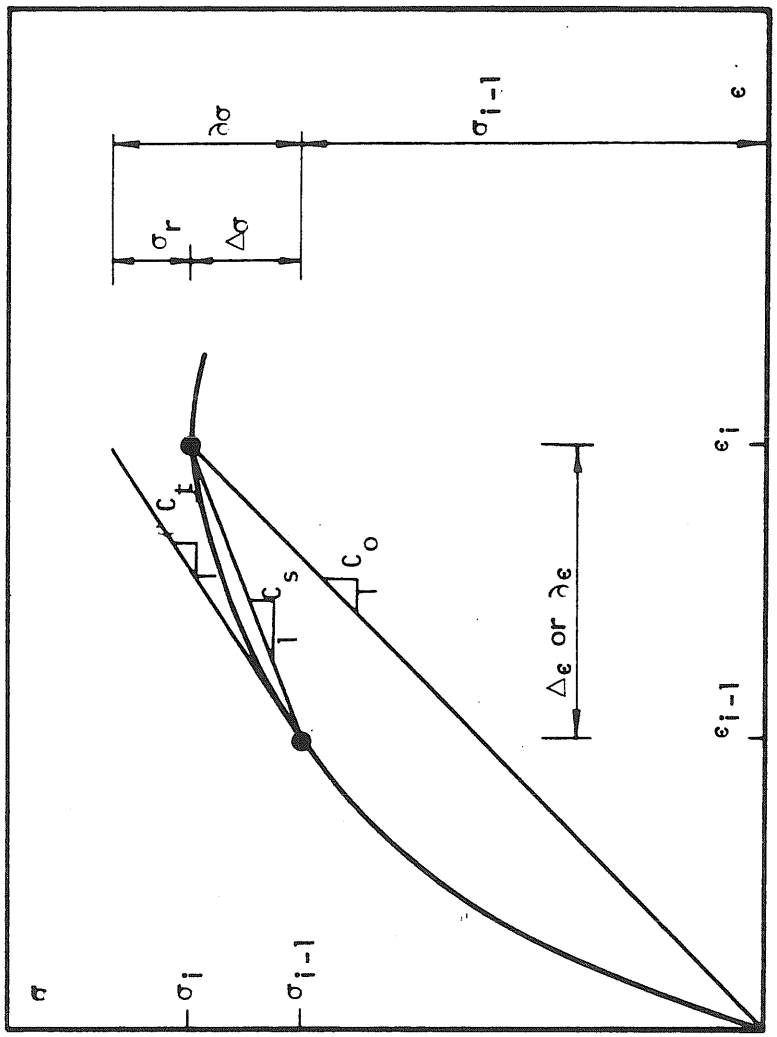

Fig. A.2 Stress-Strain Relation of a Filament

APPENDIX B

THE PROPERTIES OF A REINFORCED CONCRETE ELEMENT

B.1 Introductory Comments

A column segment is considered as a finite element in this study. The static force-displacement relation for a finite element will be developed in the following, using the moment-curvature relations derived in Appendix A. The tangential load-displacement relations of the finite elements are required for the incremental dynamic analysis of a reinforced concrete system. The procedure followed in the dynamic analysis will be presented in Appendix C.

The axial force in the finite elements are assumed to be constant through the loading history. Then the tangential variation of the axial force vanishes and only the lateral degrees of freedom are considered in the tangential force-displacement relations. The effect of the axial load on the lateral stiffness (the P-Δ effect) is incorporated in the derivations. The torsional degree of freedom of the finite elements are not considered in the following derivations. However, a torsional dynamic degree of freedom is incorporated in the dynamic analysis procedure by including the elastic torsional stiffnesses of the elements in the force-displacement relations.

B.2 Relation Between Internal and End Displacements

Consider the finite element shown in Fig. B.1. Assuming the internal displacements v and w of the element can be expressed in the form of cubic polynomials in x, the constants in these polynomials can be obtained using the boundary conditions prescribed by the end displacements and end rotations. The following relation between the internal and end displacements can then be obtained (21):

$$[u] = \begin{bmatrix} f_1 & 0 & 0 & f_2 & f_3 & 0 & 0 & f_4 \\ 0 & f_1 & -f_2 & 0 & 0 & f_3 & -f_4 & 0 \end{bmatrix} [U] \qquad (B.1)$$

where [u] contains the internal displacements v and w, [U] contains the end displacements and rotations v_A, w_A, θ_{1A}, θ_{2A}, v_B, w_B, θ_{1B}, θ_{2B}. The relating matrix contains the following functions

$$f_1 = 1 - 3\left(\frac{x}{L}\right)^2 + 2\left(\frac{x}{L}\right)^3$$

$$f_2 = \left\{\frac{x}{L} - 2\left(\frac{x}{L}\right)^2 + \left(\frac{x}{L}\right)^3\right\} L$$

$$f_3 = 3\left(\frac{x}{L}\right)^2 - 2\left(\frac{x}{L}\right)^3$$

$$f_4 = \left\{-\left(\frac{x}{L}\right)^2 + \left(\frac{x}{L}\right)^3\right\} L$$

Defining the relating matrix by [p], expression (B.1) becomes:

$$[u] = [p]\ [U] \qquad (B.2)$$

A relation between the internal curvatures and the end displacements can be obtained in the following manner. By definition:

$$[k] = \begin{bmatrix} -w_{,xx} \\ v_{,xx} \end{bmatrix} \qquad (B.3)$$

where the operator $(\ )_{,x}$ indicates partial differentiation with respect to x. Differentiating both sides of expression (B.2) twice and making the the appropriate row and sign changes

$$[k] = [B]\ [U] \qquad (B.4)$$

where

$$[B] = \begin{bmatrix} 0 & -f_{1,xx} & f_{2,xx} & 0 & 0 & -f_{3,xx} & f_{4,xx} & 0 \\ f_{1,xx} & 0 & 0 & f_{2,xx} & f_{3,xx} & 0 & 0 & f_{4,xx} \end{bmatrix}$$

can be obtained.

B.3 Relation Between End Forces and Displacements

Relations developed in sections A.2 and B.2 will be used to formulate the tangential stiffness relation of the finite element which is required for incremental dynamic analysis. Assume that the finite element is in equilibrium under the end forces [F] and the corresponding internal stresses [σ]. The virtual work should vanish at an equilibrium state (13). Denoting virtual quantities by "δ", the external virtual work δW_e can be expressed as:

$$\delta W_e = [\delta U]^T [F] - N\, \delta u \Big|_o^L \tag{B.5}$$

where $-N\, \delta u \Big|_o^L$ is the virtual work of the axial force which is positive in compression. [F] contains the end forces F_{2A}, F_{3A}, M_{1A}, M_{2A}, F_{2B}, F_{3B}, M_{1B}, M_{2B}. The virtual axial displacement can be expressed in the form:

$$\delta u \Big|_o^L = \int_L \delta u_{,x}\, dx \tag{B.6}$$

A second order approximation for the centroid strain ϵ_o, which is positive in compression, is:

$$\epsilon_o = -\left(u_{,x} + \frac{1}{2} v_{,x}^2 + \frac{1}{2} w_{,x}^2\right) \tag{B.7}$$

$\delta u,_x$ can be obtained from (B.7) as:

$$\delta u,_x = -\delta\varepsilon_o - \delta v,_x \, v,_x - \delta w,_x \, w,_x \tag{B.8}$$

Introducing (B.8) and (B.6) in (B.5), the external virtual work becomes:

$$\delta W_e = [\delta U]^T[F] + N \int_L (\delta\varepsilon_o + [\delta u],_x^T [u],_x) \, dx \tag{B.9}$$

The internal virtual work, δW_i, can be expressed in the form:

$$\delta W_i = -\int_L (\delta\varepsilon_o \, N + [\delta k]^T[m]) \, dx \tag{B.10}$$

By virtue of the principle of virtual work,

$$\delta W_e + \delta W_i = 0 \tag{B.11}$$

Substituting (B.9) and (B.10) in (B.11) and simplifying:

$$[\delta U]^T[F] + N\int_L [\delta u]_x^T[u],_x \, dx - \int_L [\delta k]^T[m] \, dx = 0 \tag{B.12}$$

can be obtained.

Assume that another equilibrium configuration is defined by the end forces $[F + \partial F]$ and the internal stresses $[\sigma + \partial\sigma]$. The principle of virtual work can be applied at this equilibrium state, yielding,

$$[\delta U]^T[F + \partial F] + N \int_L [\delta u]_x^T[u + \partial u],_x \, dx$$

$$-\int_L [\delta k]^T[m + \partial m] \, dx = 0 \tag{B.13}$$

Subtracting (B.12) from (B.13) and rearranging after simplifying:

$$[\delta U]^T[\partial F] = \int_L ([\delta k]^T[\partial m] - N[\delta u]^T_{,x}\,[\partial u]_{,x})\,dx \tag{B.14}$$

is obtained.

Differentiating both sides of (B.2),

$$[u]_{,x} = [p]_{,x}\,[U] \tag{B.15}$$

and rewriting (B.4) for tangential quantities,

$$[\partial k] = [B]\,[\partial U] \tag{B.16}$$

is obtained. Introducing (A.15), (B.15) and (B16) in (B.14) and simplifying

$$[\partial F] = \{\int_L ([B]^T[D_t^*][B] - N[p]^T_{,x}\,[p]_{,x})\,dx\}\,[\partial U] \tag{B.17}$$

is obtained. The relating expression is the tangential stiffness matrix including the effect of the axial force. Defining this relation by $[K_t]$, expression (B.17) becomes:

$$[\partial F] = [K_t]\,[\partial U] \tag{B.18}$$

The stiffness matrix of the columns can be obtained by assembling the stiffness matrices of the finite elements. In a lumped mass idealization of the columns in dynamic analysis, the stiffness relation between the forces and displacements at the column top are required. The internal degrees of freedom in the column stiffness matrix can be condensed to obtain this relation (21).

B.4 Residual End Forces

If the tangential stiffness relation in expression (B.18) is used to obtain incremental end forces resulting from incremental changes in the end displacements, an error will be introduced since the actual force-displacement relation is nonlinear. The filaments will have residual stresses σ_r as shown in Fig. A.2. During inelastic analysis, the change in the displacements corresponding to a change in the end forces can be obtained by an iterative procedure similar to the "Initial Stress Method" (27). Equivalent residual end forces corresponding to the residual filament stresses are introduced and the displacements are corrected by the additional displacements resulting from these equivalent residual end forces. Defining the residual end forces by $[P_r]$ and the residual section stresses, N_r, M_{1r}, M_{2r}, arising from the residual filament strains σ_r (section A.4), by $[\sigma_r]$, the principle of virtual work can be used to obtain an expression for $[P_r]$. The external virtual work of the residual end forces can be expressed as:

$$\delta W_e = [\delta U]^T [P_r] - N_r \, \delta u \Big|_o^L \tag{B.19}$$

the corresponding internal virtual work is:

$$\delta W_i = -\int_L (\delta e_o \, N_r + [\delta k]^T [m_r]) \, dx \tag{B.20}$$

Following the procedure in section B.3,

$$[P_r] = \int_L [B]^T [m_r] dx - N_r \{ \int_L [p]_{,x} [p]_{,x} dx \} \, [U] \tag{B.21}$$

can be obtained. For known residual filament strains, the corresponding residual section stresses $[m_r]$ and N_r can be obtained from expression (A.17).

B.5 Numerical Evaluation of the Tangential Stiffness Matrix and the Residual End Forces

The "Gaussian Quadrature" technique (27) can be used to evaluate the tangential stiffness matrix and the residual end forces numerically. In both relations (B.17) and (B.21) integration of the second term, "$\int_L [p]^T_{,x} [p]_{,x} \, dx$" is evaluated in closed form for the finite element. For the first terms, "$\int_L [B]^T [D_t^*] [B] dx$" and "$\int_L [B]^T [m_r] \, dx$", a number of checkpoints are assigned along the finite element. The locations of these checkpoints correspond to the position of the Gaussian integration sample points. The matrices $[B]$, $[D_t^*]$ and $[m_r]$ and the residual axial force N_r can be obtained at each checkpoint. Integration of the first terms can then be performed in the following manner:

$$\int_L [B]^T [D_t^*] [B] \, dx = \sum_{j=1}^{q} H_j [B_j]^T [D_{tj}^*] [B_j] \tag{B.22}$$

$$\int_L [B]^T [m_r] dx = \sum_{j=1}^{q} H_j [B_j]^T [m_{rj}] \tag{B.23}$$

where H_j is the Gaussian integration weighing coefficient at the sample point "j" and $[B_j]$, $[D_{tj}^*]$ and $[m_{rj}]$ are evaluated at the location of the sample point "j". "q" is the number of sample points. Evaluating the first terms in the integrals in this manner, the expressions for the stiffness matrix and the residual end forces for a finite element become:

$$[K_t] = \sum_{j=1}^{q} H_j [B_j]^T [D_{tj}^*] [B_j] - N \int_L [p]^T_{,x} [p]_{,x} \, dx \tag{B.24}$$

$$[P_r] = \sum_{j=1}^{q} H_j\{[B_j]^T[m_{rj}]\} - \frac{\sum_{j=1}^{q} N_{rj}}{q}\left(\int_L [p]^T_{,x}[p]_{,x}\,dx\right)[U] \qquad (B.25)$$

where the residual axial load N_r is evaluated at the checkpoints "j".

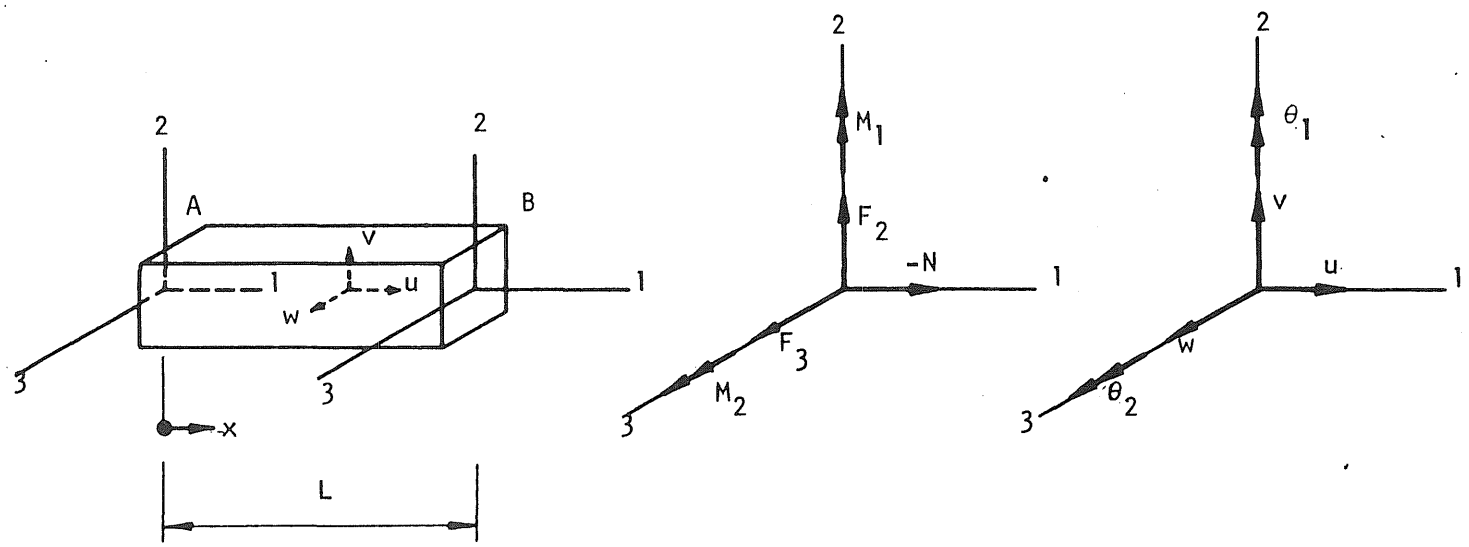

Fig. B.1 Finite Element, End Forces and Displacements

APPENDIX C

PROCEDURE FOR DYNAMIC ANALYSIS

C.1 Introductory Comments

The force-displacement and residual force relations developed in Appendix B for a single column segment can be used in the dynamic analysis of any ductile, moment resisting space frame system. In this study, these relations will be used to analyse a single lumped mass system as shown in Fig. C.1. Three dynamic degrees of freedom at the mass point and two lateral components of base acceleration are considered. The single lumped mass system represents single story systems with an arbitrary number of columns and a stiff girder or slab system or multistory systems with flexible first story columns and stiffened upper stories.

The mass of the columns is neglected. The dynamic degrees of freedom at the mass point results in lateral relative column displacements as well as torsional deformations. The stiffness relation developed in Appendix B does not include the torsional degree of freedom; elastic torsional stiffnesses of the columns are introduced in the force-displacement relations after these are obtained for the lateral degrees of freedom.

C.2 The Equations of Motion

The equations of motion in terms of the relative displacements of the mass point can be expressed in an incremental form as follows:

$$[M]\ [\Delta\ddot{X}] + [C]\ [\Delta\dot{X}] + [\Delta F] = -[M]\ [\Delta\ddot{Y}] \qquad (C.1)$$

These equations are obtained by subtracting the equations of motion expressed

at two consecutive time instances t and $t+\Delta t$. The operator Δ denotes an increment between two time steps such that $\Delta(\ ) = (\ )_{t+\Delta t} - (\ )_t$.

[M] is the diagonal mass matrix with the mass of the system as the first two diagonal elements and the rotational inertia as the third diagonal element,

[C] is the diagonal, linear viscous damping matrix,

$[\Delta\ddot{X}]$ contains relative incremental mass accelerations,

$[\Delta\dot{X}]$ contains relative incremental mass velocities,

$[\Delta\ddot{Y}]$ contains base accelerations, and

$[\Delta F]$ is the change in the resisting force of the system

Expressing $[\Delta F]$ in the form:

$$[\Delta F] = [K_{ts}]\ [\Delta X] - [\Delta P_{rs}] \tag{C.2}$$

where $[K_{ts}]$ is the tangential system stiffness and $[\Delta P_{rs}]$ is the system residual force, expression (C.1) becomes:

$$[M][\Delta\ddot{X}] + [C][\Delta\dot{X}] + [K_{ts}][\Delta X] = -[M][\Delta\ddot{Y}] + [\Delta P_{rs}] \tag{C.3}$$

Applying "Newmark's Beta Method" (15) where a special form of variation of the acceleration is assumed between two time steps, $[\Delta\ddot{X}]$ and $[\Delta\dot{X}]$ can be integrated and expressed in terms of $[\Delta X]$ and quantities at the former time step as shown in the following:

$$[\dot{X}]_{t+\Delta t} = [\dot{X}]_t + \frac{\Delta t}{2}\{[\ddot{X}]_t + [\ddot{X}]_{t+\Delta t}\}$$

$$[X]_{t+\Delta t} = [X]_t + \Delta t[\dot{X}]_t + (\frac{1}{2} - \beta)\,\Delta t^2[\ddot{X}]_t + \beta\,\Delta t^2[\ddot{X}]_{t+\Delta t} \tag{C.4}$$

where β is a constant depending on the assumed variation of acceleration (15). From Equation (C.4),

$$[\Delta\dot{X}] = \frac{1}{2\beta\Delta t}[\Delta X] - \frac{1}{2\beta}[\dot{X}]_t + \Delta t\,(1 - \frac{1}{4\beta})[\ddot{X}]_t$$

$$[\Delta\ddot{X}] = \frac{1}{\beta\Delta t^2}[\Delta X] - \frac{1}{\beta\Delta t}[\dot{X}]_t - \frac{1}{2\beta}[\ddot{X}]_t \qquad (C.5)$$

is obtained, introducing in (C.3),

$$[K^*_{ts}]\,[\Delta X] = [Q] + [\Delta P_{rs}] \qquad (C.6)$$

where

$$[K^*_{ts}] = [K_{ts}] + \frac{1}{\beta\Delta t^2}[M] + \frac{1}{2\beta\Delta t}[C]$$

$$[Q] = \{\frac{1}{\beta\Delta t}[M] + \frac{1}{2\beta}[C]\}\,[\dot{X}]_t + \{\frac{1}{2\beta}[M] + \Delta t(\frac{1}{4\beta} - 1)[C]\}[\ddot{X}]_t - [M][\Delta\dot{Y}]$$

is obtained. $[K^*_{ts}]$ is defined as the dynamic stiffness matrix of the system. $[Q]$ is defined as the dynamic load matrix.

C.3 Solution of the Equations of Motion

(C-6) are a set of linear algebraic equations for the determination of $[\Delta X]$. A direct solution is not possible since the residual forces $[\Delta P_{rs}]$ are not known in advance. A successive correction approach was followed in the study, analogous to the "Initial Stress Method" (27). Assume that the analysis is carried out until time "t" and the displacement configuration of the columns and the column segments (finite elements) as well as the stress-strain state of the filaments (at each checkpoint in all column segments) are obtained at time "t". Then the system dynamic stiffness matrix and the dynamic load matrix can be constructed knowing the system

properties at time "t". Setting up the expression (C.6) in this manner, approximate the incremental displacements $[\Delta X]$ and the system residual forces $[\Delta P_{rs}]$ between "t" and "t+Δt" by successive corrections;

$$[\Delta X] = [\Delta X]^{o} + [\Delta X]^{1} + \ldots + [\Delta X]^{n}$$

$$[\Delta P_{rs}] = [\Delta P_{rs}]^{o} + [\Delta P_{rs}]^{1} + \ldots + [\Delta P_{rs}]^{n-1} \qquad (C.7)$$

Introducing in (C.6),

$$[K^{*}_{ts}]\ ([\Delta X]^{o} + [\Delta X]^{1} + \ldots + [\Delta X]^{n}) = [Q] + [\Delta P_{rs}]^{o} + [\Delta P_{rs}]^{1} + \ldots + [\Delta P_{rs}]^{n-1} \qquad (C.8)$$

Then the successive corrections for $[\Delta X]$ can be obtained in the following manner:

$$\begin{aligned} [K^{*}_{ts}]\ [\Delta X]^{o} &= [Q] \\ [K^{*}_{ts}]\ [\Delta X]^{1} &= [\Delta P_{rs}]^{o} \\ &\vdots \\ [K^{*}_{ts}]\ [\Delta X]^{n} &= [\Delta P_{rs}]^{n-1} \end{aligned} \qquad (C.9)$$

The corrections can be carried out until a selected convergence criterion is satisfied. The system incremental residual forces for each correction are obtained through the residual filament stresses by the following procedure:

(a) Obtain the first approximation to the mass point relative displacement, $[\Delta X]^{o}$, from (C.9).

(b) Transfer $[\Delta X]^{o}$ to the column tops.

(c) Obtain the relative displacements at the interior nodes of the columns (finite element end displacements).

(d) Obtain the strains at the checkpoints along the finite elements (section B.2).

(e) Obtain the change in strain and the residual stress of each finite-filament at the checkpoints. Obtain the incremental residual section stresses at each checkpoint (section A.4).

(f) Evaluate the incremental residual end forces for the finite element (section B.4).

(g) Assemble the finite element end forces to obtain the incremental residual end forces of each column.

(h) Condense the forces at the interior nodes of the columns. Obtain the incremental residual column top (boundary) forces.

(i) Transfer the boundary forces of each column to the mass point and add to obtain the incremental system residual forces $[\Delta P_{rs}]^{o}$ for the next correction.

(j) Solve for the next correction for the relative mass point displacements, $[\Delta X]^{1}$, from expression (C.9). Repeat the procedure given in steps (a) to (j) until $[\Delta X]^{n}$ approaches zero.

(k) The above procedure to obtain the residual system forces is an alternate method of evaluating $[\Delta P_{rs}]$ in expression (C.2) through finite-filament stress-strain characteristics, rather than via the system stiffness matrix.

To reduce the number of iterations, the system stiffness can also be updated at each correction in expression (C.9). The procedure followed to update the system stiffness matrix is similar to the procedure followed

to obtain the incremental system residual forces. The finite element stiffness matrices corresponding to the filament stress-strain configurations after each correction are obtained as explained in section B.3. These are assembled to construct the column stiffness matrix. The degrees of freedom at the interior nodes are condensed and the column top stiffness is obtained. Repeating for each column, the column top stiffnesses are transferred to the mass point and added after including the elastic torsional stiffness terms. Obtaining the tangential system stiffness in this manner, this is introduced in the dynamic stiffness matrix for the next correction.

Since the solution process is iterative, an error in the form of a residual force will remain at the end of each time step. To avoid the accumulation of this error it is included in the solution for the next time step. The solution process considering the residual error from the previous time step, defined as [R], and updating the stiffness matrix at each correction becomes:

$$
\begin{aligned}
&[K^{*}_{ts}]^{n}_{i} \quad [\Delta X]^{o}_{i+1} = [Q]_{i+1} + [R]_{i} \\
&[K^{*}_{ts}]^{o}_{i+1} \quad [\Delta X]^{1}_{i+1} = [\Delta P_{rs}]^{o}_{i+1} \\
&\vdots \\
&[K^{*}_{ts}]^{n-1}_{i+1} \quad [\Delta X]^{n}_{i+1} = [\Delta P_{rs}]^{n-1}_{i+1}
\end{aligned}
\qquad \text{(C.10)}
$$

where the subscript i denotes the quantities at the ith time step, i+1 denotes the next time step. After the solution process is stopped for the ith time step and $[\Delta X]^{n}_{i}$ is computed, the system dynamic stiffness, $[K^{*}_{ts}]^{n}_{i}$ including

the effect of $[\Delta X]_i^n$ is evaluated. The residual error $[R]_i$ is obtained and the solution process for the i+1th time step starts as demonstrated by (C.10). A graphical representation of this solution process is presented in Fig. C.2.

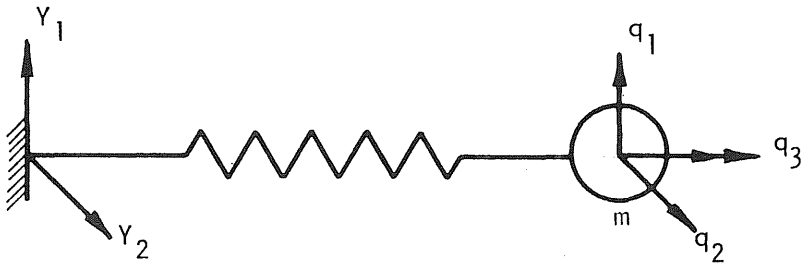

relative displacements [X] = [q] - [Y]

Fig. C.1 Single Mass System

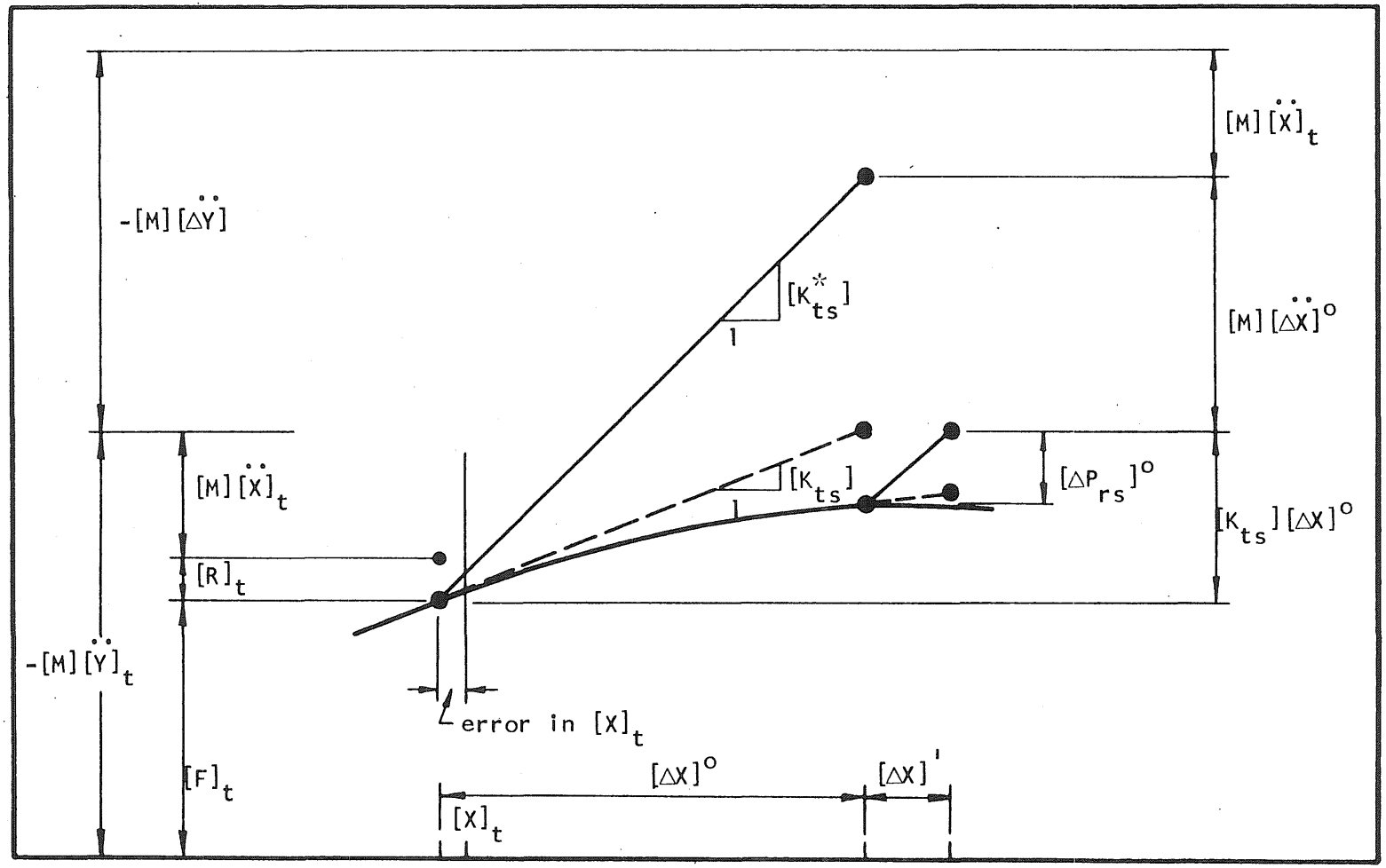

Fig. C.2 Schematic Representation of the Iteration Procedure

APPENDIX D

NOTATION

All symbols used in the text are defined when they are first introduced. For convenient reference they are listed below.

1D	=	One-dimensional
2D	=	Two-dimensional
A	=	Area of finite-filament
[B]	=	Relation between internal and end displacements of a finite element
C_o	=	Initial secant to the finite-filament stress-strain curve
C_s	=	Intermediate secant to the finite-filament stress-strain curve
C_t	=	Tangent to the finite-filament stress-strain curve
[C]	=	Viscous damping matrix
[D]	=	Relation between the stresses and strains of a section
$[D^*]$	=	Relation between the moments and curvatures of a section
[F]	=	External forces
[G]	=	Matrix containing finite-filament geometry
H	=	Gaussian integration weighing factor
I_y, I_z	=	Moments of inertia of the finite-filament along the y and z axes
I_{yz}	=	Product of inertia of the finite-filament
K	=	Curvature
[K]	=	Stiffness matrix
$[K^*]$	=	Dynamic stiffness matrix
L	=	Length of finite element

M = Bending Moment

$[M]$ = Mass matrix

N = Axial force

$[P]$ = End forces arising from internal stresses

$[Q]$ = Dynamic load matrix

$[R]$ = Error in the form of force resulting at the end of iteration

$[U]$ = End displacements of a finite element

W_e = External work

W_i = Internal work

$[X]$ = Relative displacements of mass point

$[\dot{X}]$ = Relative velocities of mass point

$[\ddot{X}]$ = Relative accelerations of mass point

Y = Section modulus of finite-filament along the y axis

$[\ddot{Y}]$ = Base acceleration

Z = Section modulus of finite-filament along the z axis

f = Function of x

$[k]$ = Curvatures of a section

$[m]$ = Bending moments of a section

$[p]$ = Relation between internal and end displacements

t = Time

u = Internal displacement along the x-axis

v = Internal displacement along the y-axis

w = Internal displacement along the z-axis

x = Coordinate axis

y = Coordinate axis

z = Coordinate axis

β = Constant defining the variation of relative mass accelerations between two time steps

ε = Axial strain at finite-filament centroid

$[\varepsilon]$ = strains of a section (axial centroid strain and curvatures)

ε_o = Axial strain at section centroid

σ = Axial stress

$[\sigma]$ = Stresses of a section (axial force and bending moments)

$\Delta(\ )$ = Incremental quantity

$\delta(\ )$ = Virtual quantity

$\partial(\ )$ = tangential change in a quantity

$(\ )_r$ = Residual quantity

$(\ )_s$ = Quantity related to the system

$(\ )_t$ = Tangential quantity

$(\ )_{,x}$ = Partial differentiation with respect to x

$[\ ]$ = Matrix

$[\ ]^T$ = Transposed matrix